LONGSHORE CURRENTS IN THE VICINITY OF A BREAKWATER

by

PETER EDWARD DANIEL
B.Sc., University of British Columbia, 1974

A THESIS SUBMITTED IN PARTIAL FULFILMENT OF
THE REQUIREMENTS FOR THE DEGREE OF
MASTER OF SCIENCE

in the Department
of
Physics

We accept this thesis as conforming to the required standard

THE UNIVERSITY OF BRITISH COLUMBIA

In presenting this thesis in partial fulfilment of the requirements for an advanced degree at the University of British Columbia, I agree that the Library shall make it freely available for reference and study. I further agree that permission for extensive copying of this thesis for scholarly purposes may be granted by the Head of my Department or by his representatives. It is understood that copying or publication of this thesis for financial gain shall not be allowed without my written permission.

Department of Physics

The University of British Columbia
Vancouver, Canada

Date August 22, 1978

ABSTRACT

Several theoretical models of the wave-induced current circulation in the vicinity of a breakwater extending from shore are presented. The models, which are patterned after a local field site, include several numerical models which take into account variable sea-floor topography and which compare the effects of linear and non-linear bottom friction as well as an analytical model characterized by semi-infinite beaches and uniform sea-floor topography.

In general (for a given angle of wave incidence) the circulation patterns show two counter-rotating cells driven by wave-induced longshore currents which flow along both the breakwater and natural beaches toward their common intersection corner, with an offshore return flow in the form of a rip current. The qualitative features of the models are consistent with observations of sediment transport taken at the study site.

Differences in the linear and non-linear bottom friction models do not become apparent until an off-shore trench parallel to the breakwater is introduced to the sea-floor topography. The non-linear model shows a deflection of the off-shore return flow into the trench in agreement with preliminary analysis based on a one-dimensional model. The linear results, however, differ considerably from those of the non-linear model and are difficult to interpret, showing an inordinate increase in transport over the trench.

During the development of the analytical model difficulties were encountered due to the complexities of the analysis which necessitated that part of the solution be solved numerically. The results, while showing the same general features as the numerical models, exhibit a much more strongly divergent off-shore return flow. This difference, while unresolved, appears to be one of scale rather than of form.

TABLE OF CONTENTS

Chapter Page

LIST OF FIGURES

Figure | Page

Figure Page

LIST OF SYMBOLS

a: wave amplitude

C: (i) a drag coefficient of $O(10^{-2})$
(ii) a friction coefficient defined by $\tau = C\rho|\underset{\sim}{u}_o|\underset{\sim}{u}_o$

C_o: $=\sqrt{gd_o}$ where d_o is the total water depth at the breaker-line

d: the total water depth equal to the sum of the local still water depth h, and the mean displacement of the water surface from the still water level, $\tilde{\eta}$; thus $d = h + \tilde{\eta}$

d_o: the total water depth at the breaker-line

E: energy density of the waves (see (3.3))

f: a friction coefficient which is a function of the total depth 'd' and wave amplitude (see (3.1) and (3.2))

g: acceleration due to gravity

h: local still water depth

h_f: a characteristic depth

H: the wave height equal to twice the amplitude 'a'

$J_{3/2}(ax)$: a Bessel function of the first kind (see (5.10))

k: the wave number

m_1, m_2: slope of the mean surface inside surfzones I and II respectively

n: $= \frac{1}{2}\left(1 + \frac{2kh}{\sinh(2kh)}\right)$

S_{ij}: radiation stress tensor

S(x): Fresnel integral (see (5.42))

T_i: force per unit mass due to divergence of radiation stress tensor (see (3.6))

$\bar{u}_{max}$: the maximum orbital velocity of the waves

u_o: the instantaneous total velocity vector just outside the bottom boundary layer (see (3.18))

U: the mean velocity component in the longshore direction

$\underset{\sim}{U}$: the velocity vector, assumed to be purely horizontal and depth independent

V: the mean velocity component in the offshore direction

x_b: width of surfzone II in analytic model (see Figure 27)

y_b: width of surfzone I in analytic model (see Figure 27)

β: angle of wave incidence relative to the normal to the breaker-line of surfzone I

γ: ratio of wave amplitude to mean water depth in the surfzone (see (4.11))

δ: angle of beach-breakwater intersection

η: the mean displacement of the water surface from the still water level

θ: angle of wave incidence relative to the normal to the breaker-line of surfzone II

ρ: the water density

τ: bottom shear stress in the presence of steady flow or long period waves (see (3.18))

ϕ: the angle of wave incidence relative to the normal to the shoreline

ψ: transport stream function (see (3.15))

ACKNOWLEDGEMENTS

I would like to thank Dr. P.H. LeBlond for directing me to this topic and for many helpful discussions concerning this work.

This work was done with the aid of a National Research Council grant.

CHAPTER I

INTRODUCTION

The need to understand littoral processes has become ever more apparent as our coastal environment is increasingly subject to human exploration and exploitation. The dispersal of pollutants, the erosion and accretion of shorelines, and the behavior of waves are but a few of the processes and phenomena which affect and are themselves, in turn, affected by human activity. The consequences of our encroachment upon the coastal environment need to be well understood, since man-made structures may have important effects (James, 1972).

It is in this vein of understanding our impact upon the coastal environment, in light of the behavior of waves that we have undertaken this study of longshore currents in the vicinity of an isolated breakwater extending from shore. We shall thus be examining the effects upon nearshore circulatory systems of one of the more common types of structures to have been built along our coasts. The exercise shall consist of the development of theoretical models of the current circulation near a breakwater and a comparison of their results, where practicable, to observations taken at a field location.

Related studies of longshore currents and their interaction with coastal structures have been conducted, for example, by Dalrymple et al (1977), who used several model basins to check their theoretical predictions of the effects of placing a wall in the path of a longshore current, and Mei and Liu (1976), with their study of the combined effects of refraction and diffraction on wave-induced mean currents in the vicinity of a breakwater.

This study shall investigate the current circulation resulting from wave-induced longshore currents generated along both breakwater and natural beach surfzones. It shall be presented in the following manner.

We shall first discuss the evidence for longshore currents at the field location as indicated by sediment transport along the beaches, inspection of groynes, aerial photographs, etc., and from these surmise as to the prevailing circulation pattern present in the area.

We shall then develop several models of the current circulation in a beach-breakwater configuration patterned after the field site. These will consist of:

i/ several numerical models using finite beaches in closed basins, with consideration given to variable sea-floor topography, as well as linear and non-linear forms of bottom friction

ii/ an analytical model employing semi-infinite beaches.

We shall conclude with a discussion of the theoretical results in light of the simplifying assumptions made throughout the analysis, and a comparison of the various models' results.

It should be pointed out that this thesis shall not attempt to resolve the practical quantitative aspects of sedimentation in a particular area; it is rather a study of the nature of longshore currents in a type of natural beach-breakwater configuration as inspired by a specific field location.

CHAPTER 2

DISCUSSION OF THE FIELD SITE

I General Location

The area which has inspired the study is a portion of the tidal-zone of the Fraser River Delta near the south end of Roberts Bank (see Figure 1).

It is bounded to the north by the Tsawwassen Ferry causeway - a breakwater extending in a south-westerly direction for a distance of approximately 3000 m. - and to the east by the Tsawwassen Beach - a narrow beach backed by 100 m. high cliffs extending in a southerly direction for a distance of approximately 6000 m. to the southern tip of Point Roberts. The angle formed by the intersection of the causeway and Tsawwassen Beach, to the south, is approximately 60°.

Our interest lies in observing, and subsequently modelling the current circulation over this portion of Roberts Bank resulting from wave-induced longshore currents along the Tsawwassen and causeway beaches.

II Geology, Geometry, Oceanography

With the exception of an off-shore trench - the result of dredging operations to procure fill for the causeway - the southern end of Roberts Bank is a shallow mudflats region having base sediments of sand and silty-sand.

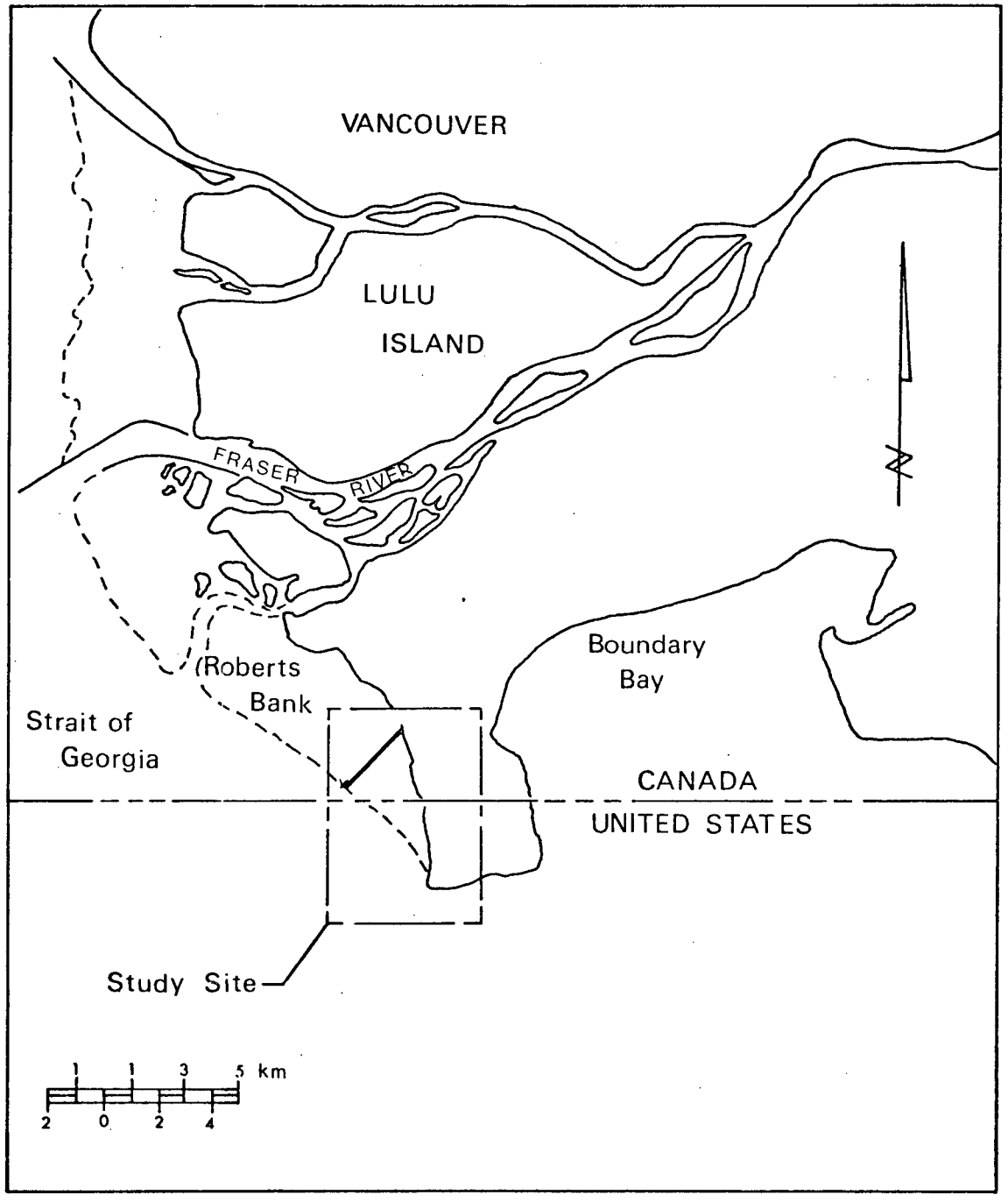

Figure 1. General location of the study site

As can be seen in Figure 2, the trench runs parallel to the causeway, across most of the width of Roberts Bank. It is approximately 150 m. wide, having mean low and high tide depths of 10 m. and 5 m. respectively, and stands approximately 250 m. from the southeast side of the causeway.

Our chosen study site will thus afford us the opportunity of isolating an aspect of variable sea-floor topography and studying its effect upon the local current circulation.

The remainder of the Bank has a mean high tide depth of approximately 5 m. and drains completely at low tide (see Figure 2), thus dictating that longshore currents will be relevant to shore erosion only during periods of high tide.

Also note that the off-shore edge of Roberts Bank, which falls with a slope of approximately 5 in 1 to a depth of approximately 100 m., does not run parallel to Tsawwassen Beach, but rather in a more south-easterly direction, effectively tapering from a distance of 3000 m. offshore with respect to the mean high tide line at the causeway, to 100 m. off-shore at Point Roberts.

III Discussion of Prevailing Winds and Local Topography

Since longshore currents are the result of waves breaking at an angle on a beach, let us examine the basic features affecting the waves which strike the causeway and Tsawwassen beaches, these being

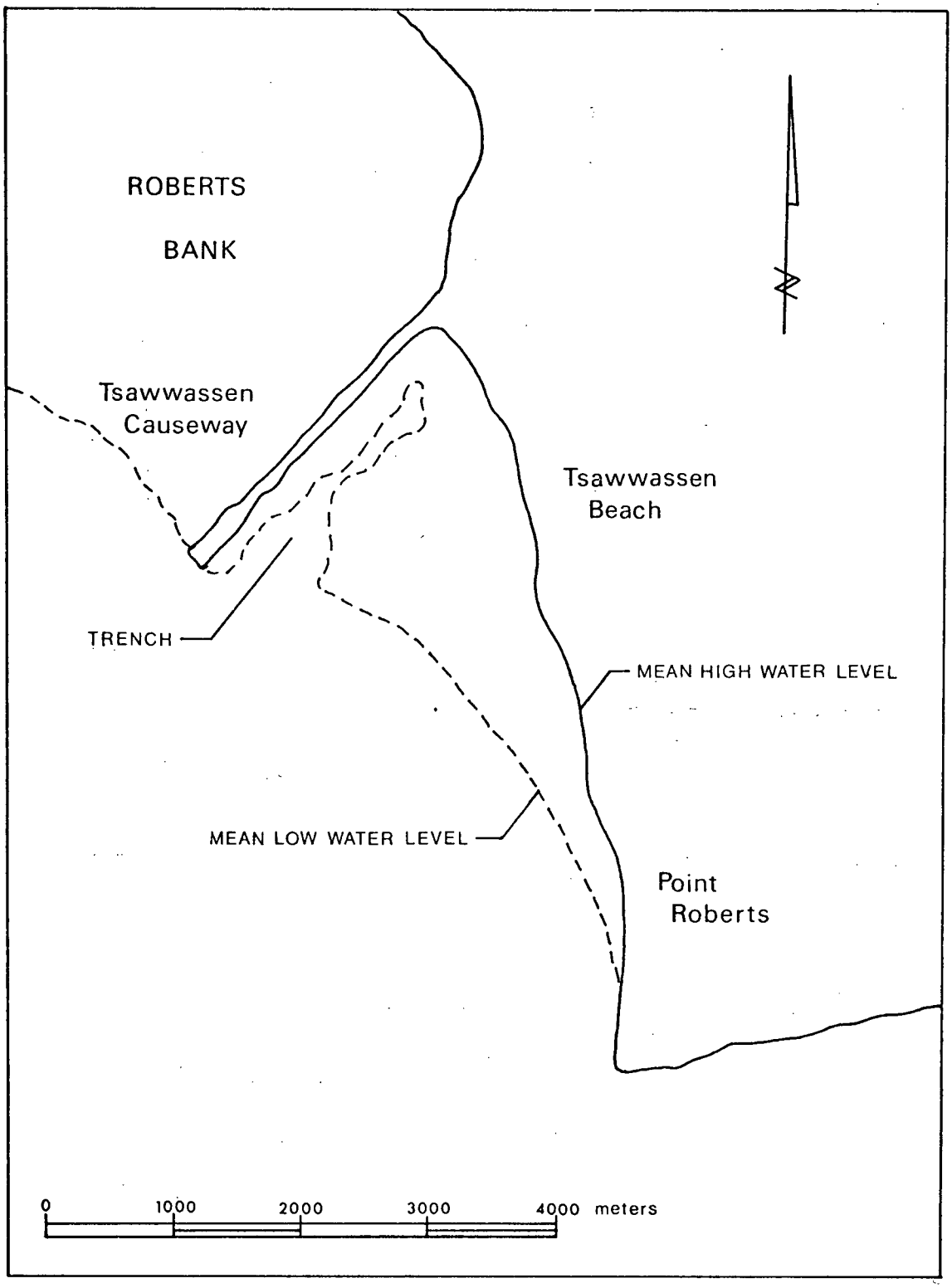

Figure 2. Detailed view of the study site

a/ the nature of the prevailing winds

b/ the local topography

Keeping in mind the orientation of the study area and its boundaries, it is apparent that it is open to attack only by wave trains incident from the southern quarter. Figure 3 indicates that a significant percentage of the local winds are, indeed, from the southern quarter, particularly from the south and south-east.

Wave trains approaching from the south will clearly have components of their propagation vector parallel to both the causeway and Tsawwassen beaches, suggesting the generation of longshore currents, whose direction of flow, in each instance, would be toward the intersection apex (see Figure 4). At first glance it appears as though Point Roberts shields the area from southeasterly waves. However, it has been suggested by Wood (1970), that southeasterly wavestrains passing the Point are diffracted and then refracted to approach the study area in a more southerly direction. Thus, they too will add to the effect of southern storms, their contribution, however, being less than if they had come over an uninterrupted fetch.

The predominant nature of the winds (from the south and south-east) together with the topographical effects of Point Roberts and Roberts Bank are thus conducive to the generation of longshore currents along both the Tsawwassen and causeway beaches.

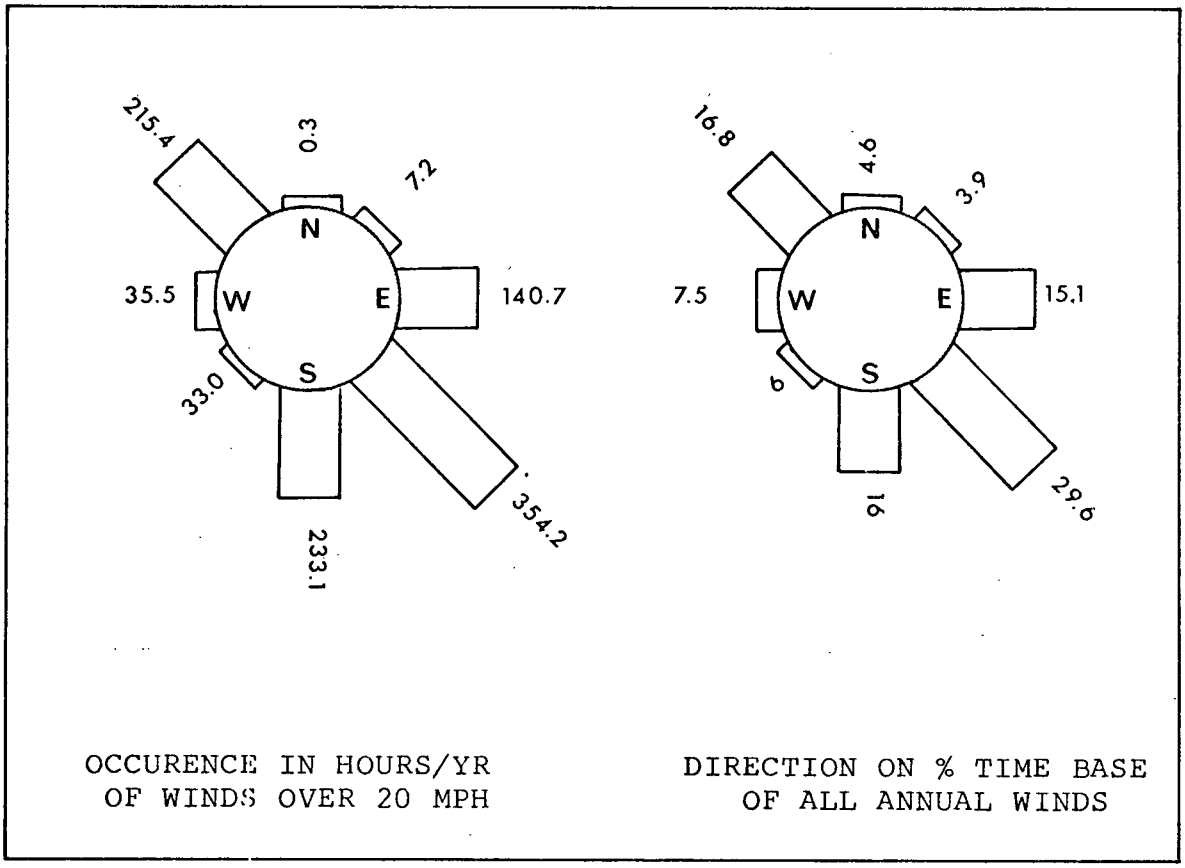

Figure 3. Wind characteristics at the Tsawwassen causeway (Wood, 1970) (Winds are from the direction shown.)

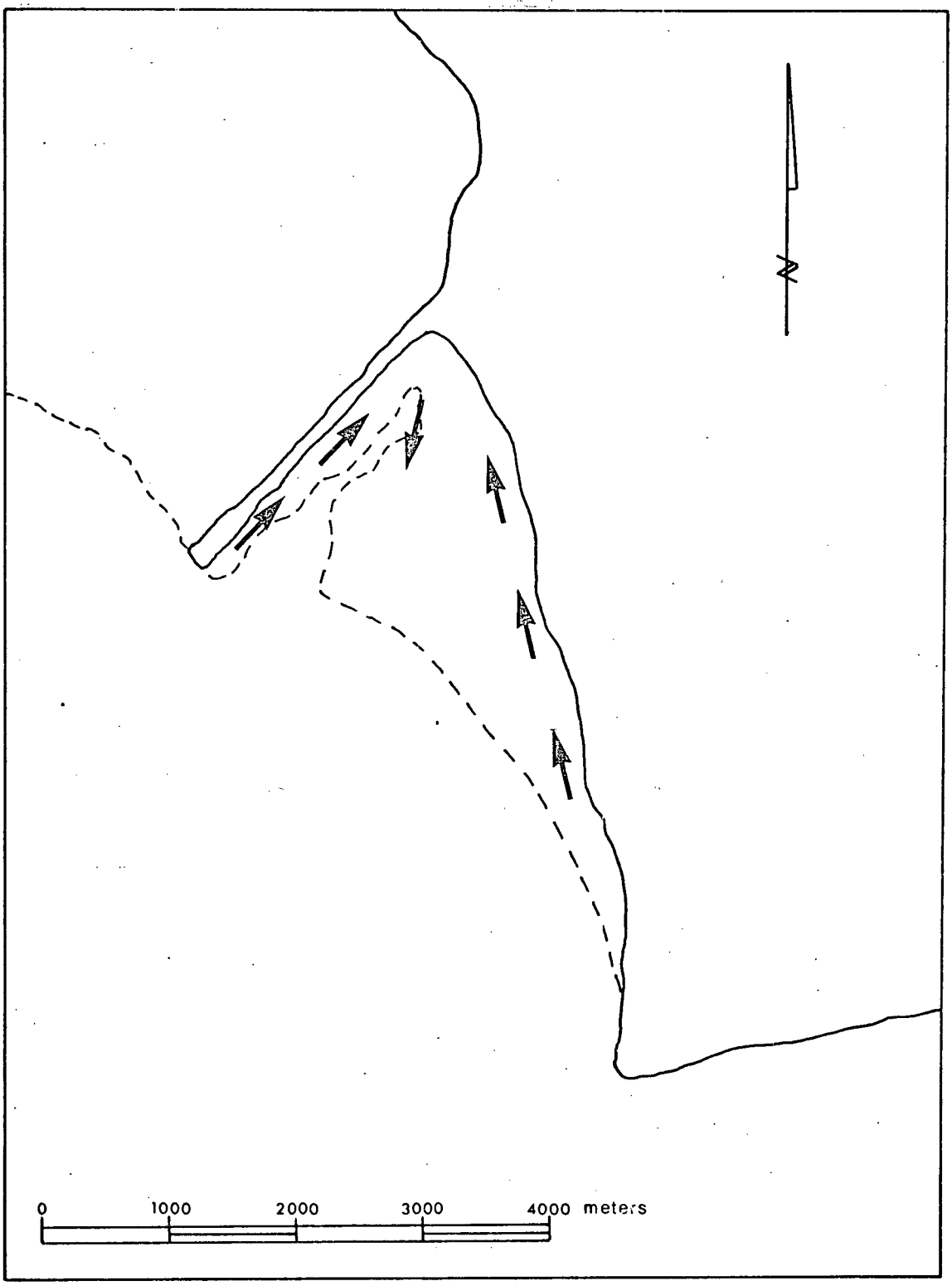

Figure 4. Speculative diagram of the wave-induced longshore current flow at the study site

IV Morphological Evidence of Longshore Currents

Since longshore movement of beach material is due almost entirely to longshore currents (Komar, 1976), let us now discuss the evidence for sediment transport along the Tsawwassen and causeway beaches as indicated by aerial photographs, inspection of groynes, etc.

Causeway Beach

Aerial photographs have shown the growth of two bulges in the beach on the south side of the causeway near the ferry terminal, with erosion between them, at times, threatening to undercut the highway as shown in Figure 5 (Hodge, 1970).

In a study conducted by Hodge in 1971, the region of the bulges was mapped and the movement of beach material measured. He concludes that "actual measurement quantitatively confirms the observed morphological changes - beach materials are moving along the causeway to the NNE," that is, toward the intersection apex.

Tsawwassen Beach

Although direct sand transport measurements along Tsawwassen Beach are unavailable, we can nevertheless indirectly evaluate the littoral drift by examining the shoreline configuration in the vicinity of several groynes built along the beach. The direction of the littoral drift during the immediately preceding period can be inferred from the entrapment of sand on either side of the groynes.

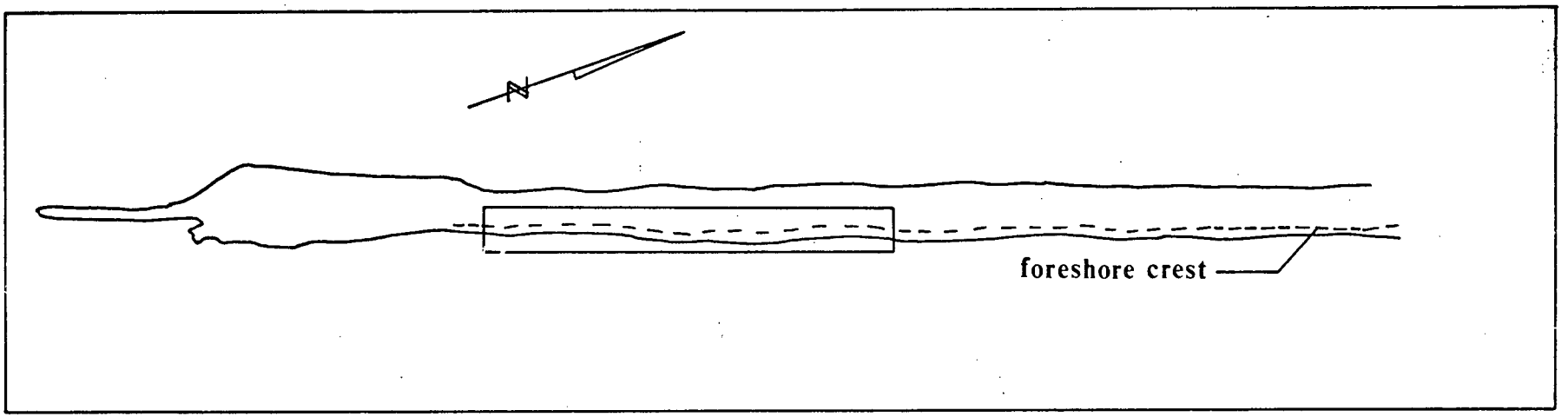

(a) May 18, 1963. (from Aerial Photograph BC 5073:38)

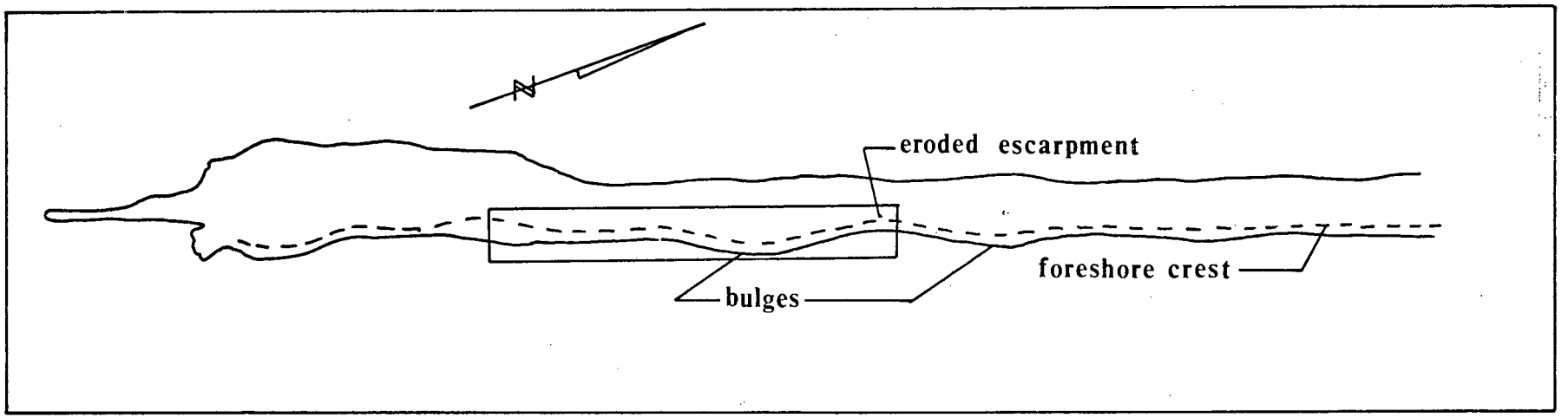

(b) May 31, 1970. (from Aerial Photograph BC 5371:108)

Figure 5. Air-photo comparison of the growth of "bulges" south-side Tsawwassen causeway. (Hodge, 1971)

Periodic inspection of these groynes has shown, that at all of them, there is a significant drop in beach level from south to north, indicative of a predominantly northern littoral drift and accompanying sediment transport toward the intersection apex of the two beaches. Of particular note is a groyne approximately 400 m. south of the causeway having a drop in cross-sectional elevation of 0.5 m. with characteristic depositon of beach sediment on its south (up-current) side and erosion to the north (down-current) side (see Figures 6 and 7).

In light of the evidence for sediment transport along both the beaches (toward the intersection apex) we should, quite reasonably, expect to find a build-up of beach materials in the corner. Field inspection of the corner shows it to be an area of stagnation, a gathering point of seaside debris - drift-wood, seaweed, etc. - while aerial photographs (taken in the years following construction of the causeway) clearly show the corner to be filling up (see Figures 8 and 9).

Morphological evidence is then consistent with earlier expectations based upon the nature of the prevailing winds together with local topographical effects that longshore currents are present in the study area and are responsible for the transport of beach materials along both the Tsawwassen and causeway beaches toward their intersection apex. Under conditions of high tides accompanied by winds from the southern quarter, we can reasonably expect a circulation pattern

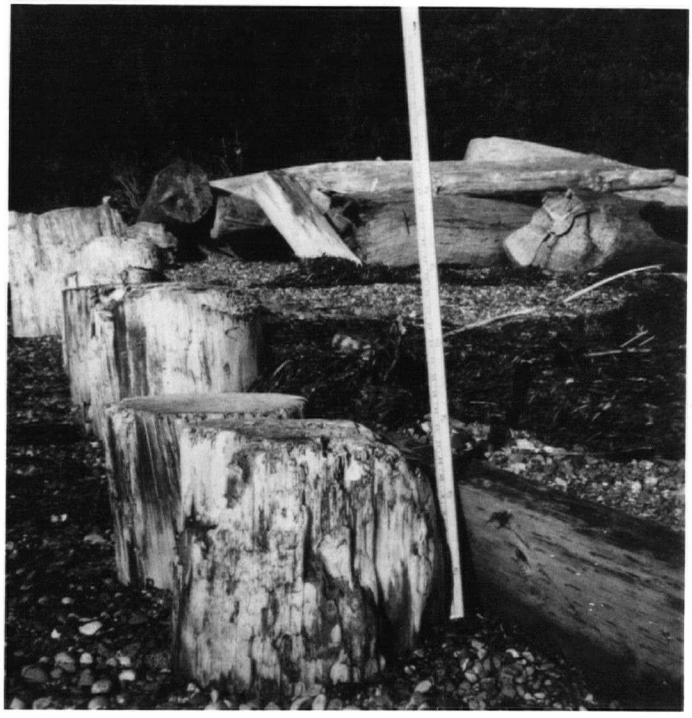

Figure 6. Shows a portion of a groyne on the Tsawwassen beach approximately 200 m. south of the causeway. A south to north (right to left) drop in beach elevation of approximately 0.25 m. is indicated.

Figure 7. Taken at a groyne on the Tsawwassen beach approximately 400 m. south of the causeway. It shows a drop in beach elevation from south to north (right to left) of approximately 0.5 m.

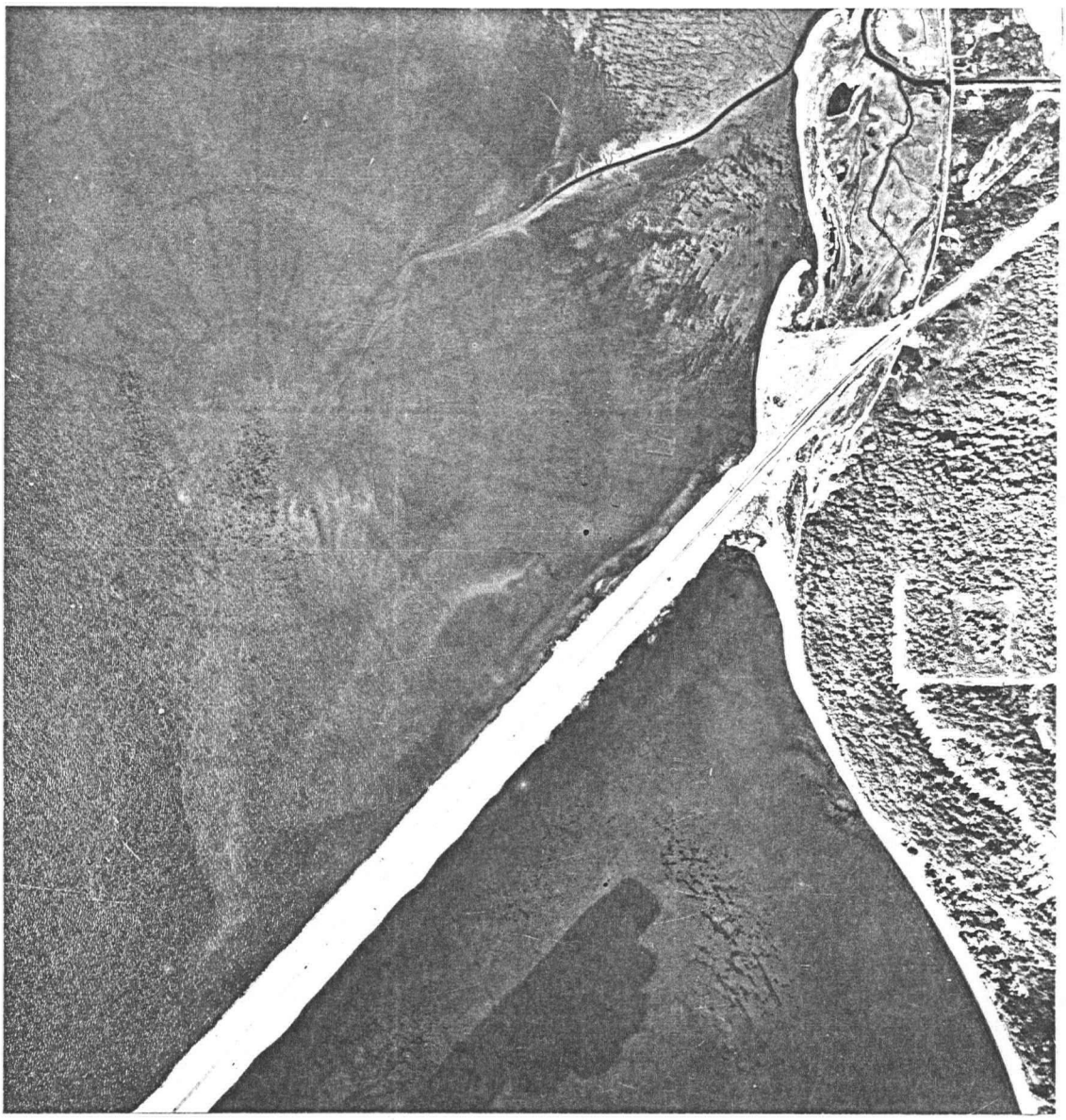

Figure 8. Aerial photograph of the intersection corner taken in 1963.

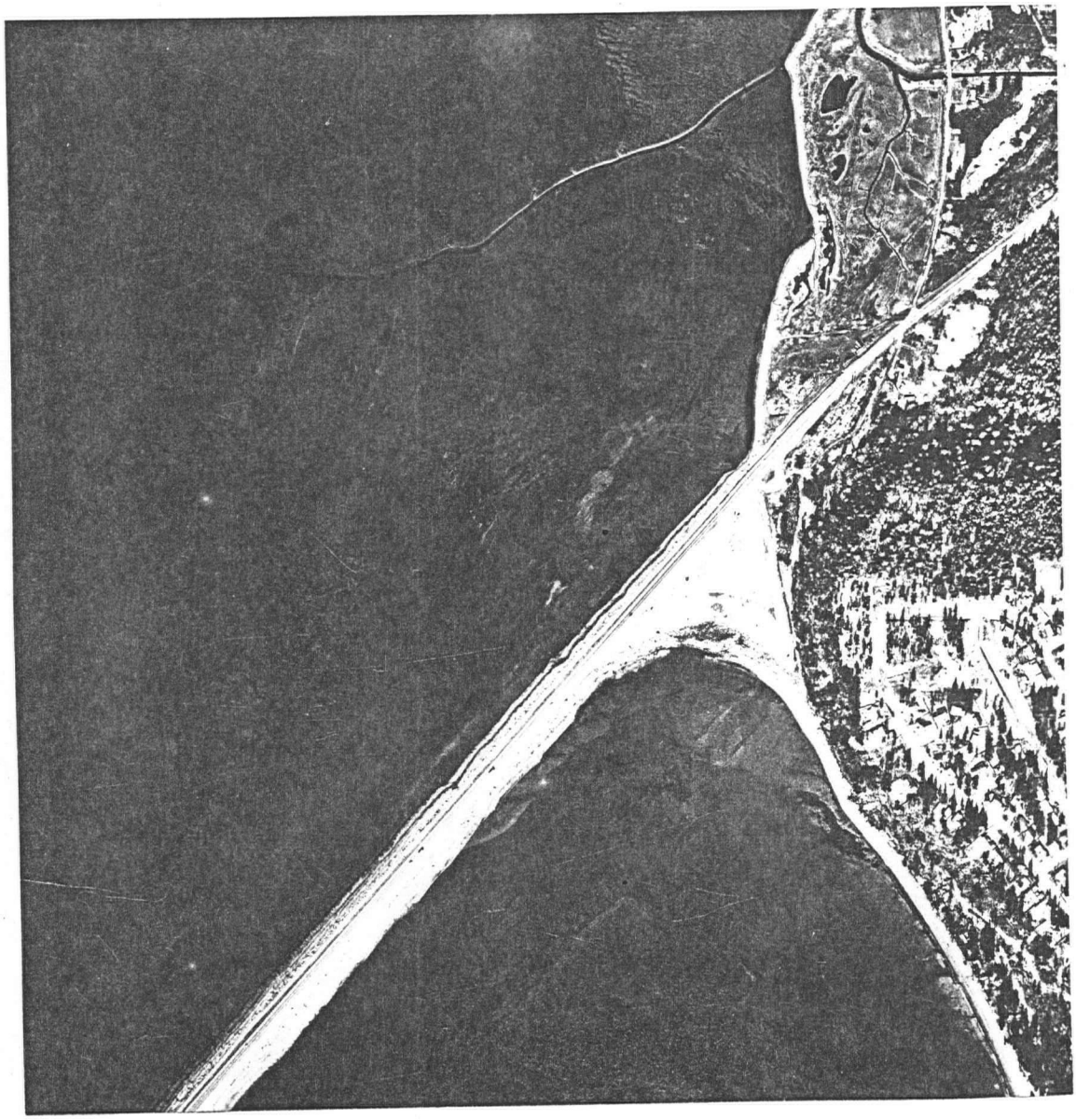

Figure 9. Aerial photograph of the intersection corner in 1975.

to develop consisting of longshore currents flowing along both the Tsawwassen and causeway beaches toward their common corner with some form of return flow out over Roberts Bank. It is this circulation pattern that we now wish to model.

We should, perhaps, make a note here with regards to the nature of the littoral processes at work at the Tsawwassen location. It is highly likely that a combination of very high tides together with stronger than normal winds acting over a relatively short period of time will do as much to alter the coastal configuration as will months of moderate winds in conjunction with normal high tides. Hence, the transport of sediments at the Tsawwassen site may be of a highly non-linear nature and should not be viewed as being solely the result of a continuous process.

CHAPTER 3

THEORY

I Review of the Theory of Longshore Currents

Before beginning the detailed analysis let us briefly review the mechanism by which wave-induced longshore currents are generated.

A longshore current is defined as the depth and time averaged total velocity in the longshore direction. It is observed to reach a maximum in the surfzone (James, 1972).

The mean wave-induced current is driven by the spatial variation of the radiation stress - which is the excess flow of momentum associated with a progressive or standing wave - a concept developed by Longuet-Higgins and Stewart (1964) and applied to longshore currents by Bowen (1969a). This extra "kinetic" pressure term in the presence of waves is due to the components of velocity corresponding to the orbital motion of wave particles - it is a quadratic non-linear quantity which arises from time averaging over the wave oscillation and integrating over the depth of the water. The subject has been reviewed recently by Miller and Barcilon (1976).

The momentum transfer that produces circulation (the spatial variation of the radiation stresses) is directly proportional to energy dissipation. If there were no dissipation there would be no currents, since it is the gradients of the radiation stress term which are responsible for the forcing.

These gradients will be balanced by set-up or set-down except when dissipation is present.

Bowen (1969a) and Longuet-Higgins (1970) both used first order sinusoidal (or 'Airy') waves as a basis for calculating momentum and energy fluxes in the near-shore region. On the basis of 1^{st} order theory and the assumption of negligible wave energy dissipation outside the surfzone there are no spatial variations in the radiation stress and therefore no driving outside the breaker-lines. Inside the surfzone, if the assumption is made that wave height is proportional to depth, there exist variations in the radiation stress across the surfzone and hence a driving force for the longshore current (Miller and Barcilon, 1976).

Under steady state conditions, the driving force must be balanced by friction. In shallow water, bottom friction is most important. However (James, 1972), lateral mixing also contributes and allows the longshore current to spread seawards of the surfzone.

In this chapter we shall derive the set of governing equations which are valid for a general beach with arbitrary bottom topography. Chapter 4 will be devoted to a discussion of some numerical models while in Chapter 5 we shall apply these equations to an analytical model.

II Formulation of the Problem

We shall begin our analysis with the mean momentum equations for a steady wave field as given by O'Rourke and LeBlond (1970).

$$U\frac{\partial U}{\partial x} + V\frac{\partial U}{\partial y} = -g\frac{\partial \tilde{\eta}}{\partial x} - \frac{1}{\rho d}\left\{\frac{\partial S_{xx}}{\partial x} + \frac{\partial S_{yx}}{\partial y}\right\} - \frac{fU}{\rho d} \qquad (3.1)$$

$$U\frac{\partial V}{\partial x} + V\frac{\partial V}{\partial y} = -g\frac{\partial \tilde{\eta}}{\partial y} - \frac{1}{\rho d}\left\{\frac{\partial S_{xy}}{\partial x} + \frac{\partial S_{yy}}{\partial y}\right\} - \frac{fV}{\rho d} \qquad (3.2)$$

where;

d is the total water depth equal to the sum of the local still water depth h, and the mean displacement of the water surface from the still water level, $\tilde{\eta}$;
thus $d = h + \tilde{\eta}$

$f = \frac{2\rho C}{\pi} u_{max}$
with C a drag coefficient of $O(10^{-2})$

ρ is the water density

$u_{max} = \gamma(gh_f)^{\frac{1}{2}}$, with $0.3 < \gamma < 0.6$

h_f, a characteristic depth (Longuet-Higgins, 1970, Part 1)

g is the acceleration due to gravity

U, V are the mean velocity components in the longshore (x) and offshore (y) directions respectively. They include the mean current as well as the mass transport of the waves and are assumed to be depth independent.

The radiation stress terms for a train of monochromatic small amplitude waves of amplitude a and wave number k, propagating over a nearly flat bottom are given by

$$S_{xx} = \frac{E}{2}(2n-1) + En\cos^2\phi$$
$$S_{xy} = S_{yx} = \frac{En}{2}\sin^2\phi \qquad (3.3)$$
$$S_{yy} = \frac{E}{2}(2n-1) + En\sin^2\phi$$

where; $E = \frac{1}{2}\rho g a^2$

$$n = \frac{1}{2}\left(1 + \frac{2kh}{\sinh(2kh)}\right)$$

ϕ is the angle of incidence relative to the normal to the shore-line

Note, that as a means of simplifying the analysis we shall ignore horizontal eddy viscosity, the effects of which (with respect to the profile of a longshore current along an infinite beach) have been discussed by Longuet-Higgins (1970, Part 2).

In shallow water and for small angles of incidence the radiation stress terms reduce to (Longuet-Higgins and Stewart, 1964)

$$S_{xx} = \frac{3}{4}\rho g a^2$$
$$S_{xy} = S_{yx} = \frac{1}{2}\rho g a^2 \sin\phi \qquad (3.4)$$
$$S_{yy} = \frac{1}{4}\rho g a^2$$

The vertically integrated continuity equation is expressed as

$$\frac{\partial U}{\partial x}(h+\tilde{\eta}) + \frac{\partial V}{\partial y}(h+\tilde{\eta}) = -\frac{\partial \tilde{\eta}}{\partial t} \tag{3.5}$$

Let us define the vectors $\underset{\sim}{T}$ and $\underset{\sim}{F}$ such that (O'Rourke and LeBlond, 1970)

$$T_1 = \frac{1}{\rho d}\left\{\frac{\partial S_{xx}}{\partial x} + \frac{\partial S_{yx}}{\partial y}\right\} \tag{3.6}$$

$$T_2 = \frac{1}{\rho d}\left\{\frac{\partial S_{xy}}{\partial x} + \frac{\partial S_{yy}}{\partial y}\right\}$$

$$F_1' = -\frac{\rho U}{\rho d} \quad ; \quad F_2' = -\frac{\rho V}{\rho d}$$

Substituting these into equations (3.1) and (3.2) we get

$$U\frac{\partial U}{\partial x} + V\frac{\partial U}{\partial y} + T_1 = -g\frac{\partial \tilde{\eta}}{\partial x} + F_1' \tag{3.7}$$

$$U\frac{\partial V}{\partial x} + V\frac{\partial V}{\partial y} + T_2 = -g\frac{\partial \tilde{\eta}}{\partial y} + F_2' \tag{3.8}$$

along with the steady state continuity equation

$$\frac{\partial U}{\partial x}(h+\eta) + \frac{\partial V}{\partial y}(h+\tilde{\eta}) = 0 \tag{3.9}$$

Writing them in vector notation, the momentum equations take the form

$$(\underset{\sim}{U}\cdot\nabla)\underset{\sim}{U} + \underset{\sim}{T} = -g\nabla\eta + \underset{\sim}{F}' \tag{3.10}$$

We can eliminate the term in $\underset{\sim}{\eta}$ by taking the curl of equation (3.10), to get

$$-\nabla \times (\underset{\sim}{U} \cdot \nabla) \underset{\sim}{U} + \nabla \times \underset{\sim}{T} = \nabla \times \underset{\sim}{F} \qquad (3.11)$$

As a further simplification of the analysis we shall now neglect the remaining non-linear terms in equation (3.11), on the basis of work done by Arthur (1962), who showed their effects to be a narrowing of off-shore flows and a widening of on-shore flows. Thus, while the non-linear terms affect the details of the currents we trust that their absence will not greatly affect their general form and will allow us to obtain an analytic solution.

Equation (3.11) then becomes

$$\nabla \times \underset{\sim}{T} = \nabla \times \underset{\sim}{F} \qquad (3.12)$$

In the seaward zone (where there is no energy dissipation and hence no spatial variation of the radiation stress), the driving torques vanish and (3.12) reduces to

$$\nabla \times \underset{\sim}{F} = 0 \qquad (3.13)$$

In the surfzone, where there is a dynamic balance between the drive due to wave stress and the retarding effect of bottom friction we have

$$\nabla \times \underset{\sim}{T} = \nabla \times \underset{\sim}{F} \tag{3.14}$$

Let us now define a transport stream function $\psi(x,y)$ from the steady state continuity equation (3.9) such that

$$U = \frac{1}{(h+\tilde{\eta})} \frac{\partial \psi}{\partial y} \tag{3.15}$$

$$V = -\frac{1}{(h+\tilde{\eta})} \frac{\partial \psi}{\partial x}$$

Substituting these into equations (3.13) and (3.14) the governing equation in the seaward zone becomes

$$\frac{\partial^2 \psi}{\partial x^2} + \frac{\partial^2 \psi}{\partial y^2} - \frac{2}{d}\left(\frac{\partial d}{\partial x}\frac{\partial \psi}{\partial x} + \frac{\partial d}{\partial y}\frac{\partial \psi}{\partial y}\right) = 0 \tag{3.16}$$

while in the surfzone we get

$$\frac{\partial}{\partial x}\left[\frac{1}{\rho d}\left(\frac{\partial S_{xy}}{\partial x} + \frac{\partial S_{yy}}{\partial y}\right)\right] - \frac{\partial}{\partial y}\left[\frac{1}{\rho d}\left(\frac{\partial S_{xx}}{\partial x} + \frac{\partial S_{xy}}{\partial y}\right)\right] \tag{3.17}$$

$$= -\frac{f}{\rho d}\left[\frac{\partial^2 \psi}{\partial x^2} + \frac{\partial^2 \psi}{\partial y^2} - \frac{2}{d}\left(\frac{\partial d}{\partial x}\frac{\partial \psi}{\partial x} + \frac{\partial d}{\partial y}\frac{\partial \psi}{\partial y}\right)\right]$$

We have now to solve equations (3.16) and (3.17) subject to the topographic characteristics and boundary conditions

relevant to our particular problem (as will be discussed in Chapter 4), but first let us comment on some of the assumptions made in arriving at these equations. (For a full summary of approximations see Appendix A).

1/ The use of a bottom shear stress linearized in the longshore current velocity (see equations (3.1) and (3.2)) is justifiable if this is small compared with the wave orbital velocity, which as James (1972) points out is not always true. In the presence of steady flow or long period waves, a reasonable assumption appears to be that the bottom shear stress be given by (James, 1972)

$$\tau = C\rho |\underset{\sim}{u}_o| \underset{\sim}{u}_o \qquad (3.18)$$

where; u_o is the instantaneous total velocity vector just outside the bottom boundary layer

C is a dimensionless coefficient whose magnitude may be increased by the presence of oscillatory flow.

We shall consider the use of this friction term in connection with the numerical models as discussed in Chapter 4. A recent extension to strong mean currents has been presented by Liu and Dalrymple (1978).

2/ We have neglected to include a horizontal eddy viscosity term (whose effect is to transfer momentum from the surfzone, where the driving of the longshore current

takes place, across the breaker-line where there is no driving) since such friction terms lead to a 4^{th} order equation when a stream function is introduced (whereas the linearized friction terms lead only to a 2^{nd} order equation) (Miller and Barcilon, 1976).

3/ The remaining non-linear terms in equation (3.11) have been neglected on the basis of work done by Arthur (1962) who showed that they play no causative role in the dynamics of the currents although they may affect their local characteristics.

The balance in the linear equations is then taken to be between the radiation stress terms, the pressure gradient (set-up) and the bottom friction terms.

CHAPTER 4

NUMERICAL MODELLING

I Introduction

This chapter is devoted to the discussion of several numerical models of the wave-induced circulation in a beach-breakwater configuration similar to that of the Tsawwassen site. A numerical approach will give us greater flexibility in choosing beach configurations and bottom topography (such as a trench and drop-off to deeper water) than an analytical approach (to be discussed in Chapter 5) and also allows the comparison of models using different forms (linear and non-linear) bottom friction.

II Model Layout

Each numerical model shall consist of two beaches of finite length intersecting at some angle δ ($0° < \delta \leq 90°$) enclosed within a rectangular basin (the walls of which have been put as far away as is practical so as to limit their effect upon the current circulation) as shown in Figure 10.

The seaward zone has been divided into three regions consisting of two surfzones and an off-shore zone beyond the breaker-lines.

The extent of the surfzones, the regions over which the longshore shear stresses exist, are subject to wave height changes at the breaker-lines. As discussed by O'Rourke and LeBlond (1970), accurate determination of the

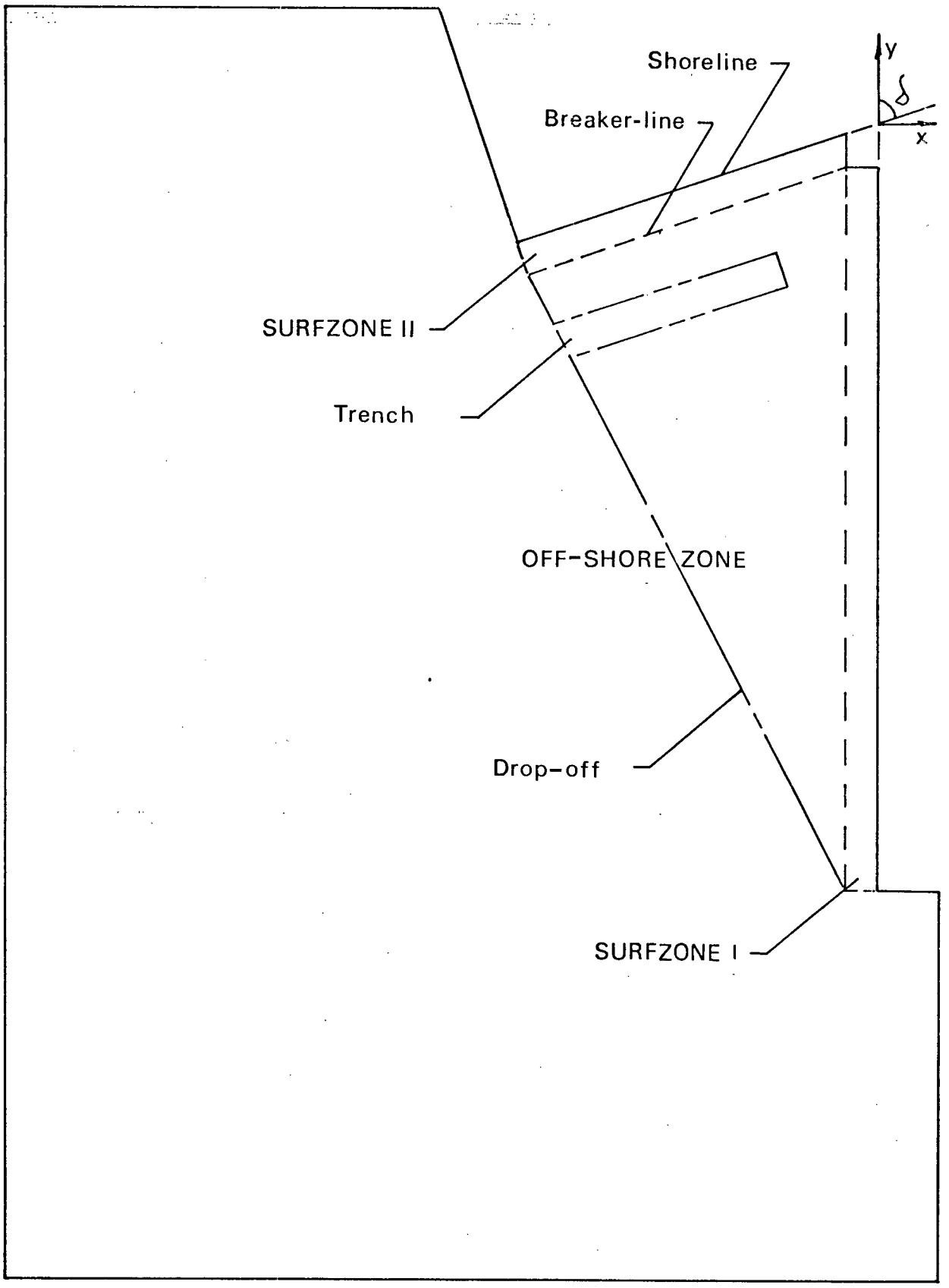

Figure 10. Plan view of the numerical model geometry

position of the shore and breaker-lines would lead to tedious matching problems at these boundaries which would do little to alter the overall current patterns. Hence the boundaries of the surfzones shall be taken as the space-averaged values of the shore and breaker-lines. To conform to the Tsawwassen configuration the natural beach shall be approximately twice as long as that corresponding to the causeway.

The ratios of surfzone length to width, in the models, are 10:1 and 20:1 for the causeway and natural beach respectively. The models presented as such exhibit a discrepancy with respect to scale, when compared directly to field dimensions, since they then yield highly unrealistic surfzone widths of approximately 300 m. Attempts to present models which are scaled more realistically would, however, due to restrictions of space, result in surfzones of negligible width. The models then strike a compromise, allowing us to study the currents in a configuration for which the surfzones are much longer than they are wide yet still retain some degree of detail.

Note that we have removed the surfzones' intersection corner to ease the specification of the boundary conditions there, the rationalization being that if the surfzone widths are sufficiently small in comparison to their lengths, then removing the corner will have little effect upon the major features of the current circulation, an assumption which shall be justified a posteriori.

The off-shore zone shall accomodate variations in bottom topography in the following manner. Immediately seaward of the breaker-lines is a shallow shelf region which in some models fills the remainder of the basin. In other models the off-shore zone is further sub-divided (see Figure 10) to incorporate a much deeper region beyond the shelf-zone typical of the drop-off into Georgia Strait found at the Tsawwassen loction; while still others will include a submarine trench running parallel to the causeway across the width of the shelf-zone. We shall thus have an opportunity to study the effects of these variations in bottom topography upon the wave-induced circulation.

Let us first consider the configuration shown in Figure 11, for which the beach intersection angle is 90°.

We shall assume surfzone I to be approximately uniform in the y-direction so that

$$d_1(x,y) = h_1(x) + \eta_1(x,y) \sim h_1(x) \tag{4.1}$$

that is

$$\frac{\partial d_1}{\partial y} \sim 0 \tag{4.2}$$

The slope $m_{1)}$ in this region shall be defined by

$$m_1 x = d_1 \tag{4.3}$$

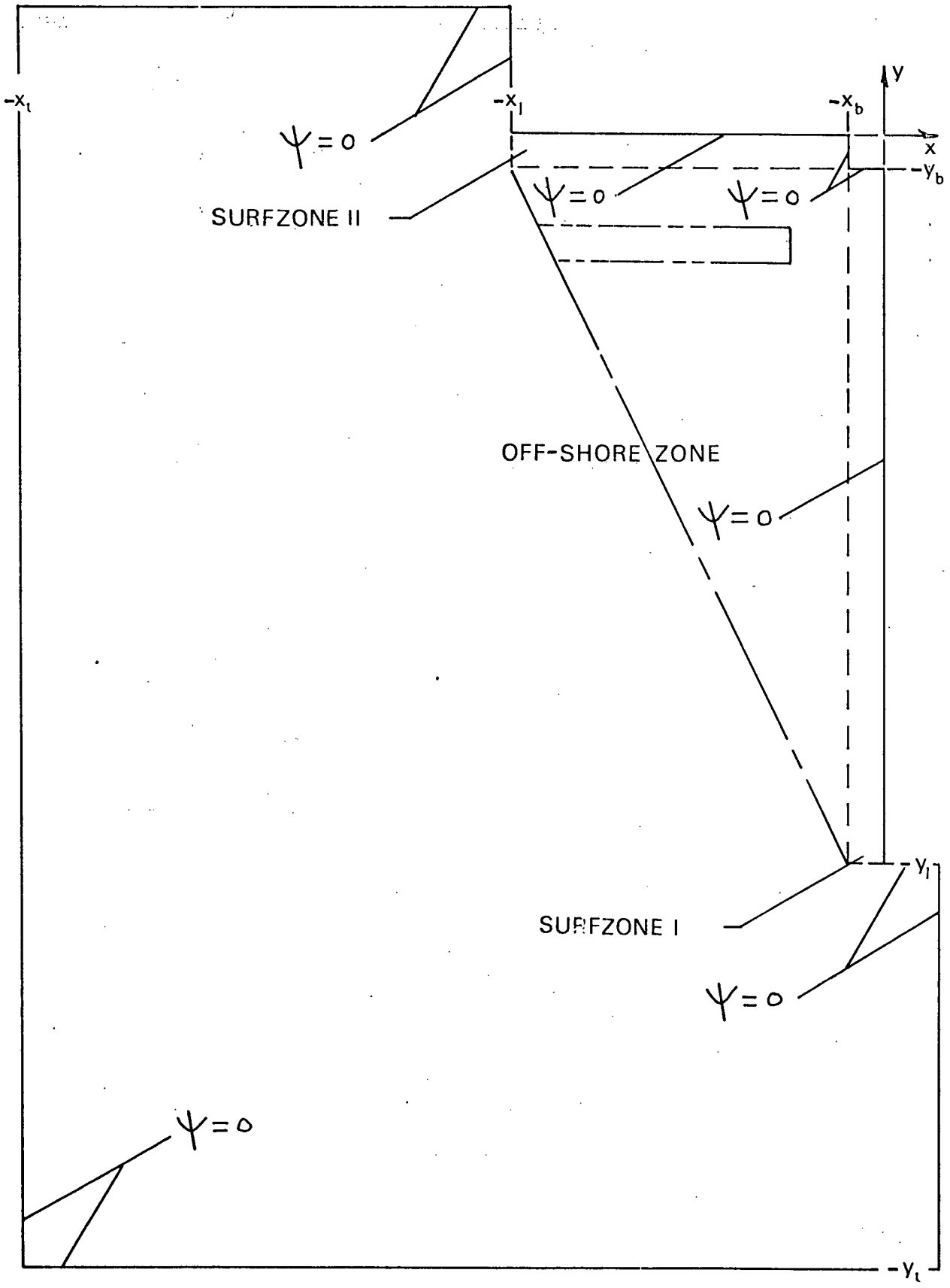

Figure 11. Boundary conditions for the particular case of a perpendicular beach intersection.

Similarly, we shall assume surfzone II to be approximately uniform in the x-direction, which gives us

$$d_2(x,y) = h_2(y) + \eta_2(x,y) \tag{4.4}$$

$$\sim h_2(y)$$

so that

$$\frac{\partial d_2}{\partial x} \sim 0 \tag{4.5}$$

The slope m_2, in this region shall be defined by

$$m_2 y = d_2 \tag{4.6}$$

Subject to the above approximations the governing equations (3.10) and (3.17) for the surfzones and off-shore zone become

1. Surfzone I

$$-\frac{1}{\rho d_1^2}\left[\frac{\partial p_1}{\partial x}\left\{\frac{\partial S_{xy}}{\partial x}+\frac{\partial S_{yy}}{\partial y}\right\}\right] \tag{4.7}$$

$$+\frac{1}{\rho d_1}\left[\left(\frac{\partial^2}{\partial x^2}-\frac{\partial^2}{\partial y^2}\right)S_{xy}+\frac{\partial^2}{\partial x \partial y}\left(S_{yy}-S_{xx}\right)\right]$$

$$=-\frac{f}{\rho d_1^2}\left[\frac{\partial^2 \psi}{\partial x^2}+\frac{\partial^2 \psi}{\partial y^2}-\frac{2}{d_1}\frac{\partial p_1}{\partial x}\frac{\partial \psi}{\partial x}\right]$$

2. Surfzone II

$$\frac{1}{\rho d_2^2}\left[\frac{\partial d_2}{\partial y}\left\{\frac{\partial S_{xx}}{\partial x}+\frac{\partial S_{xy}}{\partial y}\right\}\right] \tag{4.8}$$

$$+\frac{1}{\rho d_2}\left[\left(\frac{\partial^2}{\partial x^2}-\frac{\partial^2}{\partial y^2}\right)S_{xy}+\frac{\partial^2}{\partial x\partial y}\left(S_{yy}-S_{xx}\right)\right]$$

$$=-\frac{f}{\rho d_2^2}\left[\frac{\partial^2\psi}{\partial x^2}+\frac{\partial^2\psi}{\partial y^2}-\frac{2}{d_2}\frac{\partial d_2}{\partial y}\frac{\partial\psi}{\partial y}\right]$$

3. Off-shore zone

$$\psi_{xx}+\psi_{yy}-\frac{2}{d_3}\frac{\partial d_3}{\partial x}\frac{\partial\psi}{\partial x}-\frac{2}{d_3}\frac{\partial d_3}{\partial y}\frac{\partial\psi}{\partial y}=0 \tag{4.9}$$

Consider now equation (4.7), the governing equation for surfzone I, into which we shall substitute the expressions for the radiation stress terms (equations (3.4)), to get

$$-\frac{ga_1}{\partial d_1^2}\left[\frac{\partial d_1}{\partial x}\left\{2\cdot\frac{\partial a_1}{\partial x}\sin\beta+\frac{\partial a_1}{\partial y}\right\}\right]+\frac{g}{\partial d_1}\left[2\sin\beta\left\{\left(\frac{\partial a_1}{\partial y}\right)^2\right.\right. \tag{4.10}$$

$$\left.\left.-\left(\frac{\partial a_1}{\partial x}\right)^2+a_1\left(\frac{\partial^2 a_1}{\partial x^2}-\frac{\partial^2 a_1}{\partial x^2}\right)\right\}+\left\{\frac{\partial a_1}{\partial x}\frac{\partial a_1}{\partial y}+a_1\frac{\partial^2 a_1}{\partial x\partial y}\right\}\right]$$

$$=-\frac{f}{\rho d_1^2}\left[\psi_{xx}+\psi_{yy}-\frac{2}{d_1}\frac{\partial d_1}{\partial x}\frac{\partial\psi}{\partial x}\right]$$

Taking the wave amplitude in the surfzone to be proportional to the mean water depth (Munk, 1949) so that

$$a_1 = \gamma d_1 \tag{4.11}$$

gives us

$$\frac{\partial a_1}{\partial y} = \gamma \frac{\partial d_1}{\partial y} \sim 0 \tag{4.12}$$

and

$$\frac{\partial a_1}{\partial x} = \gamma \frac{\partial d_1}{\partial x} \tag{4.13}$$

so that equation (4.10) reduces to

$$-g\gamma^2 \sin\beta \left[\frac{2}{d_1}\left(\frac{\partial d_1}{\partial x}\right)^2 + \frac{\partial^2 d_1}{\partial x^2} \right] = -\frac{f}{\rho d_1^2}\left[\psi_{xx} + \psi_{yy} - \frac{2}{d_1}\frac{\partial d_1}{\partial x}\frac{\partial \psi}{\partial x} \right] \tag{4.14}$$

or

$$\psi_{xx} - \frac{2}{x}\psi_x + \psi_{yy} = \frac{2\rho d_1 g \gamma^2 \sin\beta \omega_1^2}{f} \tag{4.15}$$

Assuming that Snell's law of refraction holds in the surfzone (Longuet-Higgins, 1956) so that

$$\frac{\sin\beta_1}{\sqrt{g d_1}} = \frac{\sin\beta_0}{\sqrt{g d_0}} = \frac{\sin\beta_0}{C_0} \tag{4.16}$$

(where β_o and d_o are the angle of incidence and the depth at the breaker-line) equation (4.15) for surfzone I becomes;

$$\psi_{xx} - \frac{2}{x}\psi_x + \psi_{yy} = \left[2\rho g^{3/2} \gamma^2 m_1^{7/2} \frac{\sin\beta_o}{fC_o} \right] x^{3/2} \qquad (4.17)$$

$$= K_1 x^{3/2}$$

Similarly for surfzone II we get

$$\psi_{xx} - \frac{2}{y}\psi_y + \psi_{yy} = -\left[2\rho g^{3/2} \gamma^2 m_2^{7/2} \frac{\sin\theta_o}{fC_o} \right] y^{3/2} \qquad (4.18)$$

$$= -K_2 y^{3/2}$$

In summary then, the governing equations for the three zones of our numerical model are

1. Surfzone I

$$\psi_{xx} - \frac{2}{x}\psi_x + \psi_{yy} = K_1 x^{3/2} \qquad (4.19)$$

2. Surfzone II

$$\psi_{xx} - \frac{2}{y}\psi_y + \psi_{yy} = -K_2 y^{3/2} \qquad (4.20)$$

3. Off-shore zone

$$\psi_{xx} + \psi_{yy} - \frac{2}{d}\frac{\partial d}{\partial x}\frac{\partial \psi}{\partial x} - \frac{2}{d}\frac{\partial d}{\partial y}\frac{\partial \psi}{\partial y} = 0 \qquad (4.21)$$

The values of the stream function, in each model, shall be calculated from these governing differential equations by the Gauss-Seidel iterative technique (as discussed in Appendix B) subject to the constraint that the stream function is identically zero along the shore-line, the seaward edges of the intersection corner and the boundaries of the seaward zone as shown in Figure 11.

III A Simple Configuration

The first model we shall present is shown in Figure 12, and shall serve to illustrate those properties common to all the models. This configuration shows a perpendicular beach-breakwater intersection with no off-shore depth variations and currents of equal strength. Models incorporating features which conform more closely to the field site will follow.

Illustrated in Figure 12 is the entire field of according to equations (4.19), (4.20) and (4.21). In steady flow, the streamlines are equivalent to the pathlines of the fluid particles.

Note, that in order to avoid cluttering the current circulation diagrams, the breaker-lines and drop-off will not be shown. Their positions may be determined by referring to Figure 10 - the breaker-lines originate in the intersection corner and run parallel to the shore-lines for the length of the surfzones while, as will be seen, the location of the drop-off, in those models incorporating it, will be apparent. The position of the off-shore trench, when present, will always be indicated.

The circulation pattern consists of two counter-rotating cells, each cell driven by one of the wave-induced currents generated in the surfzones. The streamlines of the longshore currents converge toward the intersection apex where they merge to form a rip current which then flows out over the shelf region. Having travelled a distance across the shelf,

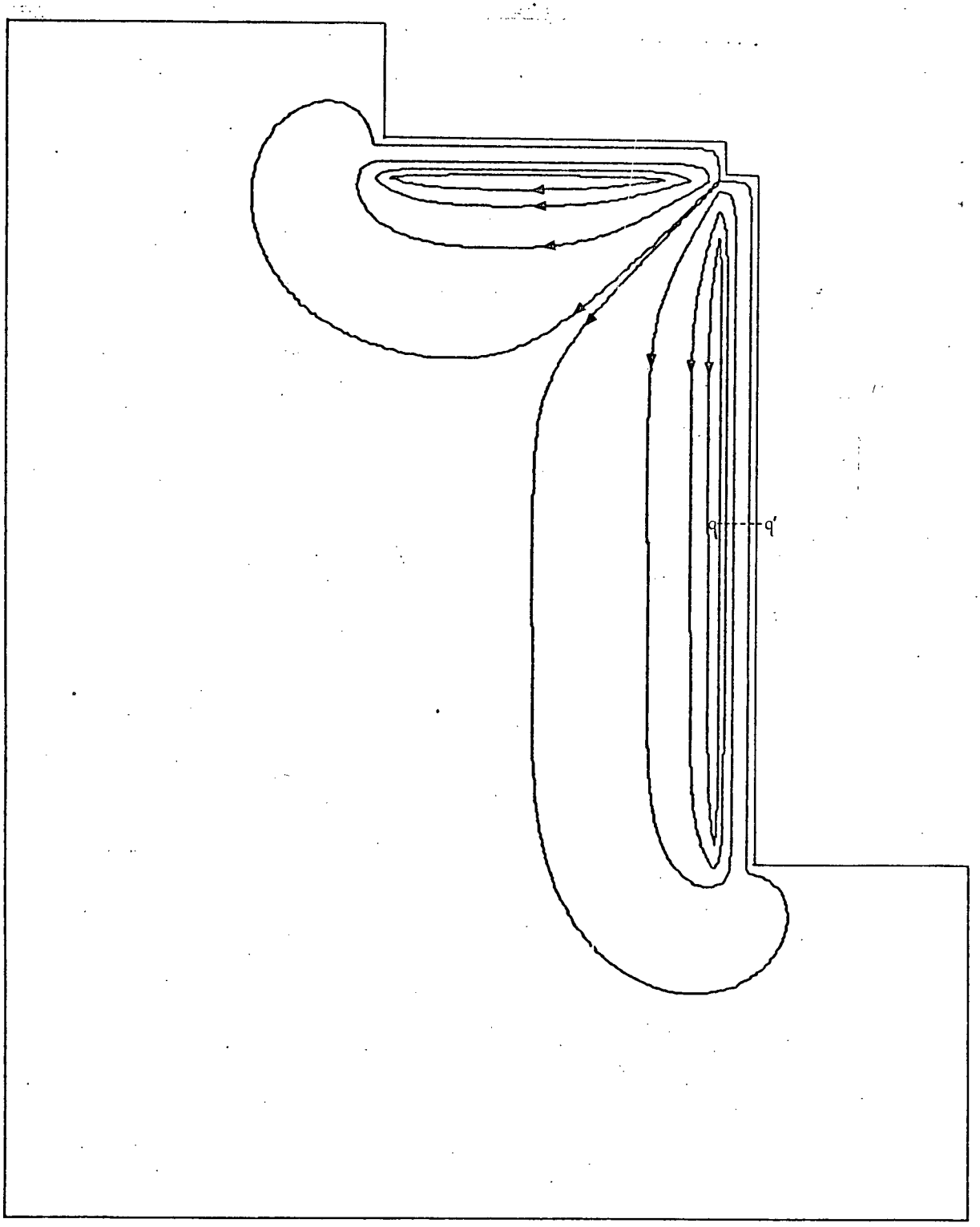

Figure 12. Current circulation for perpendicular beach intersection, equal current strengths and no off-shore depth variations.

the return flow must divide - each branch turning to complete its cell - due to continuity.

The qualitative aspects of the circulation pattern are then consistent with observations and measurements of sediment transport taken at the Tsawwassen site. The longshore currents flowing toward the intersection apex are conducive to sediment transport toward the corner, as was found at the field site, with the off-shore return flow now predicted to take the form of a rip current.

The effect of the convective inertial terms which we neglected in Chapter 3 will be to strengthen the return flow as it comes out of the corner because the current there is flowing into deeper water, and to weaken the currents which feed back into the ends of the surfzones since the flow there is into shallower water.

The exclusion of horizontal eddy viscosity (that is, lateral mixing) in the governing equations generally leads to the velocity being greater inside the surfzones and falling off more rapidly seaward of the breaker-lines than experimental results indicate (James, 1972). To include horizontal eddy viscosity in the equations would

i/ alter the surfzone velocity profiles so as to decrease the velocity maxima near the breaker-lines and increase the velocity at points closer to the shore, that is, to effectively flatten the profiles, and

ii/ result in the velocity outside the surfzones falling off less sharply than linear theory, with only bottom friction, predicts.

IV The Corner Geometry

In section II of this chapter we discussed the need to remove the intersection corner in order to ease the specification of the boundary conditions there, and justified it on the grounds that if the widths of the surfzones were sufficiently small in comparison to their lengths then removing the corner would have little effect upon the overall circulation. Figure 13 shows a model configuration identical to that of Figure 12 with the exception that the corner has now been included. The assumption has been made that the zero-valued stream line would emerge from the corner at the same angle at which it crosses the shelf zone (as shown in Figure 12), hence we have specified the boundary condition in the corner accordingly - that the stream function must be identically zero along the line bisecting the intersection angle (for the case of equal current strengths). The results, as shown in Figure 13, justify the arguments for removing the corner since the effect on the overall flow pattern is indeed negligible. Note also that Figure 13 shows a stagnation point in the corner thus indicating a possible location for the deposition of beach materials (which have been carried along the surfzones by the longshore currents). This is again consistent with observations at the Tsawwassen location which show the corner to be filling up.

A normalized streamline profile taken half-way along the breakwater surfzone of Figure 12 is shown in Figure 14,

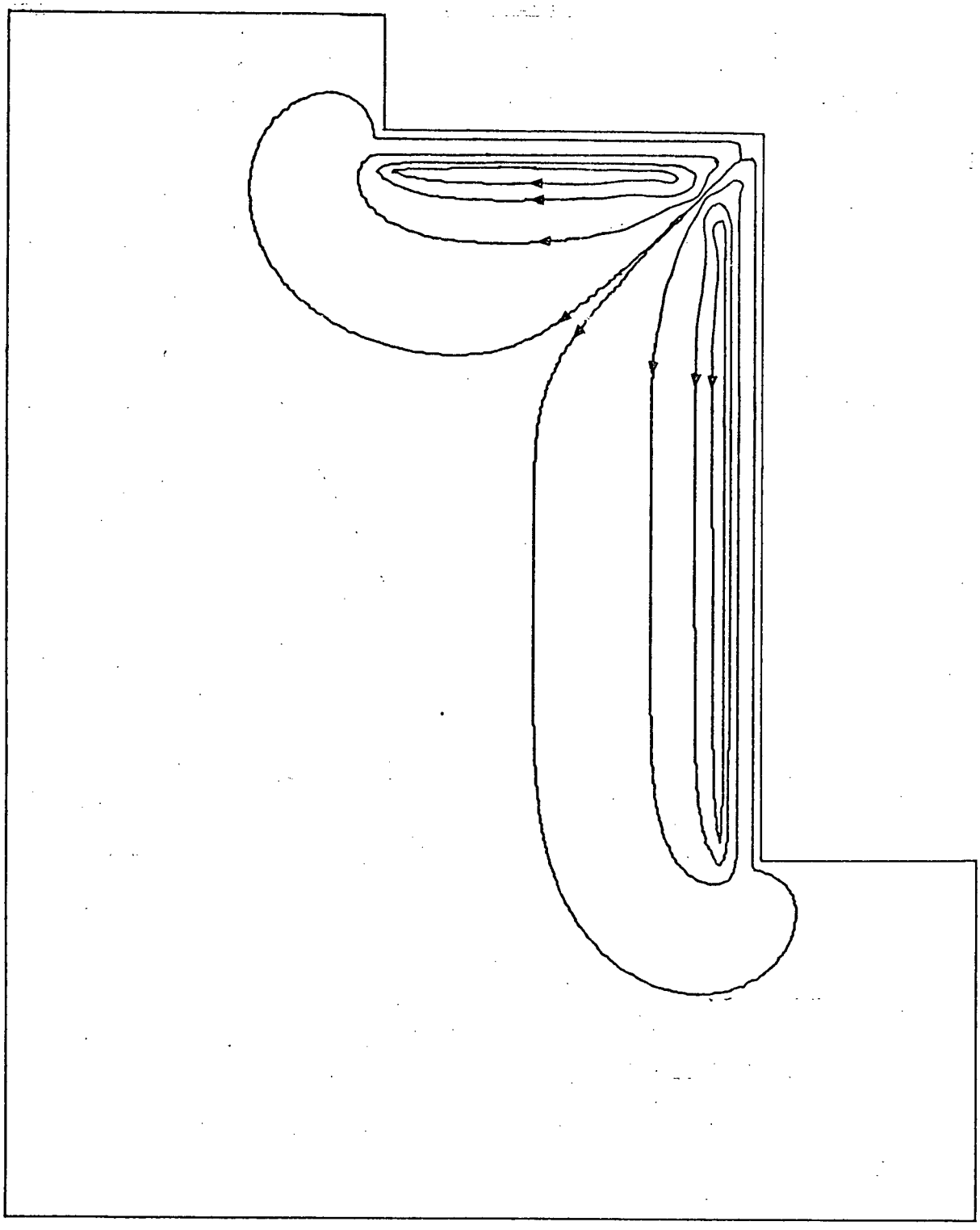

Figure 13. Perpendicular beach intersection model with the corner replaced. (The small 'corner' appearing in the streamline pattern is a numerical artifact.)

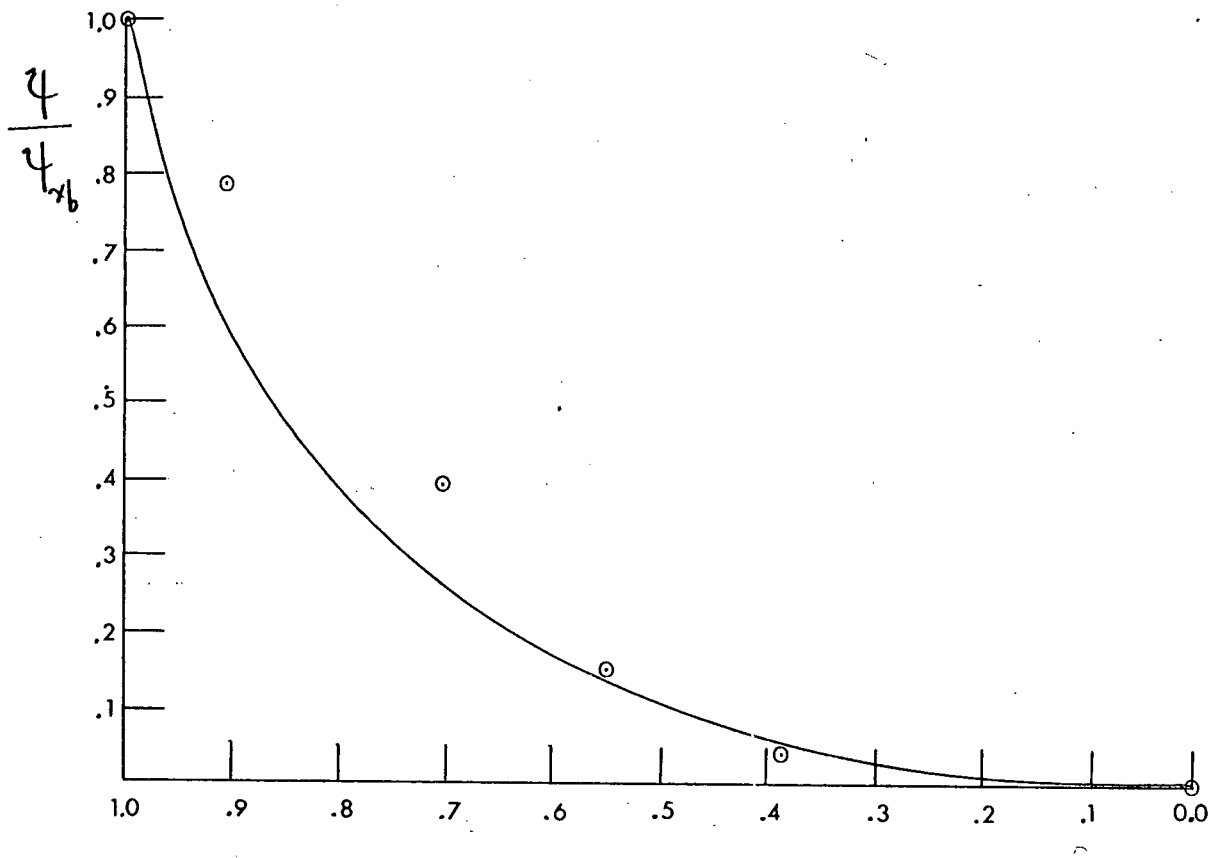

Figure 14. Normalized streamline profile taken across the surfzone along cross-section qq' in Figure 12 (shown as a solid line), together with that of an infinite beach model from Dalrymple et al (1977) (shown as ⊙): where ψ_{xb} is the value of the stream function at the breaker-line, the width of which is x_b.

together with that for the infinite beach model developed by Dalrymple et al (1977). They compare very closely, the longshore current profile half-way along the breakwater surfzone approaching that of an infinite beach.

V Acute Intersection Angle

To conform more closely to the configuration at the Tsawwassen site, the beach-breakwater intersection angle must be reduced to approximately 60° as has been done in Figure 15, which shows the circulatory system for equal current strengths and no variations in off-shore bottom topography. The general features are similar to those of the 90° beach intersection model: the cross-surfzone streamline profile is unchanged and the off-shore return flow again bisects the beach intersection angle. (The 'steps' in the streamlines adjacent to the natural beach are a computational artifact caused by the fact that, in the acute angle models, the natural beach runs diagonally to the (finitely spaced) grid lattice used in the numerical models).

The effects of varying current strength (due perhaps to relative differences in angle of wave incidence at the breaker-lines, beach slopes, surfzone widths etc., or combinations thereof) are shown in Figures 16 and 17. We shall not specify the exact values of factors necessary to account for the variations in relative current strength but merely present the results for ratios of natural beach

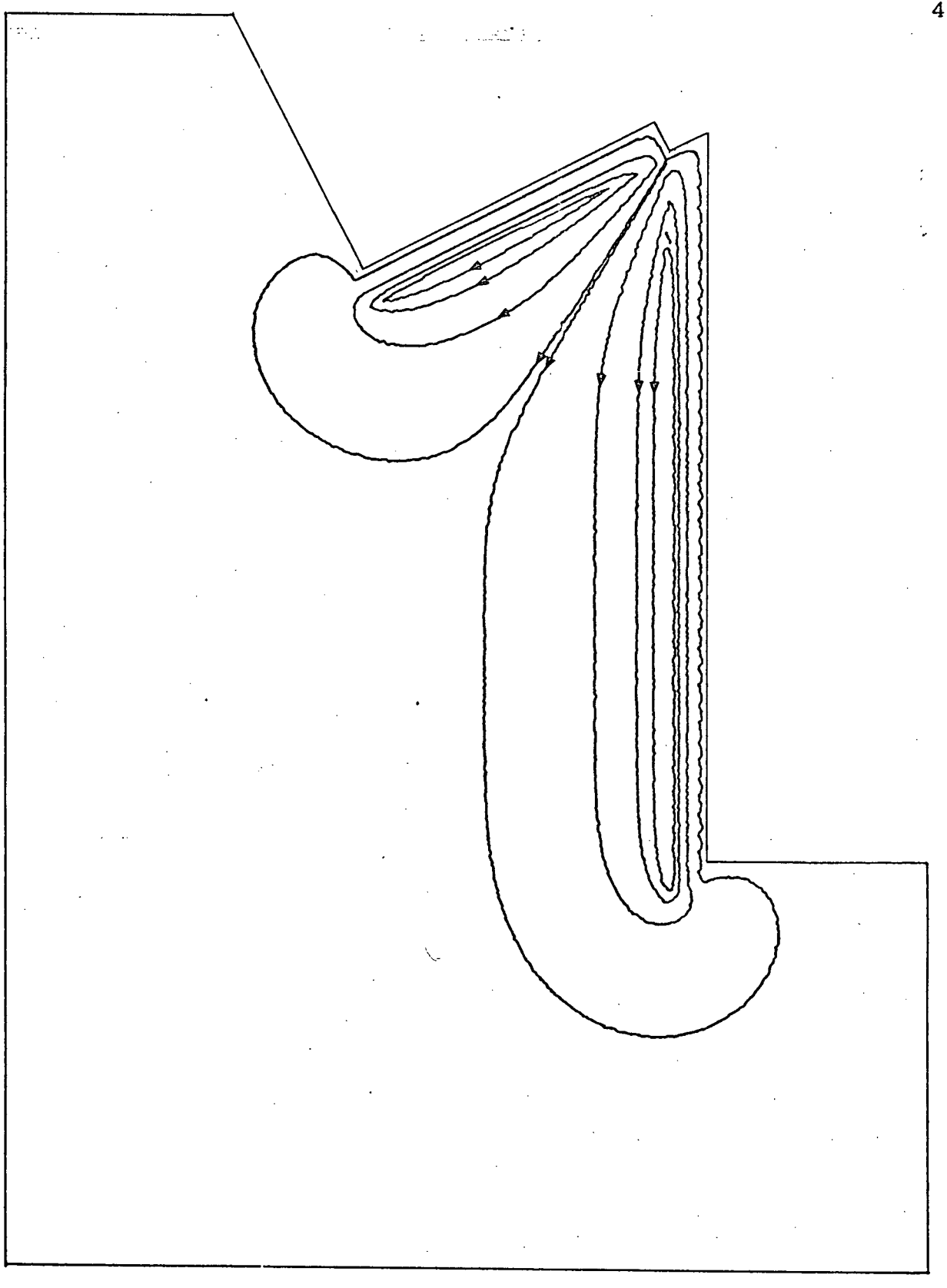

Figure 15. Current circulation for acute beach-breakwater intersection (δ =60°), equal current strengths and no offshore depth variations.

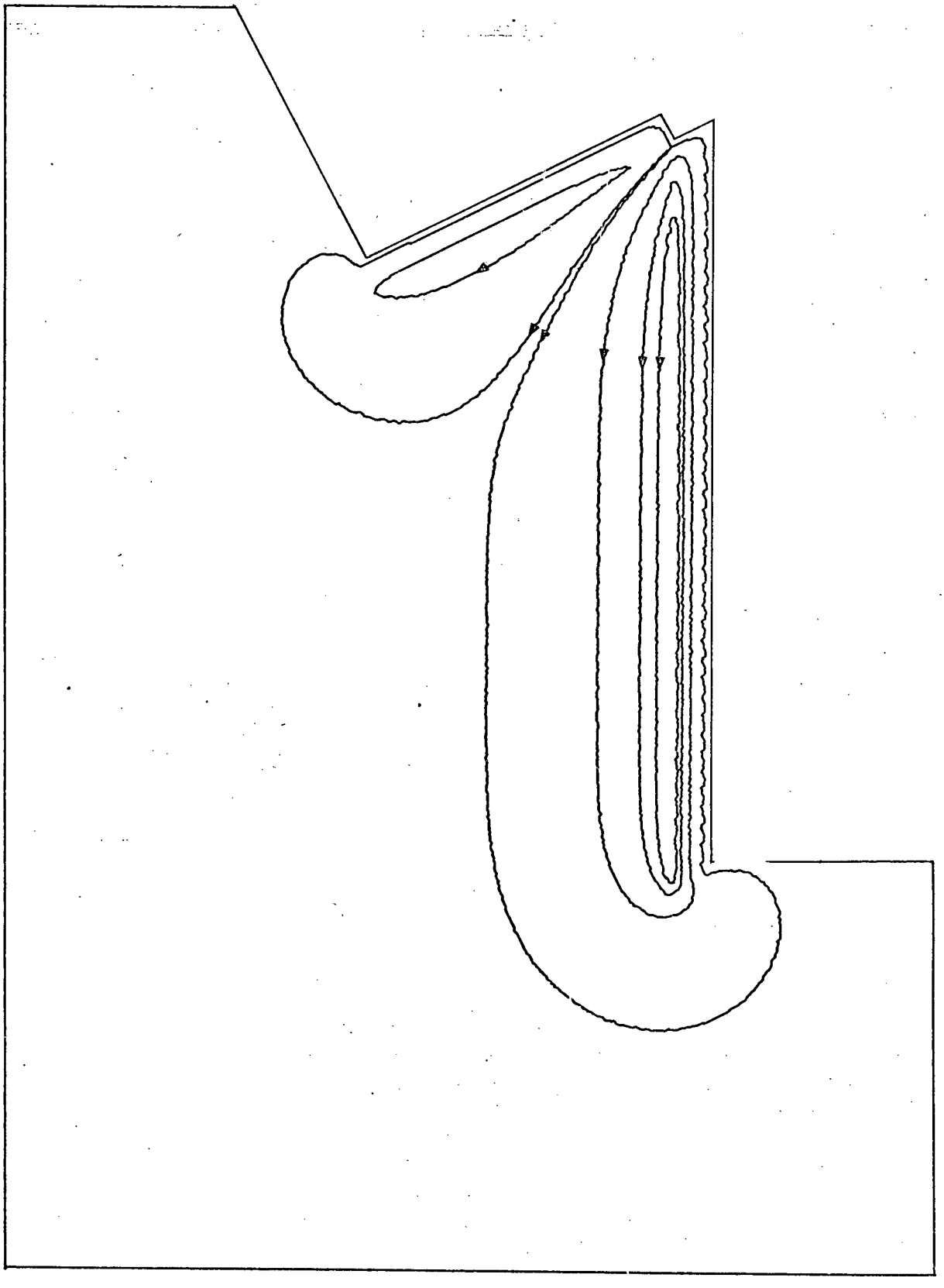

Figure 16. Circulatory pattern for a ratio of natural beach current strength to causeway beach current strength of 2:1. There are no off-shore depth variations.

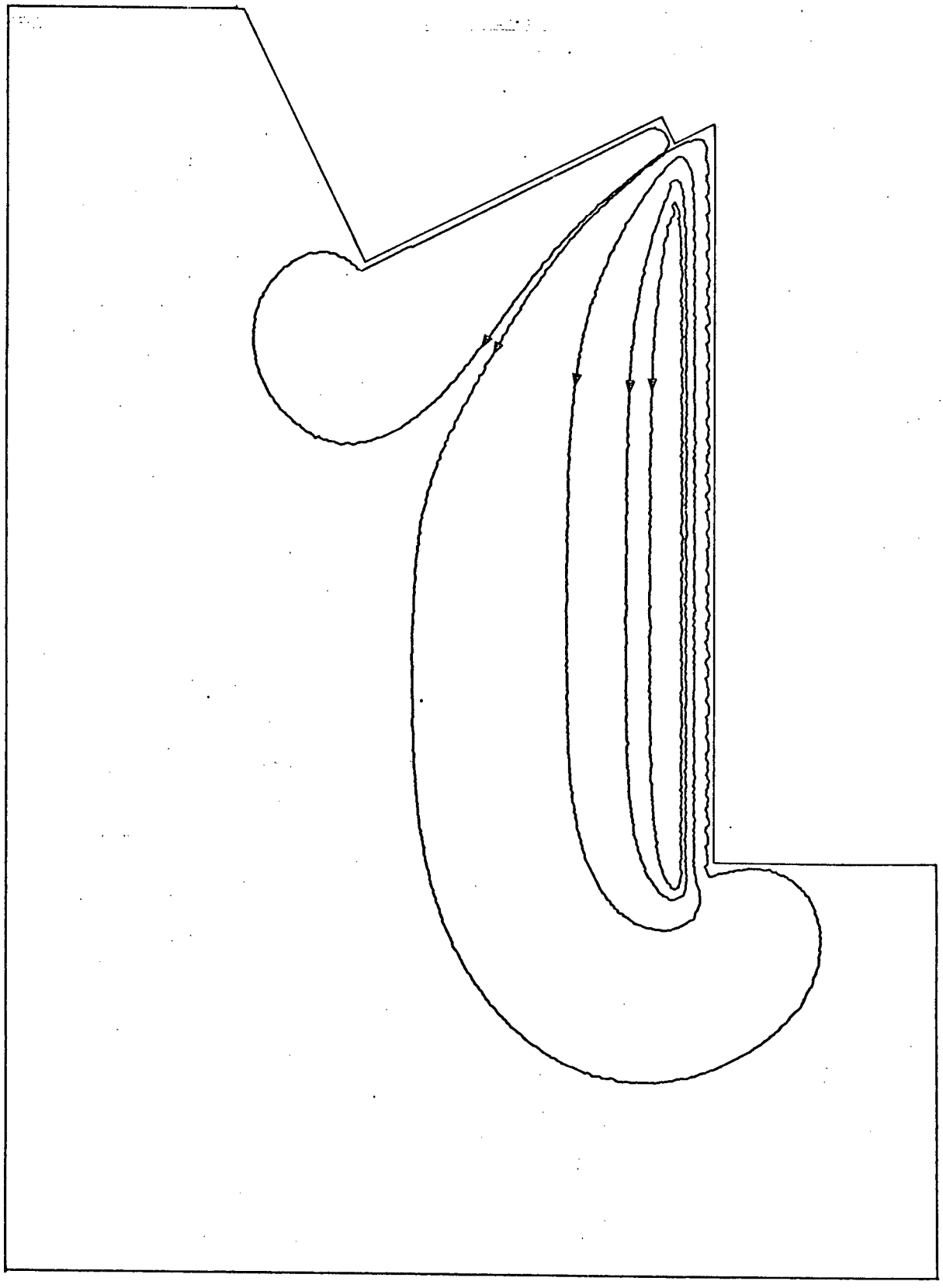

Figure 17. Circulatory pattern for a ratio of natural beach current strength to causeway beach current strength of 4:1. There are no off-shore depth variations.

current strength to causeway beach current strength of 2:1 and 4:1 respectively. The results are what we should intuitively expect, with the cell driven by the stronger current dominating the circulation pattern as the ratio of the current strengths increases. The off-shore return flow is deflected toward the causeway in such a way that its tangent divides the angle of beach intersection δ, into angles whose ratios vary as the current strengths, that is, 2:1 and 4:1 respectively.

VI Variable Bottom Topography

The next models to be presented incorporate variations in the bottom topography of the type to be found at the Tsawwassen location, that is, a drop-off from the shallow shelf region to much deeper water as from Roberts Bank to Georgia Strait, and an off-shore trench which runs parallel to the causeway across the width of the shelf-zone (see Figure 10 for the basic layout).

Shown in Figure 18 is the circulation pattern for a model featuring the drop-off to deeper water (for currents of equal strength). The deeper zone has been given a depth of 100 m. compared to the shelf depth of 5 m., a ratio of 20:1.

The results show a pronounced deflection of the stream-lines as they approach the large mass of water beyond the drop-off and a discontinuity in the tangential velocity

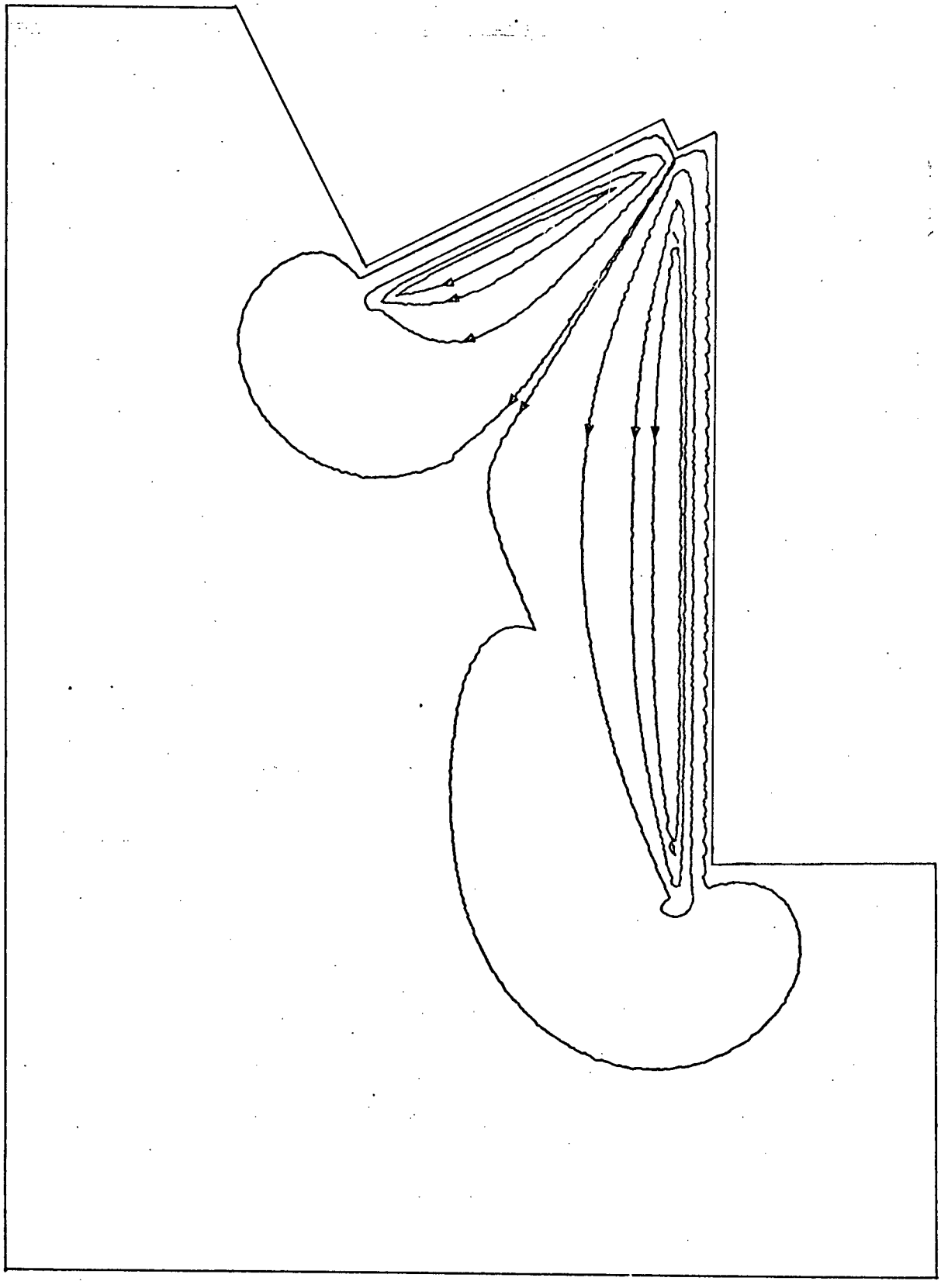

Figure 18. Circulatory pattern for the linear bottom friction model incorporating a drop-off to deep water.

as they cross the boundary from shallow to deep water. Such a discontinuity is allowed by the absence of lateral friction in the model.

An off-shore trench is next introduced to the bottom topography. It is rectangular in shape, with a mean high tide depth of 10 m. (twice that of the shelf) and tranverses most of the width of the shelf as shown in Figure 10, its off-shore end emptying into the deep off-shore zone.

The results are given in Figure 19; the influence of the trench may be seen by comparing this figure with Figure 18. The results are surprising; in addition to the channeling of the off-shore flow into the trench, which is what we would intuitively expect, we see a large increase in the total transport of the off-shore flow. A large eddy forms with seaward flow over the trench and return flow between the trench and the causeway.

Let us pause here to reflect upon the validity of these results. Recall that the linear form of bottom friction, while simple, is not realistic, being dependent upon two rather severe restrictions:

i/ that the longshore current velocity be small compared to the wave orbital velocity in the surfzone and

ii/ that the angle of wave incidence be very small.

As pointed out by James (1972) and Liu and Dalrymple (1978) these assumptions are not always satisfied. Furthermore, in the off-shore zone, the wave orbital velocity at

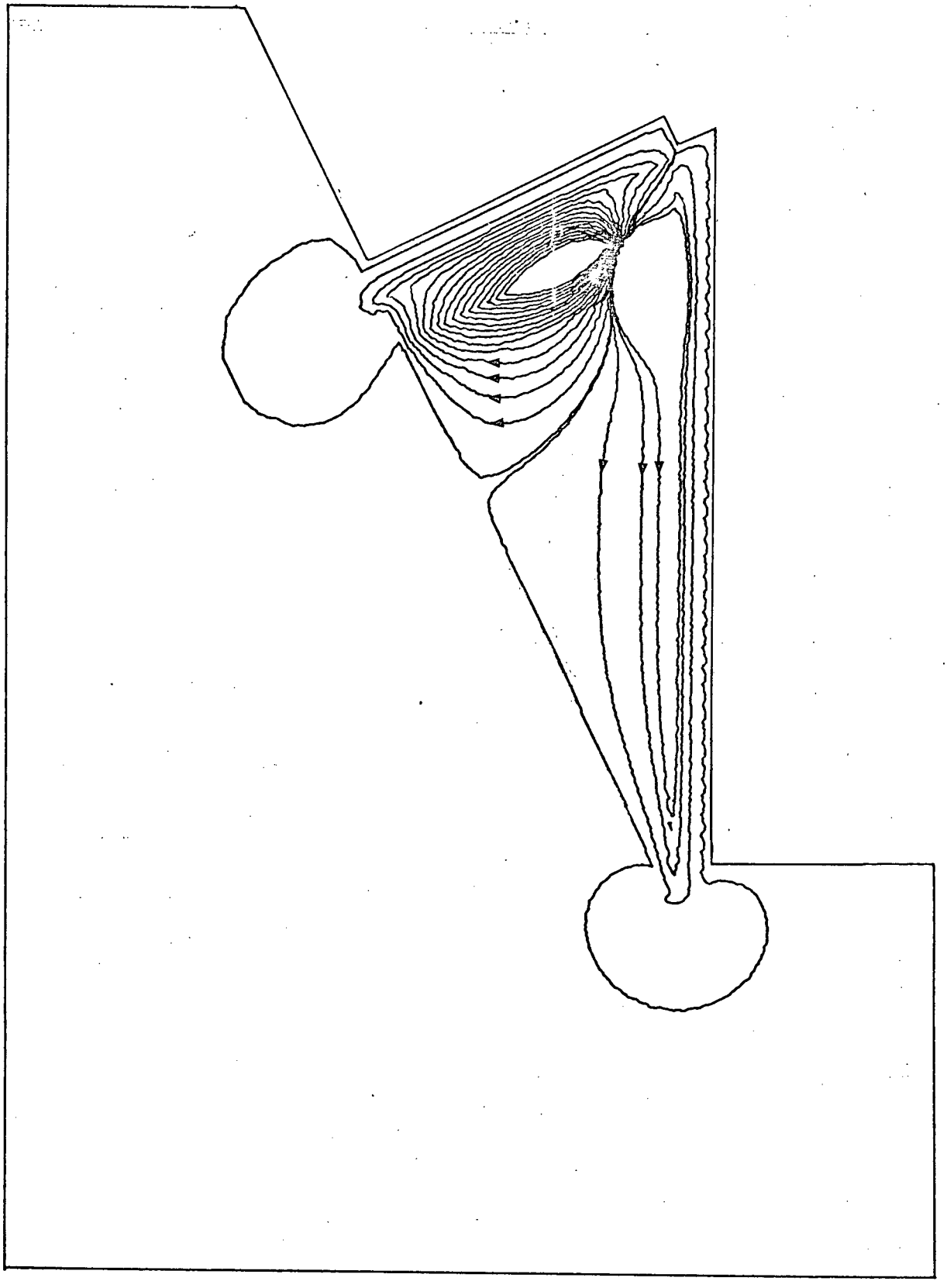

Figure 19. Circulatory pattern for the linear bottom friction model incorporating a drop-off to deep water and an offshore trench running parallel to the causeway.

the bottom is likely to be smaller than the mean current; a linearization of the bottom stress, in the form given below is then clearly inappropriate.

Hence, in light of the questionable validity of these assumptions and the difficulty in interpreting the results so derived, we shall not speculate further upon the linear results.

Rather, let us proceed to discuss the properties of models using the more realistic form of bottom friction

$$\tau = C\rho |\underset{\sim}{u}_0| \underset{\sim}{u}_0$$

in the off-shore zone, as mentioned in Chapter 3. (The relevant finite difference equation is given in Appendix B).

The results as derived for

i/ a model with no variations in bottom topography and

ii/ a model featuring only the drop-off to deeper water

are given in Figures 20 and 21, which exhibit negligible differences in comparison to their linear counterparts (Figures 15 and 18).

However, the flow pattern for the non-linear model incorporating both the drop-off and the trench (as shown in Figure 22) differs considerably from the linear model (Figure 19). Upon comparison of Figures 22 and 21, we see a definite channeling of the off-shore return flow into the trench, again as expected, but without the inordinate amplification of the flow pattern.

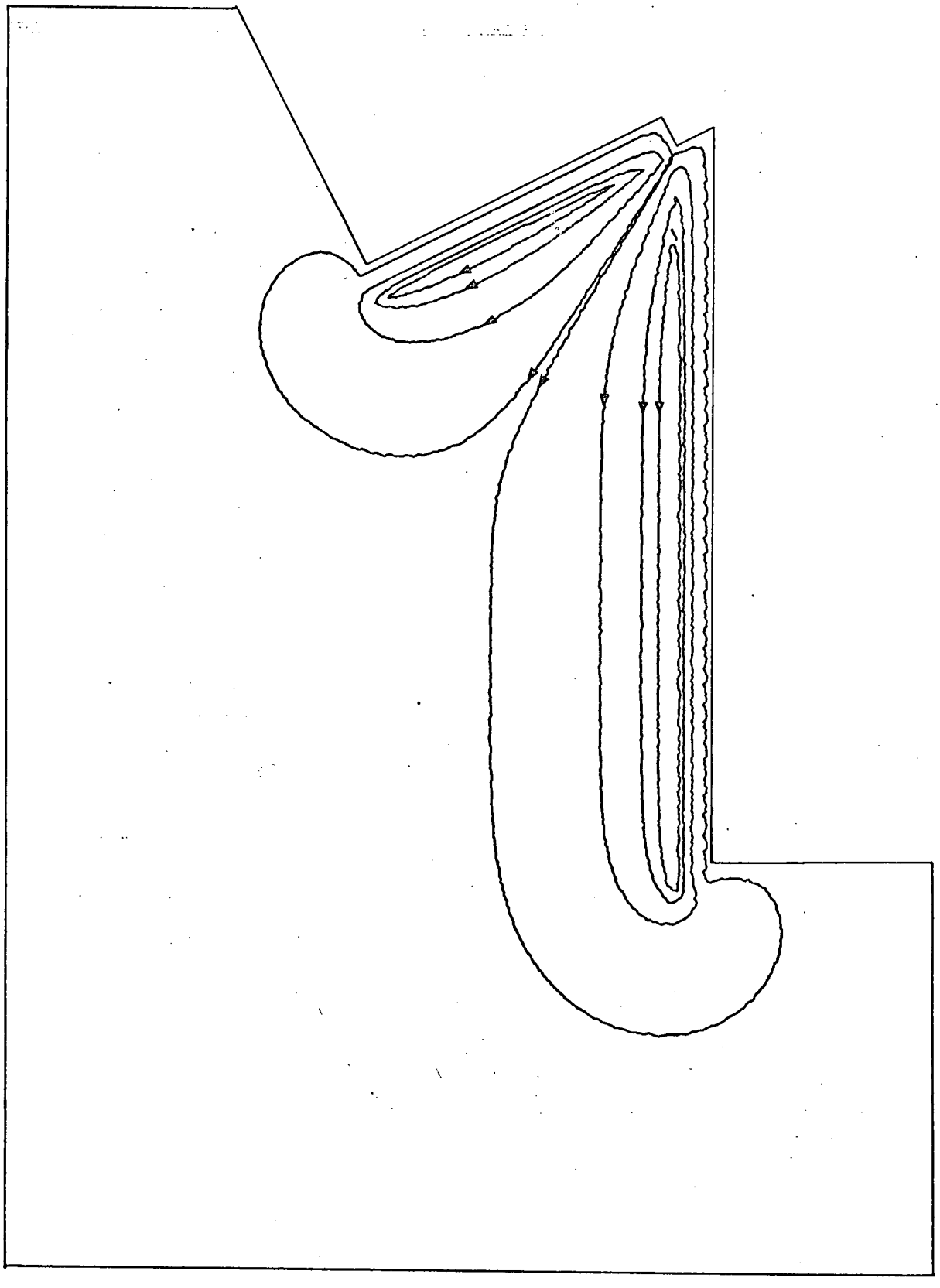

Figure 20. Circulatory pattern for the non-linear bottom friction model with currents of equal strength and no off-shore depth variations.

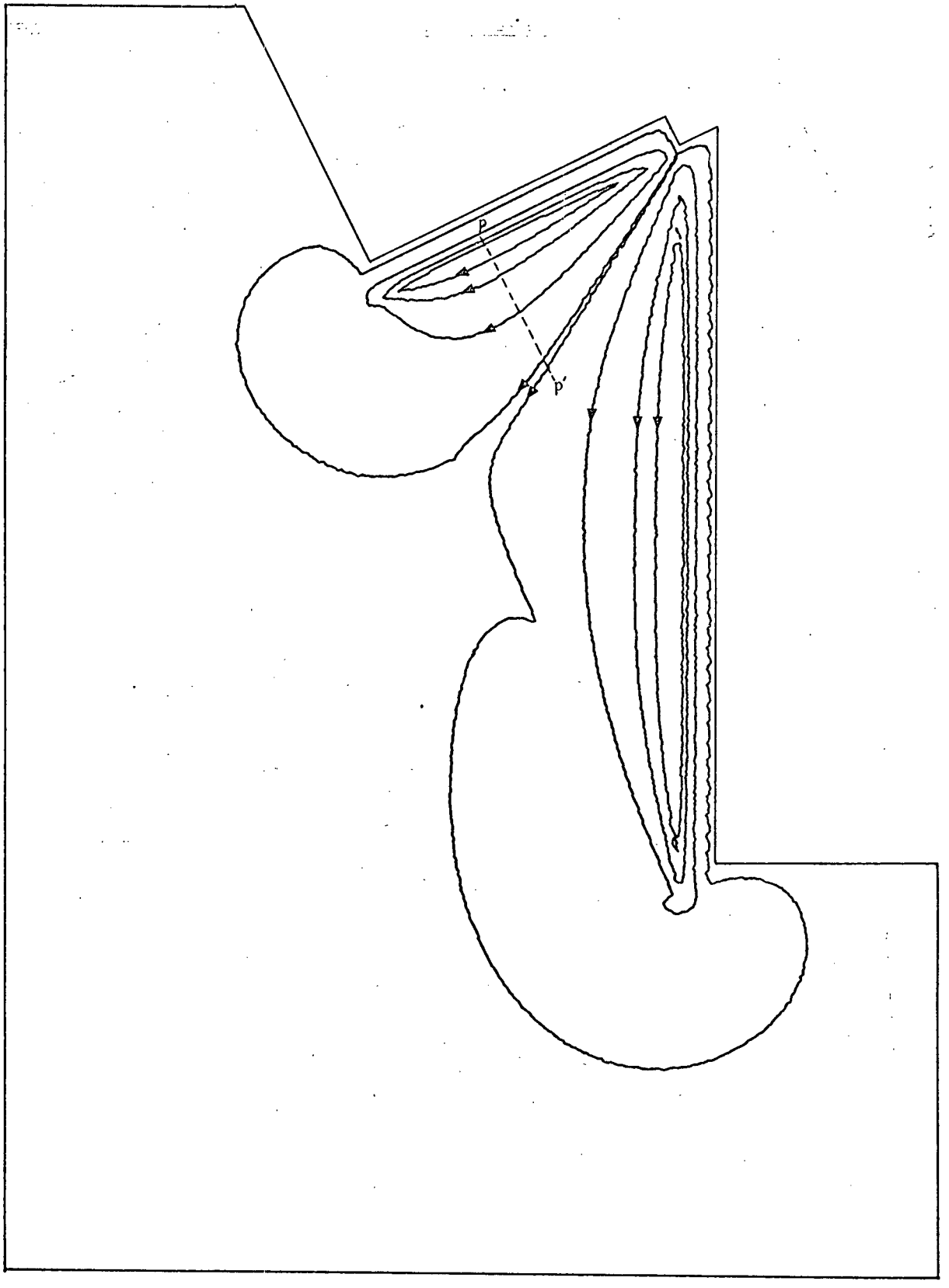

Figure 21. Current circulation for the non-linear bottom friction model incorporating a drop-off to deep water.

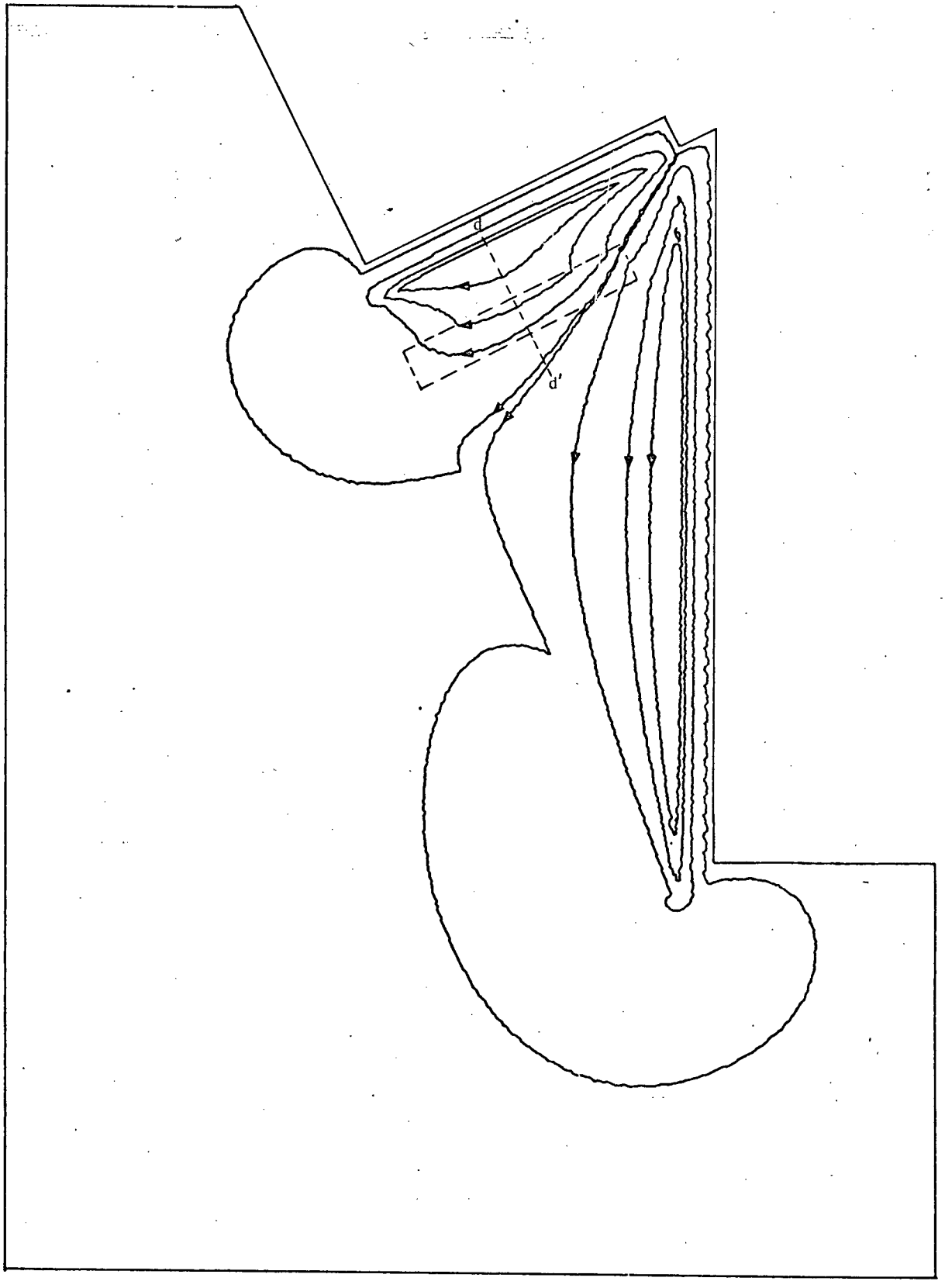

Figure 22. Current circulation for the non-linear bottom friction model incorporating a drop-off to deep water and an off-shore trench running parallel to the causeway.

The deflection of the current is most apparent on the causeway side of the trench, as is shown by a decrease in transport there, with a corresponding increase in the trench as water is drawn into it.

Velocity profiles taken along cross-sections pp' and dd' of Figures 21 and 22 respectively are compared in Figure 23, and found to be similar in form. The lower profile, from Figure 21, shows the velocity in the absence of a trench. The flow is slightly slower in the presence of the trench (upper curve) but the transport is nevertheless increased in the trench because the increase in depth more than compensates for the decrease in speed.

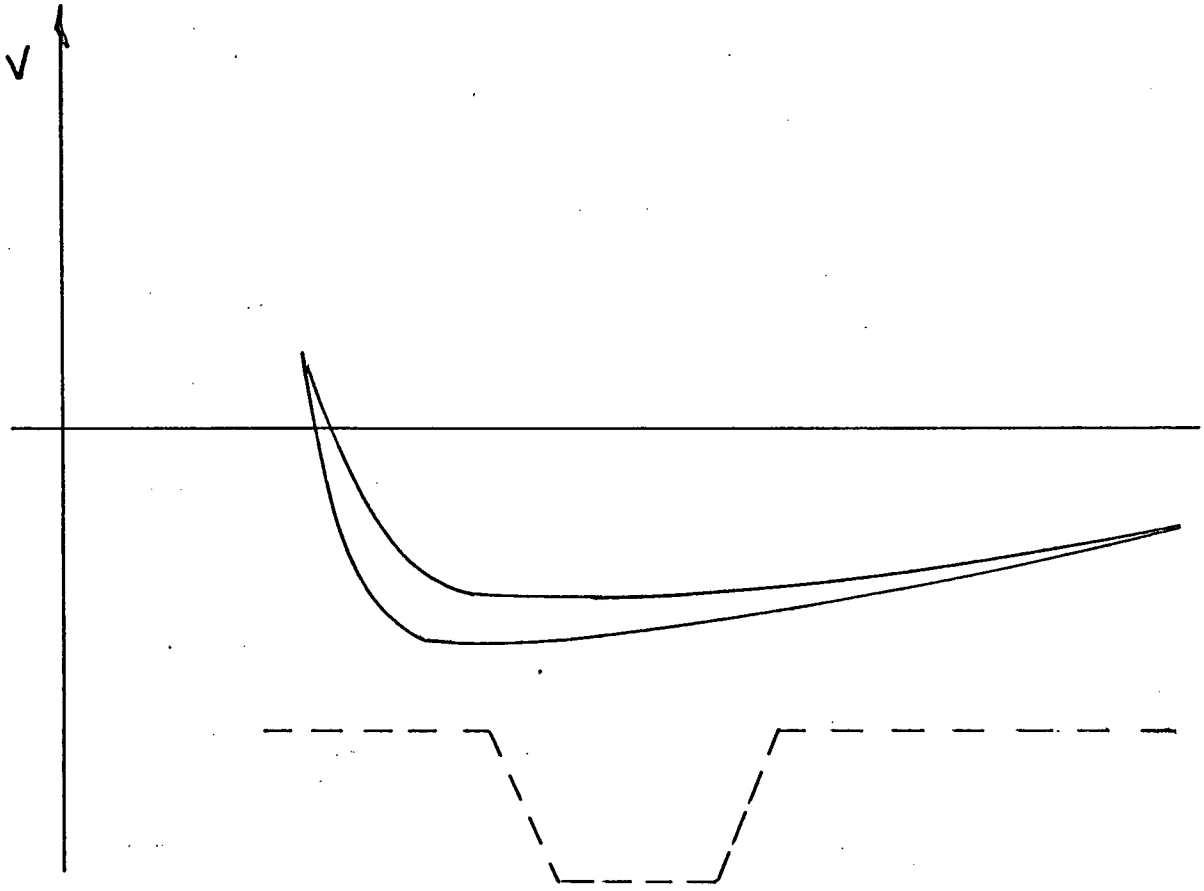

Figure 23. Velocity profiles taken along cross-sections pp' and dd' of Figures 21 and 22 respectively. The upper profile is taken from the trench model (Figure 22). The position of the trench is shown by the dashed line.

VII The Influence of Depth Variations

Let us consider further the effects of variations in bottom topography upon the local current circulation.

We begin with the x and y components of velocity respectively;

$$u = \frac{1}{h}\frac{\partial \psi}{\partial y} \tag{4.22}$$

$$v = -\frac{1}{h}\frac{\partial \psi}{\partial x} \tag{4.23}$$

so that in the case of a flat bottom we have

$$\nabla(\underset{\sim}{u}\cdot h) = 0 \tag{4.24}$$

while, for a bottom which is not flat

$$\nabla\left(\frac{1}{h}\nabla\psi\right) = 0 \tag{4.25}$$

Consider now the bottom to be nearly flat, so that

$$\begin{aligned} h &= h_0(1+\epsilon\eta) + \cdots \\ \psi &= \psi_0 + \epsilon\psi_1 + \cdots \end{aligned} \tag{4.26}$$

To zeroth order, we have from (4.24) and (4.25)

$$\nabla^2\psi_0 = 0 \tag{4.27}$$

while to 1st order

$$\nabla^2 \psi_1 = \nabla\eta \cdot \nabla\psi_0 \tag{4.28}$$

where $\nabla^2\psi_1$, is a measure of the departure from average at a point, so that if $\nabla^2\psi_1 > 0$ then ψ is increasing.

What then are the effects of a variation in depth upon the velocity and transport?

Consider the one-dimensional situation as illustrated in Figure 24, where all the motion is in the x-direction, so that

$$\psi_x \equiv 0$$
$$\psi_y = uh \tag{4.29}$$

which gives us

$$\psi_0 = (0, u_0 h_0 y) \tag{4.30}$$

$$\nabla\psi_0 = (0, u_0 h_0) \tag{4.31}$$

and

$$\nabla^2 \psi_1 = \nabla\eta \cdot \nabla\psi_0 \tag{4.32}$$

(=0 if $\nabla\eta$ has no y-component)

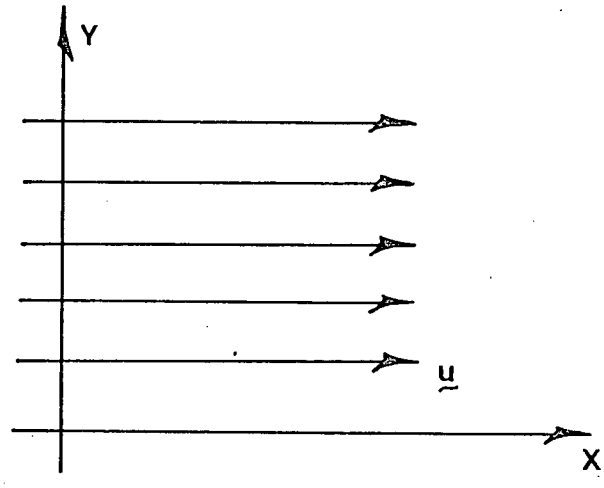

Figure 24. Velocity field for the one-dimensional model.

Is the velocity changed? (that is, is $u_1 \neq 0$?)

From (4.22) we have

$$u = \frac{1}{h}\psi_y$$

$$(u_0 + \epsilon u_1) = \frac{1}{h_0(1+\epsilon\eta)} \cdot (\psi_0 + \epsilon\psi_1)_y$$

or, to 1st order

$$u_1 h_0 = \psi_{1y} - u_0 h_0 \eta \qquad (4.33)$$

To determine ψ_{1y}, let

$$\eta = \left(\frac{h_1}{h_0}\right)_0 = y(y-1) \qquad \text{(as shown in Figure 25)}$$

so that $$\nabla^2\psi_1 = \nabla\eta \cdot \nabla\psi_0$$
$$= (2y-1) \cdot h_0 u_0$$

that is

$$\psi_{1y} = \eta h_0 u_0 \qquad (4.34)$$

giving us

$$u_1 h_0 = 0 \qquad (4.35)$$

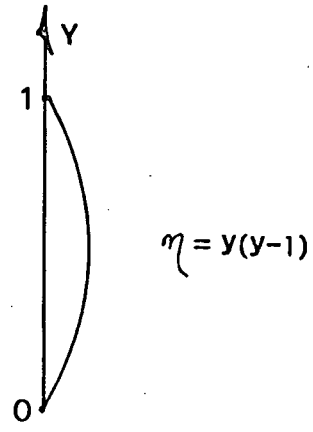

Figure 25. Variation in depth as defined by $\eta = y(y-1)$.

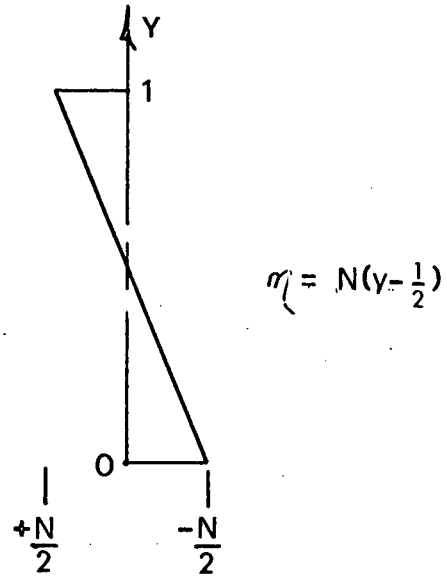

Figure 26. Variation in depth as defined by $\eta = N(y-\frac{1}{2})$.

So that to 1st order, $u_1 = 0$, hence the speed of the current is not changed in this one-dimensional case.

A slightly different case is as follows: consider a variation in depth, as shown in Figure 26, such that the average depth is not changed, by letting

$$\eta = N\left(y - \tfrac{1}{2}\right) \tag{4.36}$$

so that we have

$$\begin{aligned} \int_0^1 h\,dy &= \int_0^1 h_0(1+\epsilon\eta)\,dy \\ &= h_0 = \text{constant} \end{aligned} \tag{4.37}$$

Then we have

$$\begin{aligned} \psi_{1yy} &= \sigma\eta \cdot \sigma\psi_0 \\ &= \eta_y \cdot \psi_{0y} \\ &= N h_0 u_0 \end{aligned} \tag{4.38}$$

and

$$\psi_{1y} = N h_0 u_0 y + \text{constant} \tag{4.39}$$

Now the total transport is not changed, that is

$$\int_0^1 (u_0 h_0 + \epsilon[u_1 h_0 + h_0 \eta u_0])\, dy = \int_0^1 u_0 h_0\, dy \tag{4.40}$$

$$h_0 \int_0^1 (u_1 + \eta u_0)\, dy = 0$$

or from (4.33)

$$\int_0^1 \psi_{1,y}\, dy = 0 \tag{4.41}$$

$$\psi_1(1) - \psi_1(0) = 0$$

Thus from (4.39) we have

$$\psi_1 = N h_0 u_0 \frac{y^3}{2} + \text{constant}_1 + \text{constant}_2 \tag{4.42}$$

Solving for the constants

$$\psi_1(y) = N h_0 u_0 \frac{(y^2 - y)}{2} \tag{4.43}$$

Again, the velocity is not affected, as is seen upon substitution of $\psi_{1,y}$ from (4.43) into

$$u_1 h_0 = \psi_{1,y} - h_0 u_0 \eta$$

Hence, with $u_1 = 0$, the transport locally is

$$uh = u_0 h_0 (1 + \epsilon \eta) \tag{4.44}$$

so that in both cases considered, the transport increases linearly with the depth of the fluid layer because to 1^{st} order, continuity alone does not require the velocity to change with small changes in depth.

The results then, for our simple one-dimensional model are in agreement with the numerical models which show an increase in transport over the trench (although there is less of an increase in the more realistic non-linear case due to the stronger effects of friction).

CHAPTER 5

ANALYTICAL MODEL

I. Physical Description

We shall now attempt to develop an analytical model of the wave-induced current circulation in the vicinity of a beach-breakwater intersection.

During the course of the discussion we shall encounter a number of difficulties (despite further simplifications to the analysis) and shall find, in fact, that we must resort to some numerical means in order to salvage a solution.

We wish then to apply equations (3.16) and (3.17) to our analytical model which consists of the intersection at right angles of two semi-infinite beaches, as shown in Figure 27. (The solution we derive for this general configuration need only be rotated 180° so as to conform more closely to that of the field site.)

As discussed in Chapter 2, the Tsawwassen and causeway beaches are of great length, hence we have replaced them in the model by semi-infinite beaches. This allows us to circumvent the need of specifying the boundary conditions at the ends of the surfzones (which we do not know a priori), since we can now simply allow the stream function profiles to approach those of the infinite beach solutions as we get further from the corner.

The quadrant of interest has again been divided into three zones, consisting of two surfzones and an off-shore

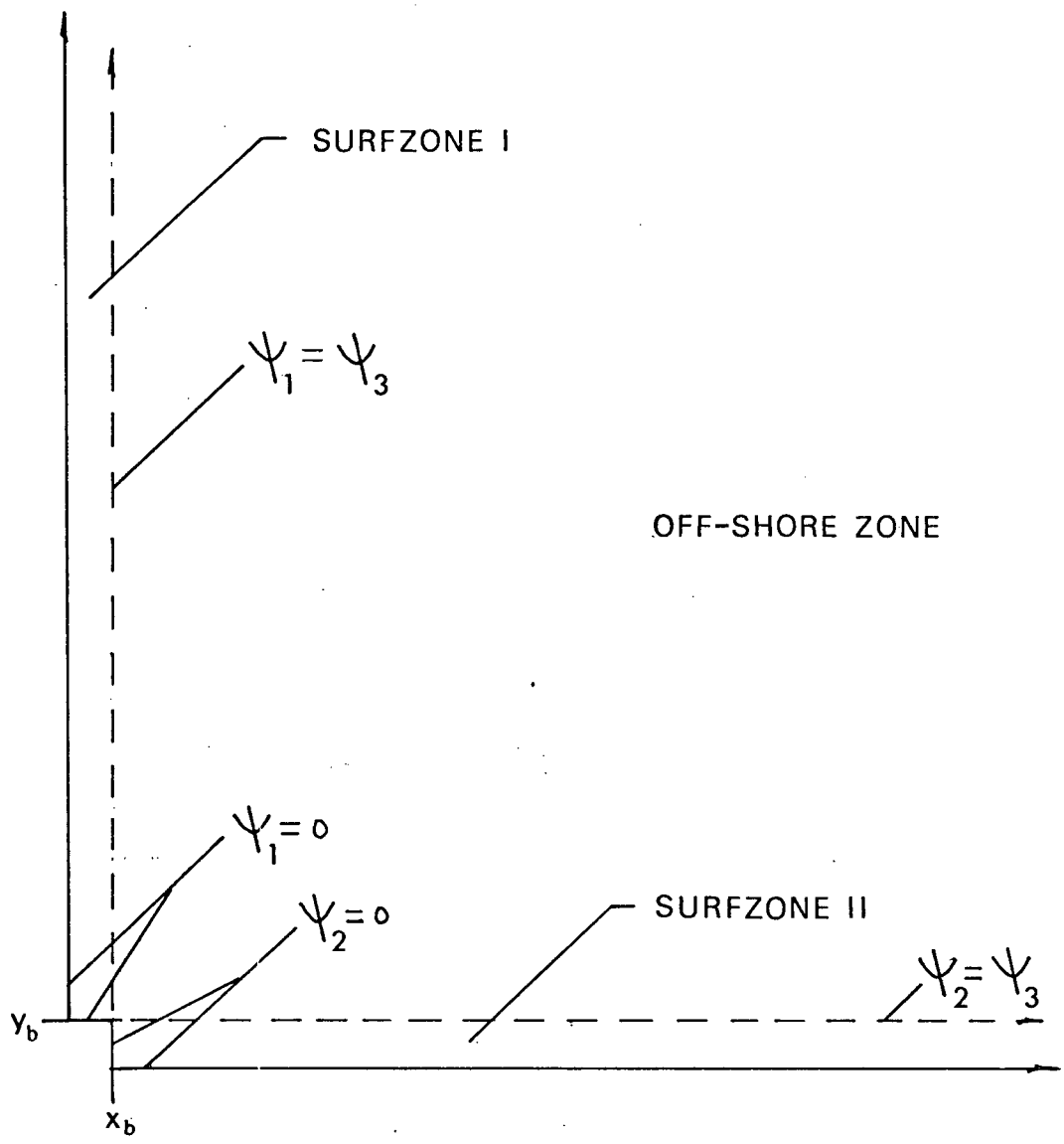

Figure 27. Plan view and boundary conditions of the analytical model.

zone seaward of the breaker-lines. The angles of approach of a wave-train with respect to the breaker-lines of surf-zones I and II will be taken as β and θ respectively.

We shall invoke the following assumptions and approx-imations as for the numerical model:

i/ the intersection corner has been removed to ease the specification of the boundary conditons there

ii/ the boundaries of the surfzones shall be taken as the space - averaged values of the shore and breaker-lines

iii/ the surfzones are assumed uniform in the long-shore directions (equations (4.1) through (4.6))

iv/ the wave amplitude in the surfzones is taken to be proportional to the mean depth of the water (equations (4.11), (4.12) and (4.13))

v/ Snell's law of refraction holds in the surfzones (equation (4.16))

Further, the off-shore zone shall now be assumed to have a uniformly flat bottom, with a depth equal to the water depth at the breaker-lines, which gives us

$$\frac{\partial d_3}{\partial x} = \frac{\partial d_3}{\partial y} \equiv 0 \qquad (5.1)$$

Under these assumptions and approximations the governing equations for the three zones of our analyt-ical model become

1. Surfzone I

$$\psi_{xxx} - \frac{2}{x}\psi_{xx} + \psi_{xyy} = K_1 x^{3/2} \qquad (5.2)$$

2. Surfzone II

$$\psi_{xxy} - \frac{2}{y}\psi_{xy} + \psi_{yyy} = -K_2 y^{3/2} \qquad (5.3)$$

3. Off-shore zone

$$\psi_{xxx} + \psi_{xyy} = 0 \qquad (5.4)$$

which differ from those for the numerical model (equations (4.19), (4.20) and (4.21)) only in the off-shore zone, where variations in the bottom topography are now forbidden.

II Analysis

Surfzone I

Let us begin with the governing equation for surfzone I (the region for which $0 \leq x < x_b$, and $y > y_b$) as given by equation (5.2),

$$\psi_{1xxx} - \frac{2}{x}\psi_{1xx} + \psi_{1xyy} = K_1 x^{3/2} \qquad (5.5)$$

which is to be solved subject to the following boundary conditions:

i/ the stream function is identically zero along the mean shore-line defined by x=0

that is, $\psi_1(0,y) \equiv 0 \quad , \quad y \geq y_b$

ii/ the stream function tends to the infinite beach solution far away from the corner, so that

$$\lim_{y \to +\infty} \psi_1(x,y) = F_1 x^{7/2} \quad , \quad 0 \leq x < x_b$$

iii/ the stream function is identically zero at the end of the surfzone

$$\psi_1(x,y_b) \equiv 0 , \qquad 0 \leq x < x_b$$

The homogeneous equation

$$\psi_{1xx} - \frac{2}{x}\psi_{1x} + \psi_{1yy} = 0 \tag{5.6}$$

can be solved using the separation of variables technique. By making the substitution

$$\psi_1(x,y) = X(x)Y(y) \tag{5.7}$$

equation (5.6) gives the following pair of ordinary differential equations

$$X'' - \frac{2}{x}X' + a^2 Y = 0 \tag{5.8}$$

$$Y'' - a^2 Y = 0 \tag{5.9}$$

where "a" is a separation constant and the primes denote differentiation with respect to the appropriate independent variable.

The solution of equation (5.8) which vanishes at x=0 is (Kamke, 1959)

$$X(x) = x^{3/2} J_{3/2}(ax) \tag{5.10}$$

(where $J_{3/2}(ax)$ is a Bessel function of the first kind:

$$J_{3/2}(ax) = \sqrt{\frac{2}{\pi}} \cdot (ax)^{-3/2} (\sin ax - ax \cos ax)$$

The general solution of equation (5.9) is

$$Y(y) = B_1 e^{+ay} + B_2 e^{-ay} \tag{5.11}$$

where B_1 and B_2 shall be determined by the boundary conditions.

As a particular solution of the non-homogeneous equation (5.5), let us take

$$B_3 x^{1/2} \tag{5.12}$$

where B_3 shall also be determined by the boundary conditions.

The general solution of the governing equation (5.5), for any one value of the separation constant "a", is then given by

$$\psi_1(r,y) = \left(B_1 e^{+ay} + B_2 e^{-ay}\right) r^{3/2} J_{3/2}(ar) + B_3 r^{7/2} \qquad (5.13)$$

to which we shall now apply the boundary conditions to determine B_1, B_2, and B_3.

i/ $\psi_1(0,y) = 0$, is identically satisfied by equation (5.13).

ii/ $\lim_{y \to +\infty} \psi_1(r,y) = \bar{F}_1 r^{7/2}$ gives us

$$B_1 \equiv 0$$

$$B_3 = \bar{F}_1 = \frac{4}{7} K_1$$

We now have, for any one given value of "a"

$$\psi_1(r,y) = B_2 e^{-ay} r^{3/2} J_{3/2}(ar) + \bar{F}_1 r^{7/2} \qquad (5.14)$$

Applying the final boundary condition

iii/ $\psi_1(r,y_b) \equiv 0$, $0 \le r < r_b$

gives us, after integrating over all possible values of "a"

$$\int_0^\infty B_2(a) e^{-ay_b} r^{3/2} J_{3/2}(ar)\, da = -\bar{F}_1 r^{7/2} \qquad (5.15)$$

or

$$\int_0^\infty J_{3/2}(\alpha x)\left[\frac{B_2(\alpha)e^{-\alpha y_b}}{\alpha}\right]\alpha\,d\alpha = -\overline{F}_1 x^2 \qquad (5.16)$$

which is of the form

$$\int_0^\infty J_{3/2}(\alpha x)\,\bar{\xi}(\alpha)\,d\alpha = \xi(x) \qquad (5.17)$$

(where $$\xi(x) = \begin{cases} -\overline{F}_1 x^2 & 0 \le x < y_b \\ 0 & y_b < x < \infty \end{cases}$$

which allows us to pass to the upper limit of x_b immediately) so that we may apply the following Hankel transformation (Morse and Feshbach, 1953, p.944)

$$\bar{\xi}(\alpha) = \int_0^{y_b} J_{3/2}(\alpha x)\,\xi(x)\,x\,dx \qquad (5.18)$$

to equation (5.16), giving us

$$\frac{B_2(\alpha)}{\alpha}e^{-\alpha y_b} = -\int_0^{y_b} J_{3/2}(\alpha x)\left[\overline{F}_1 x^2\right]x\,dx \qquad (5.19)$$

or

$$B_2(\alpha) = -\overline{F}_1\,\alpha\,e^{+\alpha y_b}\,\overline{I}_1(\alpha) \qquad (5.20)$$

where

$$I_1(\alpha) = \int_0^{x_b} J_{3/2}(\alpha x)\, x^3\, dx \tag{5.21}$$

Thus, the complete solution for the stream function subject to the governing equation (5.5) (in surfzone I defined by $0 \leq x < x_b$, $y > y_b$) now takes the form

$$\psi_1(x,y) = \int_0^\infty B_2(\alpha)\, e^{-\alpha y}\, x^{3/2}\, J_{3/2}(\alpha x)\, d\alpha + F_1\, x^{7/2}$$

$$= -F_1 \int_0^\infty e^{-\alpha(y-y_b)}\, I_1(\alpha)\, x^{3/2}\, J_{3/2}(\alpha x)\, \alpha\, d\alpha + F_1\, x^{7/2}$$

$$= F_1 \left[x^{7/2} - x^{3/2} \int_0^\infty e^{-\alpha(y-y_b)}\, I_1(\alpha)\, J_{3/2}(\alpha x)\, \alpha\, d\alpha \right] \tag{5.22}$$

Surfzone II

In surfzone II, defined by $0 \leq y < y_b$, $x > x_b$, the governing equation is (as given by equation (5.3)),

$$\psi_{2xx} - \frac{2}{y}\psi_{2y} + \psi_{2yy} = -K_2\, y^{3/2} \tag{5.23}$$

where $\psi_2(x,y)$ is subject to the following boundary conditions

i/ the stream function is identically zero along the mean shore-line defined by y=0, that is

$$\psi_2(x,0) \equiv 0 \qquad , \quad x \geq x_b$$

ii/ the stream function tends to the infinite beach configuration far away from the corner, so that

$$\lim_{x \to +\infty} \psi_2(x,y) = F_2' y^{7/2} \qquad , \quad 0 \leq y < y_b$$

iii/ the stream function is identically zero at the end of the surfzone, that is

$$\psi_2(x_b,y) \equiv 0 \qquad , \quad 0 \leq y < y_b$$

In a manner similar to the derivation of equation (5.22), we can arrive at the following expression for the stream function $\psi_2(x,y)$ (in the surfzone defined by $0 \leq y < y_b$, $x > x_b$)

$$\psi_2(x,y) = F_2' \left\{ y^{7/2} - y^{3/2} \int_0^\infty e^{-p(x-x_b)} \bar{I}_2(p)\, \bar{J}_{3/2}(py)\, p\, dp \right\}$$

$$\bar{I}_2(p) = \int_0^{x_b} \bar{J}_{3/2}(py)\, y^3\, dy$$

$$F_2' = -\frac{4}{7} K_2$$

(5.24)

"p" being the separation constant in this case

Off-shore Zone

We have now to derive an expression for the stream function $\psi_3(x,y)$ in the off-shore zone defined by $x > x_b$, $y > y_b$.

The governing equation in this region subject to the assumptions and approximations discussed earlier was found to be Laplace's equation;

$$\psi_{3_{xx}} + \psi_{3_{yy}} = 0 \tag{5.25}$$

The expression for the offshore stream function is to be found by matching it across the breaker-lines to the respective surfzone solutions, the boundary conditions being

$$\text{i/}\quad \psi_3(x_b,y) = \psi_1(x_b,y) \qquad y > y_b$$

$$\text{ii/}\quad \psi_3(x,y_b) = \psi_2(x,y_b) \qquad x > x_b$$

$$\text{iii/}\quad \psi_3(x,y) \text{ remains finite as } x \to +\infty \text{ and as } y \to +\infty \tag{5.26}$$

Let us begin by breaking this in to two simpler problems, expressing $\psi_3(x,y)$ in the following manner

$$\psi_3(x,y) = \psi_{3,1}(x,y) + \psi_{3,2}(x,y) \tag{5.27}$$

where $\psi_{3,1}$ and $\psi_{3,2}$ satisfy equations (5.28) and (5.29) respectively;

$$\text{i)}\ \nabla^2\psi_{3,1} = 0 \qquad x>x_b,\ y>y_b \qquad (5.28)$$

$$\text{ii)}\ \psi_{3,1}(x_b,y) = \psi_1(x_b,y) \qquad y>y_b$$

$$\text{iii)}\ \psi_{3,1}(x,y_b) = 0 \qquad x>x_b$$

$$\text{iv)}\ \psi_{3,1} \text{ remains bounded as } x \to +\infty$$

$$\text{i)}\ \nabla^2\psi_{3,2} = 0 \qquad x>x_b,\ y>y_b \qquad (5.29)$$

$$\text{ii)}\ \psi_{3,2}(x,y_b) = \psi_2(x,y_b) \qquad x>x_b$$

$$\text{iii)}\ \psi_{3,2}(x_b,y) = 0 \qquad y>y_b$$

$$\text{iv)}\ \psi_{3,2} \text{ remains bounded as } y \to +\infty$$

Considering first equations (5.28), let us apply separation of variables by making the substitution

$$\psi_{3,1}(x,y) = X(x)\,Y(y) \qquad (5.30)$$

into equation (5.28(i)) to get the following pair of ordinary differential equations

$$X(x) = A_1 e^{\lambda(x-x_b)} + A_2 e^{-\lambda(x-x_b)} \qquad (5.31)$$

$$Y(y) = A_3 \cos \lambda(y-y_b) + A_4 \sin \lambda(y-y_b)$$

where λ is a separation constant and the A_i's are to be found from the boundary conditions.

Applying then, boundary condition (5.28(iii)) and (5.28(iv)) to equation (5.31) yields

$$X(x) = A_2 e^{-\lambda(x-x_b)} \qquad (5.32)$$

$$Y(y) = A_4 \sin \lambda(y-y_b)$$

Integrating over all possible positive values of λ, equation (5.30) gives us

$$\psi_{3,1}(x,y) = \int_0^\infty A(\lambda) e^{-\lambda(x-x_b)} \sin \lambda(y-y_b)\, d\lambda \qquad (5.33)$$

To determine $A(\lambda)$ we apply boundary condition (5.28(ii)) to equation (5.33) to get

$$\psi_{3,1}(x_b,y) = \int_0^\infty A(\lambda)\sin\lambda(y-y_b)\,d\lambda$$

$$= \psi_1(x_b,y) \qquad (5.34)$$

or

$$A(\lambda) = \frac{2}{\pi}\int_0^\infty \psi_1(x_b,y')\sin\lambda y'\,dy' \qquad (5.35)$$

Similarly for $\psi_{3,2}(x,y)$ we get

$$\psi_{3,2}(x,y) = \int_0^\infty B(\lambda)\,e^{-\lambda(y-y_b)}\sin\lambda(x-x_b)\,d\lambda \qquad (5.36)$$

where

$$B(\lambda) = \frac{2}{\pi}\int_0^\infty \psi_2(x';y_b)\sin\lambda x'\,dx' \qquad (5.37)$$

Combining solutions for $\psi_{3,1}$ and $\psi_{3,2}$ gives us the stream function in the off-shore zone;

$$\psi_3(x,y) = \psi_{3,1}(x,y) + \psi_{3,2}(x,y)$$

$$= \int_0^\infty A(\lambda)e^{-\lambda(x-x_b)}\sin\lambda(y-y_b)\,d\lambda + \int_0^\infty B(\lambda)e^{-\lambda(y-y_b)}\sin\lambda(x-x_b)\,d\lambda \qquad (5.38)$$

$$A(\lambda) = \frac{2}{\pi}\int_0^\infty \psi_1(x_b,y')\sin\lambda y'\,dy'$$

$$B(\lambda) = \frac{2}{\pi}\int_0^\infty \psi_2(x';y_b)\sin\lambda x'\,dx'$$

The remaining task is to solve the expressions for the stream functions in the surfzones and hence arrive at a solution in the off-shore zone by matching the stream functions across their respective breaker-lines.

In summary, the expressions are;

1. Surfzone I

$$\psi_1(x,y) = F_1 \left\{ x^{1/2} - x^{3/2} \int_0^\infty e^{-\alpha(y-y_b)} I_1(\alpha) J_{3/2}(\alpha x)\, \alpha\, d\alpha \right\} \qquad (5.39)$$

$$I_1(\alpha) = \int_0^{x_b} J_{3/2}(\alpha x)\, x^3\, dx$$

2. Surfzone II

$$\psi_2(x,y) = F_2 \left\{ y^{1/2} - y^{3/2} \int_0^\infty e^{-\beta(x-x_b)} I_2(\beta) J_{3/2}(\beta y)\, \beta\, d\beta \right\} \qquad (5.40)$$

$$I_2(\beta) = \int_0^{y_b} J_{3/2}(\beta y)\, y^3\, dy$$

3. Offshore zone

$$\psi_3(x,y) = \qquad (5.41)$$

$$\int_0^\infty A(\lambda)\, e^{-\lambda(x-x_b)} \sin \lambda(y-y_b)\, d\lambda + \int_0^\infty B(\lambda)\, e^{-\lambda(y-y_b)} \sin \lambda(x-x_b)\, d\lambda$$

$$A(\lambda) = \frac{2}{\pi}\int_0^\infty \psi_1(x_b, y')\sin\lambda y' dy'$$

$$B(\lambda) = \frac{2}{\pi}\int_0^\infty \psi_2(x', y_b)\sin\lambda x' dx'$$

Before we can begin to evaluate the integral expressions for $\psi_1(x,y)$ and $\psi_2(x,y)$ we must first attend to $I_1(a)$ and $I_2(p)$, where

$$I_1(a) = \int_0^{x_b} J_{3/2}(ax)\, x^3 dx$$

$$I_2(p) = \int_0^{y_b} J_{3/2}(py)\, y^3 dy$$

The algebra is presented in Appendix C, from which we get

$$I_1(a) = \sqrt{\frac{2}{\pi}}\, a^{-4}\left[-\frac{1}{2}(ax_b)^{3/2}\cos ax_b - (ax_b)^{5/2}\sin ax_b \right. \qquad (5.42)$$

$$\left. + \frac{21}{4}(ax_b)^{1/2}\sin ax_b - \frac{21}{4}\sqrt{\frac{\pi}{2}}\, S\sqrt{ax_b}\right]$$

where $S(\sqrt{\alpha x_b}\,)$ is a Fresnel integral as given by Gradshteyn and Rhyzik (1965, p.930, 8.251(2)); and

$$I_2(p) = \sqrt{\frac{2}{\pi}}\, p^{-4}\left[-\frac{7}{2}(py_b)^{3/2}\cos(py_b) - (py_b)^{5/2}\sin py_b\right. \tag{5.43}$$

$$\left. + \frac{21}{4}(py_b)^{1/2}\sin py_b - \frac{21}{4}\sqrt{\frac{\pi}{2}}\, S\sqrt{py_b}\,\right]$$

The expressions for the surfzone stream functions $\psi_1(x,y)$ and $\psi_2(x,y)$ are now

$$\psi_1(x,y) = F_1\left[x^{7/2} - x^{3/2}\int_0^\infty e^{-a(y-y_b)}\sqrt{\frac{2}{\pi}}\cdot a^{-4}\left[-(\alpha x_b)^{5/2}\sin(\alpha x_b)\right.\right.$$

$$-\frac{7}{2}(\alpha x_b)^{3/2}\cos(\alpha x_b) + \frac{21}{4}(\alpha x_b)^{1/2}\sin(\alpha x_b)$$

$$\left.\left. - \frac{21}{4}\sqrt{\frac{\pi}{2}}\, S\sqrt{\alpha x_b}\,\right] J_{3/2}(\alpha x)\, a\, da\,\right] \tag{5.44}$$

$$= F_1\left[x^{7/2} - \frac{2x}{\pi}\int_0^\infty e^{-a(y-y_b)}\left[-\frac{7}{2}(\alpha x_b)^{3/2}\cos(\alpha x_b)\right.\right.$$

$$-(\alpha x_b)^{5/2}\sin(\alpha x_b) + \frac{21}{4}(\alpha x_b)^{1/2}\sin(\alpha x_b)$$

$$\left.\left. - \frac{21}{4}\sqrt{\frac{\pi}{2}}\, S\sqrt{\alpha x_b}\,\right]\left(\frac{\sin\alpha x}{\alpha x} - \cos\alpha x\right)\frac{da}{a^{7/2}}\,\right]$$

and $\psi_2(x,y) = \frac{1}{\Gamma_2}\left[y^{7/2} - \frac{2y}{\sqrt{\pi}} \int_0^\infty e^{-\alpha(x-x_b)} \left[-\frac{7}{2}(\beta y_b)^{3/2} \cos \beta y_b \right.\right.$

$$\left. - (\beta y_b)^{5/2} \sin(\beta y_b) + \frac{21}{4}(\beta y_b)^{1/2} \sin(\beta y_b) \right. \qquad (5.45)$$

$$\left.\left. - \frac{21}{4}\sqrt{\frac{\pi}{2}}\, S\sqrt{\beta y_b} \right] \left(\frac{\sin \beta y}{\beta y} - \cos \beta y \right) \frac{d\beta}{\beta^{7/2}} \right]$$

In each of equations (5.44) and (5.45) there are eight integrals to be evaluated. Let us first turn our attention to $\psi_1(x,y)$, for which the integrals are

$$\frac{7}{2} x_b^{3/2} \int_0^\infty e^{-\alpha y} \cos \alpha x_b \sin \alpha x \, d\alpha / \alpha^3 \qquad (5.46)$$

$$-\frac{7}{2} x_b^{3/2} \int_0^\infty e^{-\alpha y} \cos \alpha x_b \cos \alpha x \, d\alpha / \alpha^2 \qquad (5.47)$$

$$x_b^{5/2} \int_0^\infty e^{-\alpha y} \sin \alpha x_b \sin \alpha x \, d\alpha / \alpha^2 \qquad (5.48)$$

$$-x_b^{5/2} \int_0^\infty e^{-\alpha y} \sin \alpha x_b \cos \alpha x \, d\alpha / \alpha \qquad (5.49)$$

$$-\frac{21}{4}\frac{x_b^{\frac{1}{2}}}{7}\int_0^\infty e^{-ay}\sin ax_b \sin ax\,\frac{da}{a^4} \tag{5.50}$$

$$+\frac{21}{4}x_b^{\frac{1}{2}}\int_0^\infty e^{-ay}\sin ax_b\cos ax\,da/a^3 \tag{5.51}$$

$$+\frac{21}{4}\sqrt{\frac{\pi}{2}}\frac{1}{7}\int_0^\infty e^{-ay}\sin ax\,S\sqrt{ax_b}\,da/a^{9/2} \tag{5.52}$$

$$-\frac{21}{4}\sqrt{\frac{\pi}{2}}\int_0^\infty e^{-ay}\cos ax\,S\sqrt{ax_b}\,da/a^{7/2} \tag{5.53}$$

(where $y \Rightarrow y - y_b$,)

By repeatedly applying the technique of integration by parts (see Appendix D), integrals (5.46) through (5.51) can be reduced to multiples of the following standard integrals as given by Gradshteyn and Rhyzik (1965, p.492)

$$\int_0^\infty e^{-ay}\sin ax_b \sin ax\,\frac{da}{a} = \frac{1}{4}\ln\left[\frac{y^2+(x-x_b)^2}{y^2+(x+x_b)^2}\right] \tag{5.54}$$

$$\int_0^\infty e^{-\alpha y} \sin\alpha x \cos\alpha x_b \frac{d\alpha}{\alpha} = \frac{1}{2}\tan^{-1}\left(\frac{2yx}{y^2+x_b^2-x^2}\right) \tag{5.55}$$

$$\int_0^\infty e^{-\alpha y} \sin\alpha x_b \sin\alpha x \frac{d\alpha}{\alpha^2} = \frac{x_b}{2}\tan^{-1}\left(\frac{2yx}{y^2+x_b^2-x^2}\right)$$

$$+\frac{x}{2}\tan^{-1}\left(\frac{2yx_b}{y^2-x_b^2+x^2}\right) + \frac{y}{4}\ln\left[\frac{y^2+(x-x_b)^2}{y^2+(x-x_b)^2}\right] \tag{5.56}$$

Integrals (5.46) through (5.51) then give us

$$\left(-\frac{1}{8}x_b^{3/2}x - \frac{1}{8}x_b^{3/2}\frac{y^2}{x} + \frac{1}{8}x_b^{7/2}\frac{}{x}\right)\cdot\frac{1}{2}\tan^{-1}\left(\frac{2yx}{y^2+x_b^2-x^2}\right) \tag{5.57}$$

$$-\frac{1}{4}\tan^{-1}\left(\frac{2yx_b}{y^2-x_b^2+x^2}\right)$$

$$+\left(\frac{21}{8}x_b^{\frac{1}{2}}x + \frac{1}{8}x_b^{5/2} + \frac{1}{8}x_b^{\frac{1}{2}}\frac{y^2}{x}\right)\frac{y}{4}\ln\left[\frac{y^2+(x-x_b)^2}{y^2+(x+x_b)^2}\right]$$

Similarly, by applying the following integration by parts relations

$$\int_0^\infty e^{-\alpha y}\sin\alpha x \sum\sqrt{\alpha x_b}\frac{d\alpha}{\alpha^{n/2}} = \tag{5.58}$$

$$+\frac{2}{(n-2)}\sum\sqrt{\alpha x_b}\frac{\sin\alpha x}{\alpha^{\frac{n-2}{2}}}\Bigg|^0 - \frac{2y}{(n-2)}\int_0^\infty e^{-\alpha y}\sin\alpha x \sum\sqrt{\alpha x_b}\frac{d\alpha}{\alpha^{\frac{n-2}{2}}}$$

$$+\frac{2x}{(n-2)}\int_0^\infty e^{-ay}\cos ax\,S\sqrt{ax_b}\,\frac{da}{a^{\frac{n-2}{2}}} + \frac{2}{(n-2)}\sqrt{\frac{x_b}{2\pi}}\int_0^\infty e^{-ay}\sin ax\sin ax_b\,\frac{da}{a^{\frac{n-1}{2}}}$$

$$\int_0^\infty e^{-ay}\cos ax\,S\sqrt{ax_b}\,\frac{da}{a^{n/2}} =$$

$$\frac{2}{(n-2)}S\sqrt{ax_b}\cos ax\,\frac{}{a^{\frac{n-2}{2}}}\Bigg|^0 - \frac{2y}{(n-2)}\int_0^\infty e^{-ay}\cos ax\,S\sqrt{ax_b}\,\frac{da}{a^{\frac{n-2}{2}}} \qquad (5.59)$$

$$-\frac{2x}{(n-2)}\int_0^\infty e^{-ay}\sin ax\,S\sqrt{ax_b}\,\frac{da}{a^{\frac{n-2}{2}}} + \frac{2}{(n-2)}\sqrt{\frac{x_b}{2\pi}}\int_0^\infty e^{-ay}\cos ax\sin ax_b\,\frac{da}{a^{\frac{n-1}{2}}}$$

('n' a positive integer) integrals (5.52) and (5.53) can be reduced to the following form

$$\left(-\frac{1}{8}x_b^{3/2}x + \frac{1}{8}x_b^{3/2}\frac{y^2}{x} - \frac{1}{8}x_b\frac{x_b}{x}\right)\frac{1}{2}\tan^{-1}\left(\frac{2yx}{y^2+x_b^2-x^2}\right) + \frac{1}{4}\tan^{-1}\left(\frac{2yx_b}{y^2-x_b^2+x^2}\right) \qquad (5.60)$$

$$+\left(\frac{15}{8}x_b^{\frac{1}{2}}x - \frac{21}{40}x_b^{5/2}\frac{}{x} - \frac{1}{8}x_b^{\frac{1}{2}}\frac{y^2}{x}\right)\frac{y}{4}\ln\left[\frac{y^2+(x-x_b)^2}{y^2+(x+x_b)^2}\right] - \frac{2}{5}x_b^{3/2}y$$

$$+\frac{1}{105}\left[72y^2x + 16\frac{y^4}{x} - 40x^3\right]\int_0^\infty e^{-ay}\sin ax\,S\sqrt{ax_b}\,\frac{da}{a^{1/2}}$$

$$-\frac{1}{105}\left[104x^2y - 8y^3\right]\int_0^\infty e^{-\alpha y}\cos\alpha x \sum\sqrt{\alpha x_b}\,\frac{d\alpha}{\alpha^{1/2}}$$

(where $y \Rightarrow y-y_b$)

Adding equations (5.57) and (5.60) gives us, for integrals (5.46) through (5.53)

$$-x_b^{3/2}\frac{x}{2}\tan^{-1}\left(\frac{2yx}{y^2+x_b^2-x^2}\right) + \left(\frac{9}{2}x_b^{1/2}x - \frac{2}{5}x_b^{5/2}\frac{x}{\pi}\right)\frac{y}{4}\ln\left[\frac{y^2+(x-x_b)^2}{y^2+(x+x_b)^2}\right]$$

$$-\frac{2}{5}yx_b^{3/2} + \frac{1}{105}\left[72y^2x + 16\frac{y^4}{x} - 40x^3\right]\int_0^\infty e^{-\alpha y}\sin\alpha x \sum\sqrt{\alpha x_b}\,\frac{d\alpha}{\alpha^{1/2}} \qquad (5.61)$$

$$-\frac{1}{105}\left[104x^2y + 8y^3\right]\int_0^\infty e^{-\alpha y}\cos\alpha x \sum\sqrt{\alpha x_b}\,\frac{d\alpha}{\alpha^{1/2}}$$

The expression for the stream function $\psi_1(x,y)$ (equation (5.44)) then becomes

$$\psi_1(x,y) = \frac{1}{\pi}\left[x^{\pi/2} + \frac{2x}{\pi}\left[-x_b^{3/2}\frac{x}{2}\tan^{-1}\left(\frac{2yx}{y^2+x_b^2-x^2}\right)\right.\right.$$

$$\left.\left. + \left(\frac{9}{2}x_b^{1/2}x - \frac{2}{5}x_b^{5/2}\frac{x}{\pi}\right)\frac{y}{4}\ln\left[\frac{y^2+(x-x_b)^2}{y^2+(x+x_b)^2}\right] - \frac{2}{5}y^2x_b^{3/2}\right]\right. \qquad (5.62)$$

$$\left. + \frac{21}{4}\left[\frac{\pi^2}{2} - \frac{2x}{\pi}\cdot\frac{1}{105}\left[72y^2x + 16\frac{y^4}{x} - 40x^3\right]\int_0^\infty e^{-\alpha y}\sin\alpha x \sum\sqrt{\alpha x_b}\,\frac{d\alpha}{\alpha^{1/2}}\right.\right.$$

$$-\frac{21}{4}\sqrt{\frac{\pi}{2}}\cdot\frac{2x}{\pi}\cdot\frac{1}{105}\left[104yx^2+8y^3\right]\int_0^\infty e^{-\alpha y}\cos\alpha x\, S\sqrt{\alpha x_b}\,\frac{d\alpha}{\alpha^{1/2}}\Bigg\}$$

(The solution for $\psi_2(x,y)$ is arrived at in a similar manner).

Setting x = 0, gives us

$$\psi_1(0,y)=0 \tag{5.63}$$

satisfying the boundary condition (5.5(i)) at the shore line.

At the end of the surfzone, y = 0 (that is, as $y\to y_b$), $0<x<x_b$, we get

$$\psi_1(x,0)=\overline{f_1}\left\{x^{1/2}-\frac{4x^4}{\sqrt{2\pi}}\int_0^\infty \sin\alpha x\, S\sqrt{\alpha x_b}\,\frac{d\alpha}{\alpha^{1/2}}\right\}$$

Making the substitution

$$t^2=\alpha x_b$$

in the integral gives us

$$-\frac{8}{\sqrt{2\pi}}\frac{x^4}{x_b^{1/2}}\int_0^\infty \sin\left(t^2\frac{x}{x_b}\right)S(t)\,dt \tag{5.65}$$

or (Gradshteyn and Rhyzik (1965), p. 654, 6.325)

$$-\frac{8}{\sqrt{2\pi}}\cdot\frac{x^4}{x_b^{1/2}}\cdot\left(\frac{x_b}{x}\right)^{1/2}\cdot\pi^{1/2}\cdot 2^{-5/2} \tag{5.66}$$

which then gives us

$$\psi_1(x,0) \equiv 0$$

to satisfy boundary condition (5.5(iii)).

Attempts to further reduce the integrals

$$\int_0^\infty e^{-ay} \sin(ax) \sqrt{ax_b}\, da/a^{1/2}$$

$$\int_0^\infty e^{-ay} \cos(ax) \sqrt{ax_b}\, da/a^{1/2} \qquad (5.67)$$

to standard forms did not meet with success.

An attempt to solve them by Taylor series expansion of the Fresnel integral met with convergence difficulties at both limits of y (as $y \to 0$ and as $y \to +\infty$), as well as a discontinuity at the breaker-line, $x=x_b$.

Integrals (5.67) were, therefore, evaluated numerically (using the trapezoidal rule) and the results thus obtained used in equation (5.62) to calculate values for the stream function $\psi_1(x,y)$ in surfzone I. (Values for the stream function in surfzone II were calculated in a similar manner.)

The solution seaward of the breaker-lines was not calculated from the closed form (5.41), which is not of much practical use. Instead, Laplace's equation was ingrated numerically using the finite difference equation

given in Appendix B (7b), with values at the breaker-lines matched to the analytical solutions.

III Discussion

The full solution, as presented in Figure 28, has been rotated 180° from the configuration shown in Figure 27 and the surfzones truncated at lengths equal to those of the numerical models for comparison with the solutions of Chapter 4. It is realized that the surfzones thus presented are from semi-infinite, but nevertheless of sufficient length in comparison to their widths to merit presenting in this manner.

The general circulation pattern again consists of two counter-rotating cells driven by the wave-induced longshore currents - which flow toward the intersection corner. The off-shore return flow is, however, more strongly divergent than in the numerical solutions, "leaking" across the breaker-lines for most of the width of the surfzones.

Presented in Figure 29 are normalized stream-line profiles taken across the natural beach surfzone at the positions shown in Figure 28. (The stream function values have been normalized with respect to the value of the stream function at the breaker-line of cross section d.) They differ considerably from the infinite beach profile shown in Figure 14 and again illustrate the rapid divergence of the longshore currents in comparison to the numerical models.

The difference between the analytical and numerical solutions appears to be one of scale rather than of form. A thorough verification of the analysis leading to equation (5.62) has not revealed any errors in algebra. A repetition of the numerical model with doubled resolution shows the reliability of the numerical integrations and the independence of the results on grid scale. The difference between numerical and analytical models remains unresolved; in view of its complexity the analytical model does not appear to be a useful tool even in the idealized conditions studied here.

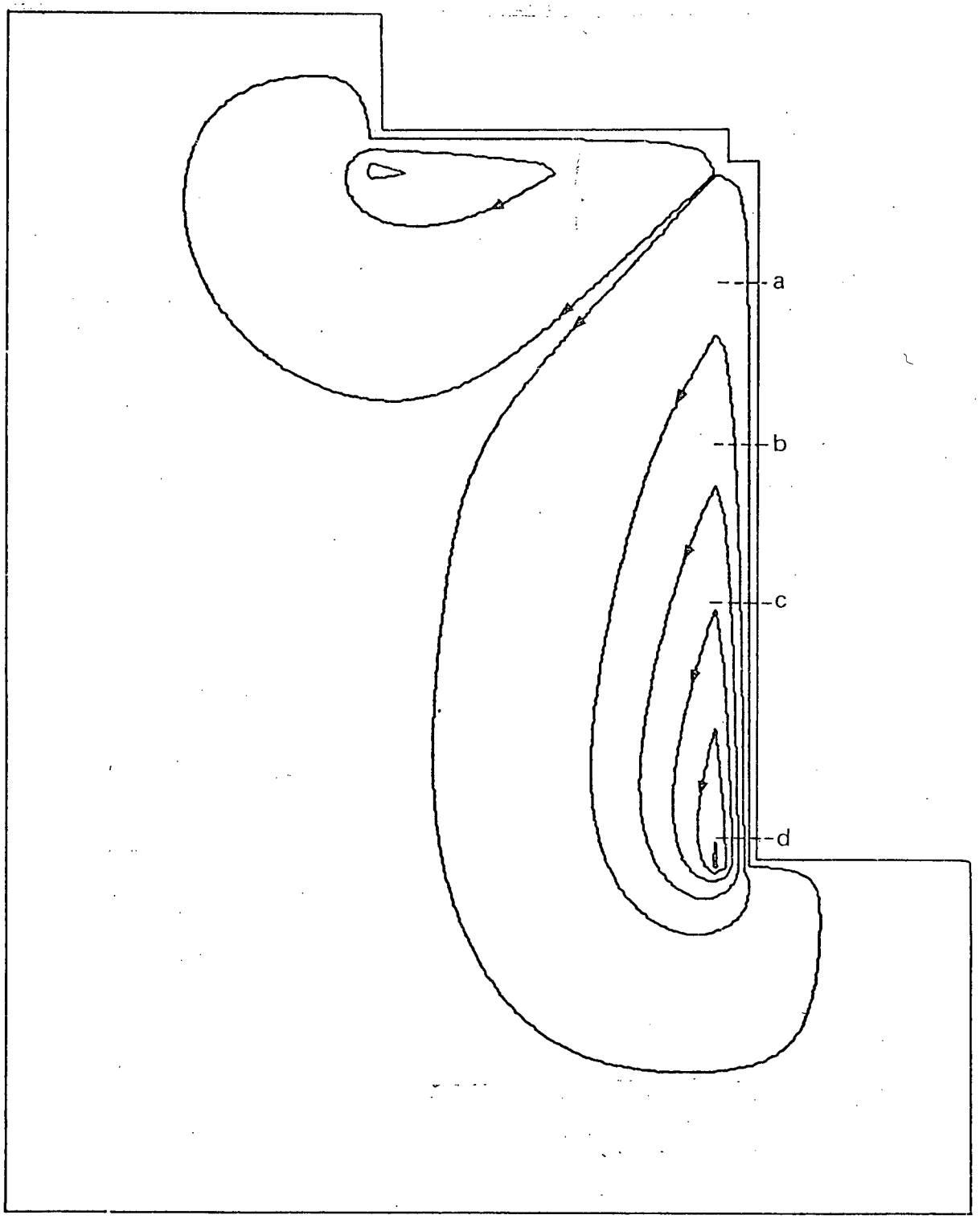

Figure 28. Current pattern for the analytical model, where the beaches have been truncated for comparison to the numerical solutions.

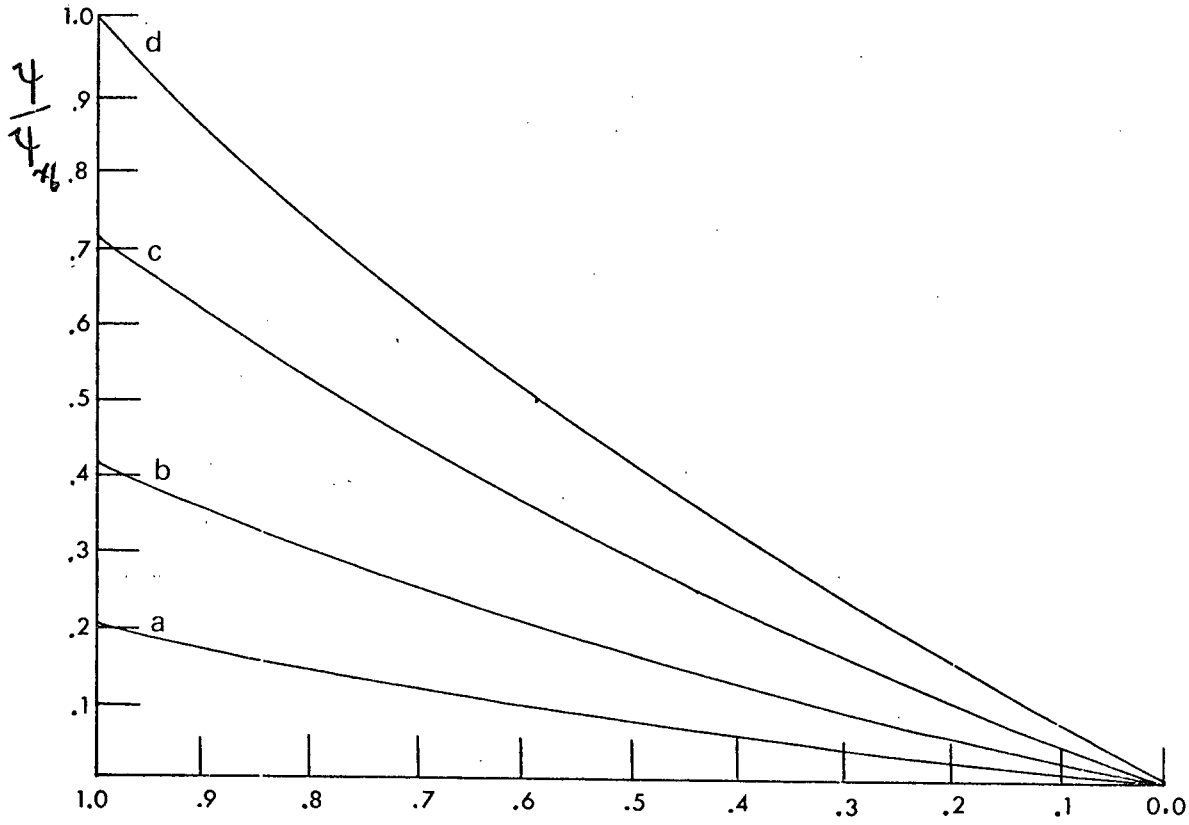

Figure 29. Normalized stream-line profiles taken across the natural beach surf zone of the analytical model at the positions shown in Figure 28

CHAPTER 6

SUMMARY

We have developed several theoretical models of the wave-induced current circulation in the vicinity of an isolated breakwater extending from shore, as inspired by a local field site. These consist of

i/ several numerical models using finite beaches in enclosed basins, where consideration has been given to variations in sea-floor topography as well as to linear and non-linear forms of bottom friction

ii/ an analytical model characterized by semi-infinite beaches and uniform sea-floor topography.

Numerical Models

In general (for a given angle of wave incidence) the circulation patterns show two counter-rotating cells driven by the wave-induced longshore currents - which flow along each beach toward the intersection apex - with a return flow out over the shelf in the form of a rip current. The maximum velocity is found in the return flow, shortly after it emerges from the intersection corner. Despite a host of simplifying assumptions and approximations, the qualitative features of the models are consistent with observations of sediment transport taken at the study site which show beach sediments to be moving along both the causeway and Tsawwassen beaches toward their common corner which is building out as a result.

Differences in the linear and non-linear bottom friction models did not become apparent until an off-shore trench parallel to the causeway, was introduced to the sea-floor topography.

The results for the non-linear model show a deflection of the off-shore return flow into the trench with a corresponding increase in transport and agree with preliminary analysis based on a one-dimensional model. However, the linear results differ considerably from those of the non-linear model, are difficult to interpret and thought to be suspect due to the restrictive assumptions upon which the linear form of bottom friction is derived. The trench model perhaps serves to illustrate another instance in which the use of the linear form of bottom friction may not be appropriate.

Analytical Model

Difficulties were encountered in the development of an analytical model of the current circulation despite the linearization of the governing equations and the use of semi-infinite beaches. As a result it was found necessary to numerically integrate two of the integrals in the surf zone solution as well as the governing equation for the region seaward of the breaker-line.

While exhibiting the same general features as the numerical models, the analytical model shows a much broader and weaker off-shore return flow. The source of this

difference has been sought in possible scaling disparities between the numerical and analytical models, but without success. In view of its algebraic complexity, the analytical model does not appear to be a useful tool, even in the relatively simple geometry studied here, and a fortiori in more realistic geometries.

Improvements to the analysis would take into account horizontal eddy viscosity (which may reduce the strength of the longshore currents), convective inertia (which may strengthen the off-shore return flow), and wave-current interaction, since the off-shore return flow may modify the wave field and cause the waves to break earlier than otherwise (Mei and Liu, 1976, part 2).

Also of interest (at the Tsawwassen location) is the added effect of the trench upon current circulation in light of tidal action, particularly the effects of an ebbing tide upon nearshore circulation as water is drawn into the trench.

To verify the models' predictions, a series of field measurements or wave tank experiments should be undertaken. That longshore currents are present at the study site has been established by evidence of sediment transport along the beaches. However, difficulties in obtaining field measurements of the total circulation at this particular location arise due to the restrictions imposed by the local bathymetry and geometry as well as the non-linearity of the littoral processes themselves. Wave tank experiments may then give a higher yield of data per input of time and effort.

The relationship between near-shore currents and coastal sediment transport is a difficult and complicated problem. Hopefully the basic understanding of the currents in a typical beach-breakwater configuration gained in this study may serve as a first step in resolving the associated quantitative aspects of sedimentation.

LIST OF REFERENCES

Arthur, R.S. (1962). A note on the dynamics of rip currents. J. Geophys. Res., 67, 2777-2779.

Abramowitz, M., and Segun, I.A. (1965). Handbook of Mathematical Functions. New York, Dover Publications Inc.

Bowen, A.J. (1969a). The generation of longshore currents on a plane beach. J. Mar. Res., 27, 206-215.

Dalrymple, R.A., Eubanks, R.A. and Birkmeier, W.A. Wave induced circulation in shallow rectangular basins. Journal of the Waterway, Port, Coastal and Ocean Division, ASCE, vol. 104, No. ww1, Proc. Paper 12749, February 1977, pp 117-134.

Gradshteyn, I.S. and Ryzhik, I.M. (1965). Table of Integrals, Series and Products. New York and London, Academic Press, 1086 pp.

Hodge, R.A.L. (1971). The movement of beach materials; south side Tsawwassen Causeway, a research project submitted during the third year of the course in applied science at the University of British Columbia.

James, I.D. (1972). Ph.D. Thesis. Cambridge University.

James, M.L., Smith, G.M. and Wolford, J.C. (1968). Applied Numerical Methods for Digital Computation with Fortran. Scranton, Pennsylvania, International Text Book Company.

Kamke, E. (1959). Differential-Gleichungen, Lösungsmethoden und Lösungen. New York, Chelsea Publishing Company, 3rd edition.

Komar, P.D. (1976). Beach Processes and Sedimentation. Englewood Cliffs, New Jersey, Prentice-Hall.

Liu, P.L.F. and Dalrymple, R.A. (1978). Bottom friction stresses and longshore currents due waves with large angles of incidence. J. Mar. Res., 36, 357-375.

Liu, P.L.F. and Mei, C.C. (1976). Water motion on a beach in the presence of a breakwater, Part 2. J. Geoph. Res., 81, 3085-3094.

Longuet-Higgins, M.S. (1970). Longshore currents generated by obliquely incident sea waves, 1 and 2. J. Geophys. Res., 75, 6778-6801.

Longuet-Higgins, M.S. (1956). The refraction of sea waves in shallow water. J. Fluid. Mech., 1, 163-176.

Longuet-Higgins, M.S., and Stewart, R.W. (1964). Radiation stress in water waves; a physical discussion with applications. Deep Sea Res., 11, 529-562.

Miller, C.D., and Barcilon, A. The dynamics of the littoral zone. Reviews of Geoph. and Space Phys., vol. 14, no. 1, February 1976, pp 81-91.

Morse, P.M., and Feshbach, H. (1953). Methods of Theoretical Physics, New York, McGraw-Hill Book Company.

Munk, W.H. (1949). The solitary wave theory and its application to surf problems. Ann. N.Y. Acad. Sci., 51, 376-424.

O'Rourke, J.C., and LeBlond, P.H. (1972). Longshore currents in a semicircular bay. J. Geophys. Res., 77, 444-452.

Wood, J.S. (1970). The Tsawwassen and Roberts Bank causeways, a paper presented at the Seminar on Coastal Engineering, University of British Columbia.

APPENDIX A

SUMMARY OF APPROXIMATIONS

The governing equations for the linear numerical models have been derived subject to the following approximations.

1. The equations have been formulated for monochromatic small amplitude wave trains propagating over a mildly sloping bottom.
2. All averaged motion is purely horizontal and depth independent.
3. The energy density of the waves E, is equal to $\frac{1}{2}\rho g a^2$, where 'a' is the amplitude of the waves.
4. Horizontal eddy viscosity has been ignored.
5. Bottom friction has been linearized.
6. The inertial convective terms have been ignored.
7. The wave amplitude in the surfzone is proportional to the mean water depth.
8. Wave-current interaction has been ignored.
9. The waves are assumed plane at the breaker-line.

In addition, for the analytical model, the off-shore zone is assumed to have a uniformly flat bottom, with a depth equal to the water depth at the breaker-line, while the non-linear numerical models do not assume the bottom friction to be linear.

APPENDIX B

COMPUTATIONAL CONSIDERATIONS

We wish to develop a computer programme which will numerically solve for the stream function $\psi(x,y)$ in the vicinity of a beach-breakwater junction.

Throughout we shall be referring to the beach configuration as shown in Figure 30, which differs slightly from the Tsawwassen configuration in angle of intersection and orientation with the general surroundings.

The region in which we are to solve for $\psi(x,y)$ shall be divided into three zones, surfzones I and II and an off-shore zone. Surfzone I (corresponding to the Tsawwassen Beach surfzone) is parallel to the y-axis from $-y_b$ to $-y_\ell$, and is of width $|x_b|$. Surfzone II (corresponding to the causeway surfzone) is parallel to the x-axis from $-x_b$ to $-x_\ell$, and is of width $|y_b|$. The intersection corner has been removed to ease the specification of the boundary conditions there.

The off-shore zone is to accomodate variations in bottom topography such as a trench running parallel to the causeway and a drop-off to much deeper water, as discussed in Chapter 4.

The problem shall be solved by the Gauss-Seidel iterative technique, the general application of which is described below. For a more detailed discussion see James, Smith and Wolford (1968).

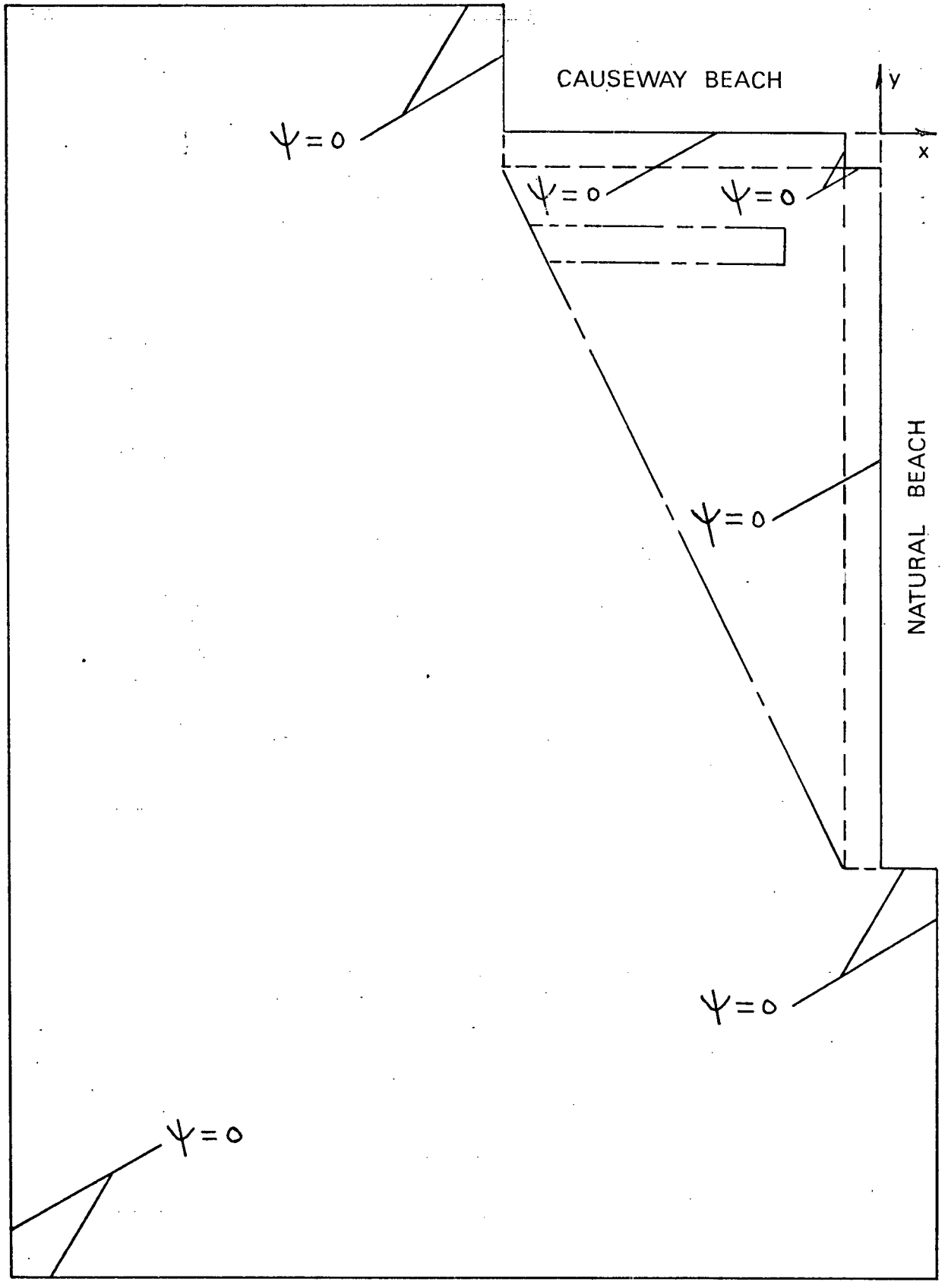

Figure 30. General lay-out and boundary conditions for the numerical models.

A lattice or grid of mesh size $\Delta x=\Delta y=h$ and of dimension x_t by y_t is superimposed upon the region in which a solution is required. The solution of the governing equations consists of determining the stream function values at the finitely-spaced grid points (i,j).

The governing equations for each region of the linear model are as given by equations (4.19), (4.20) and (4.21).

1. Surfzone I

$$\frac{\partial^2\psi}{\partial x^2} - \frac{2}{x}\frac{\partial\psi}{\partial x} + \frac{\partial^2\psi}{\partial y^2} = -K_1 x^{3/2} \qquad (1.b)$$

i) $\psi(x;y_b) = 0 \qquad -x_b < x \leq 0$

ii) $\psi(0,y) = 0 \qquad -y_\ell \leq y < -y_b$

2. Surfzone II

$$\frac{\partial^2\psi}{\partial x^2} - \frac{2}{y}\frac{\partial\psi}{\partial y} + \frac{\partial^2\psi}{\partial y^2} = -K_2 y^{3/2} \qquad (2.b)$$

i) $\psi(-x_b,y) = 0 \qquad -y_b < y \leq 0$

ii) $\psi(x,0) = 0 \qquad -x_\ell \leq x < -x_b$

3. Off-shore Zone

$$\frac{\partial^2 \psi}{\partial x^2} + \frac{\partial^2 \psi}{\partial y^2} - \frac{2}{d}\frac{\partial d}{\partial x}\frac{\partial \psi}{\partial x} - \frac{2}{d}\frac{\partial d}{\partial y}\frac{\partial \psi}{\partial y} = 0 \qquad (3.b)$$

The offshore stream function is identically zero on the walls of the basin, as shown in Figure 30, and is matched across the breaker-lines and the ends of the surf-zones to the respective surfzone stream functions.

From Taylor series expansions we have the following finite difference approximations to derivatives:

$$\frac{\partial^2 u}{\partial x^2} = \frac{u_{i+1,j} - 2u_{i,j} + u_{i-1,j}}{h^2}$$

$$\frac{\partial^2 u}{\partial y^2} = \frac{u_{i,j+1} - 2u_{i,j} + u_{i,j-1}}{h^2} \qquad (4.b)$$

$$\frac{\partial u}{\partial y} = \frac{u_{i,j+1} - u_{i,j}}{h}$$

$$\frac{\partial u}{\partial x} = \frac{u_{i+1,j} - u_{i,j}}{h}$$

which upon substitution into equations (1.b), (2.b) and (3.b) give:

1. Surfzone I

$$\psi_{i,j} = \frac{SP \cdot \psi_{i+1,j} + \psi_{i-1,j} + \psi_{i,j+1} + \psi_{i,j-1} + K_1 \cdot \mathbb{R}_x^{3/2}}{SD}$$

$$SP = 1 - \frac{2}{\mathbb{R}_x} \quad ; \quad SD = 4 - \frac{2}{\mathbb{R}_x} \tag{5.b}$$

$\mathbb{R}_x$ is the distance from the shoreline

2. Surfzone II

$$\psi_{i,j} = \frac{\psi_{i+1,j} + \psi_{i-1,j} + SP \cdot \psi_{i,j+1} + \psi_{i,j-1} - K_2 \cdot \mathbb{R}_y^{3/2}}{SD}$$

$$SP = 1 - \frac{2}{\mathbb{R}_y} \quad ; \quad SD = 4 - \frac{2}{\mathbb{R}_x} \tag{6.b}$$

$\mathbb{R}_y$ is the distance from the shoreline

3. Off-shore Zone

$$\psi_{i,j} = \frac{SP \cdot \psi_{i+1,j} + \psi_{i-1,j} + SL \cdot \psi_{i,j+1} + \psi_{i,j-1}}{SD} \tag{7.b}$$

$$SP = 3 - 2 \cdot H_{i+1,j} / H_{i,j}$$

$$SL = 3 - 2 \cdot H_{i,j+1} / H_{i,j}$$

$$SD = 8 - 2 \cdot \left[H_{i,j+1} + H_{i+1,j} \right] / H_{i,j}$$

where H_{ij} is the depth at grid point (i,j).

The problem has now been reduced to obtaining the simultaneous solution of a set of linear algebraic equations in the unknown grid-point stream function values $\psi_{i,j}$, the total number of equations depending upon the extent of the boundaries and the number of grid points used.

The steps in the Gauss-Seidel iterative method used to obtain the solutions are as follows (as given by James, Smith and Wolford, 1968).

i/ each equation is first written in a form convenient for solving for the unknown with the largest coefficient in that equation.

ii/ all unknown stream function values at the grid points are then assigned initial values on the basis of the best estimated value (the better the estimate, the more rapid the convergence to a solution).

iii/ at each point (i,j) in the lattice, an approximate value of the stream function STEMP is then calculated using the appropriate equation ((5.b), (6.b) or (7.b)). This calculated value supercedes the estimated value and is then used as the stream function value $\psi_{i,j}$, at that grid point until it, in turn, is superceded by a new calculated value

iv/ in all iterations, the latest calculated stream function values are always used in calculating newer and better points.

v/ the points on the lattice at which the STEMP values are calculated are selected in some systematic way - in this case by rows

vi/ one iteration is completed when an appropriate value has been calculated for each lattice point whose stream function value is sought

vii/ when the stream function change at all grid points between successive iterations is less than or equal to some pre-determined value or when a certain maximum number of iterations has been reached the computations are stopped.

A plotter is used to draw the contour graphs of the stream-lines as functions of i and j.

In some models a non-linear form of bottom friction (James, 1972)

$$\tau = C\rho |\underset{\sim}{u}_0| \underset{\sim}{u}_0 \qquad (8.b)$$

is used in the off-shore zone (as discussed in Chapter 3). The relevant finite difference equation then becomes

$$\psi_{i,j} = \frac{SP \cdot \psi_{i+1,j} + 2 \cdot \psi_{i-1,j} + SL \cdot \psi_{i,j+1} + 2 \cdot \psi_{i,j-1}}{SD} \qquad (9.b)$$

$$SP = 4 - 2 \cdot H_{i,j+1} / H_{i,j}$$

$$SL = 4 - 2 \cdot H_{i+1,j} / H_{i,j}$$

$$SD = 12 - 2 \cdot [H_{i,j+1} + H_{i+1,j}] / H_{i,j}$$

And finally, a note with regards to the mesh size h, used in the analysis. The models presented in Chapters 4 and 5 have a lattice spacing of 18 grid points per inch. The effects of varying the numerical models' resolution is clearly illustrated upon comparison of the acute angle model of Figure 31 with that of Figure 18, where the models differ only in their mesh size; Figure 18 showing the circulation pattern of a model having twice the resolution of that shown in Figure 31. The most noticeable effect of increasing the resolution is to decrease the size of the 'step' (which is a direct reflection of the mesh size) in the stream-lines adjacent to the natural beach which runs diagonally to the grid lattice. In addition, the 'eddies' which are present in Figure 31 would also appear to be a manifestation of poor resolution since they are not evident in the higher resolution models of Chapters 4 and 5.

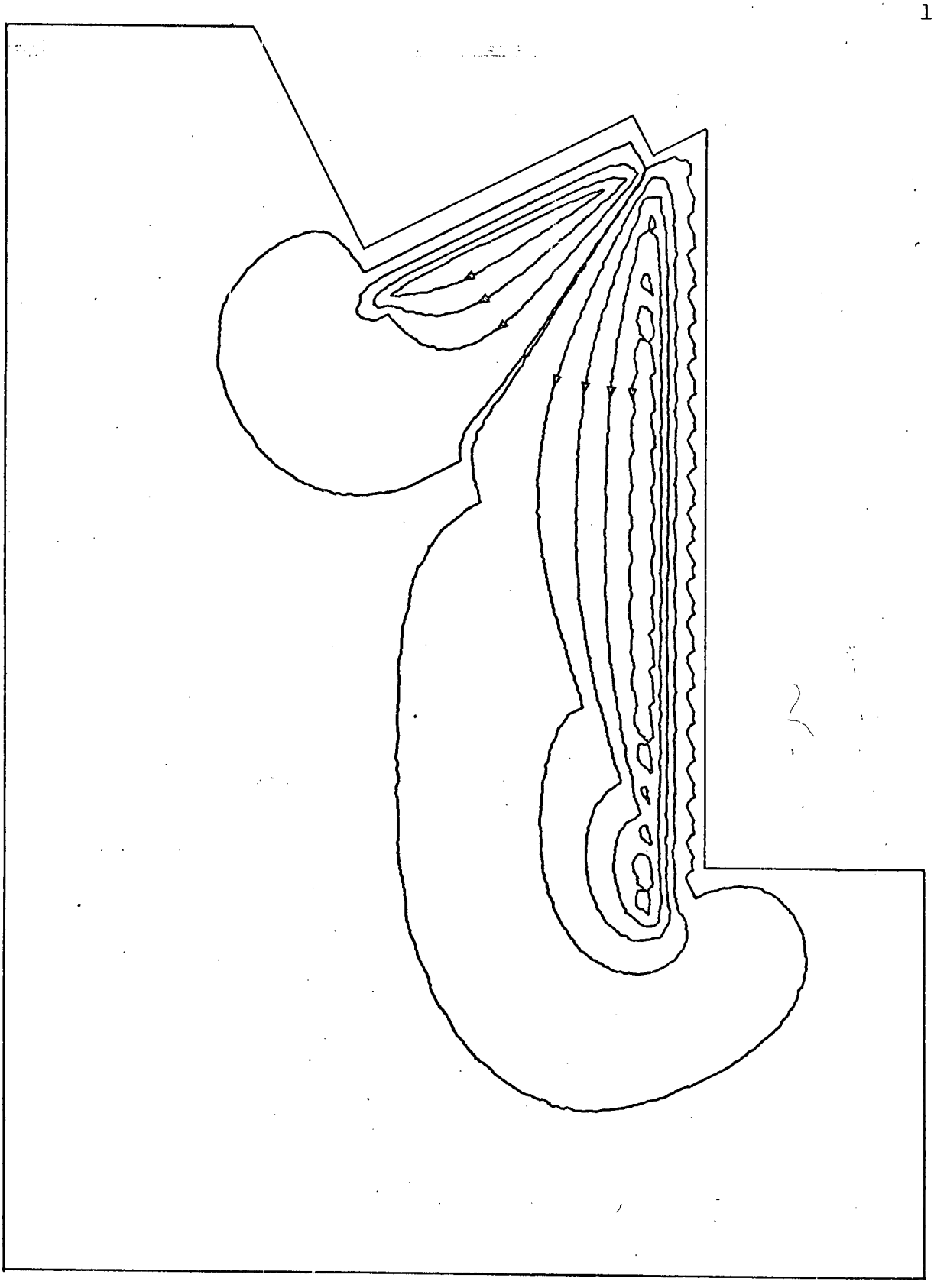

Figure 31. An example of the effects of varying the resolution of the numerical models

APPENDIX C

EVALUATION OF INTEGRALS $I_1(\alpha)$ AND $I_2(\beta)$

We wish to evaluate

$$I_1(\alpha) = \int_0^{x_b} J_{3/2}(\alpha x)\, x^3\, dx \tag{1.c}$$

where (Abramowitz and Stegun (1965), p. 437)

$$J_{3/2}(\alpha x) = \sqrt{\frac{2}{\pi}}\,(\alpha x)^{-3/2}(\sin \alpha x - \alpha x \cos \alpha x) \tag{2.c}$$

so that

$$I_1(\alpha) = \sqrt{\frac{2}{\pi}}\,\alpha^{-4}\int_0^{x_b}(\sin \alpha x - \alpha x \cos \alpha x)(\alpha x)^{3/2}\, d\alpha x \tag{3.c}$$

If we integrate by parts, letting

$$u = (\alpha x)^{3/2} \qquad du = 3/2\,(\alpha x)^{1/2}\, d\alpha x$$

$$v = \int (\sin \alpha x - \alpha x \cos \alpha x)\, d\alpha x = -(2\cos \alpha x + \alpha x \sin \alpha x)$$

equation (3.c) gives us

$$\overline{I}_1(a) = \sqrt{\frac{2}{\pi}}\, a^{-4} - (2\cos ax_b + ax_b \sin ax_b)(ax_b)^{3/2}$$

$$+ 3\int_0^{ax_b} (ax)^{1/2}\cos ax\, dax + 3/2 \int_0^{ax_b} (ax)^{3/2}\sin ax\, dax \qquad (4.c)$$

Consider now

$$3/2 \int_0^{ax_b} (ax)^{3/2}\sin ax\, dax = 3/2\, Q(ax) \qquad (5.c)$$

Again integrating by parts

$$u = (ax)^{3/2} \quad , \quad du = 3/2\,(ax)^{1/2}\, dax$$

$$v = \int \sin ax\, dax = -\cos ax$$

we get

$$3/2\, Q(ax) = 3/2\,(ax_b)^{3/2}\cos ax_b + 9/4 \int_0^{ax_b} (ax)^{1/2}\cos ax\, dax$$

so that

$$I_1(a) = \sqrt{\frac{2}{\pi}}\, a^{-4} \left[-\frac{1}{2}(ax_b)^{3/2}\cos ax_b - (ax_b)^{5/2}\sin ax_b + \frac{21}{4}\int_0^{ax_b} (ax)^{1/2}\cos ax\, dax \right] \tag{6.c}$$

Now consider

$$\int_0^{ax_b} (ax)^{1/2}\cos ax\, dax = \mathcal{R}(ax)$$

once again integrating by parts

$$u = (ax)^{1/2} \quad ; \quad du = \frac{1}{2}(ax)^{-1/2}\, dax$$

$$v = \int \cos ax\, dax = \sin ax$$

so that

$$\mathcal{R}(ax) = (ax)^{1/2}\sin(ax)\Big|_0^{ax_b} - \frac{1}{2}\int_0^{ax_b} \frac{\sin ax\, dax}{(ax)^{1/2}}$$

$$= (ax_b)^{1/2}\sin(ax_b) - \sqrt{\frac{\pi}{2}}\, S\left(\sqrt{ax_b}\right)$$

where $S(\sqrt{\alpha r_b})$ is a Fresnel integral as given by Gradshetyn and Rhyzik ((1965), p. 930, 8.251(2)).

We then have

$$I_1(\alpha) = \sqrt{\frac{2}{\pi}}\,\alpha^{-4}\left[-\frac{1}{2}(\alpha r_b)^{3/2}\cos\alpha r_b - (\alpha r_b)^{5/2}\sin\alpha r_b\right.$$

$$\left.+\frac{21}{4}(\alpha r_b)^{1/2}\sin\alpha r_b - \frac{21}{4}\sqrt{\frac{\pi}{2}}\,S(\sqrt{\alpha r_b})\right] \qquad (7.c)$$

Similarly for

$$I_2(\beta) = \int_0^{y_b} J_{3/2}(\beta y)\,y^3\,dy$$

$$= \sqrt{\frac{2}{\pi}}\,\beta^{-4}\left[-\frac{1}{2}(\beta y_b)^{3/2}\cos\beta y_b - (\beta y_b)^{5/2}\sin\beta y_b\right. \qquad (8.c)$$

$$\left.+\frac{21}{4}(\beta y_b)^{1/2}\sin\beta y_b - \frac{21}{4}\sqrt{\frac{\pi}{2}}\,S\sqrt{\beta y_b}\right]$$

APPENDIX D

INTEGRAL ANALYSIS

We wish first to evaluate integrals (5.46) and (5.47)

$$\frac{1}{2}\frac{r_b^{3/2}}{r}\int_0^\infty e^{-ay}\cos ar_b \sin ar\,\frac{da}{a^3} - \frac{1}{2}r_b^{3/2}\int_0^\infty e^{-ay}\cos ar_b\cos ar\,\frac{da}{a^2} \tag{1.d}$$

Let us start by integrating the following integral by parts

$$\frac{r_b^{5/2}}{r}\int_0^\infty e^{-ay}\sin ar\sin ar_b\,\frac{da}{a^2} \tag{2.d}$$

letting

$$u = \frac{e^{-ay}\sin ar}{a^2}\quad ;\quad dv = \sin ar_b\quad ;\quad v = -\frac{\cos ar_b}{r_b}$$

We then have

$$\frac{r_b^{5/2}}{r}\int_0^\infty e^{-ay}\sin ar\sin ar_b\,\frac{da}{a^2} =$$

$$\frac{r_b^{3/2}}{r}\frac{\sin ar}{a^2}\Bigg|^0 - \frac{r_b^{3/2}y}{r}\int_0^\infty e^{-ay}\cos ar_b\sin ar\,\frac{da}{a^2} \tag{3.d}$$

$$-2\frac{r_b^{3/2}}{r}\int_0^\infty e^{-ay}\cos ar_b\sin ar\,\frac{da}{a^3} + r_b^{3/2}\int_0^\infty e^{-ay}\cos ar_b\cos ar\,\frac{da}{a^2}$$

or

$$\frac{1}{2}\frac{x_b}{\pi}^{3/2}\int_0^\infty e^{-\alpha y}\cos\alpha x_b \sin\alpha x \frac{d\alpha}{\alpha^3} =$$

$$\frac{1}{4}\frac{x_b}{a}^{3/2}\Big|^0 - \frac{1}{4}\frac{x_b}{\pi}^{5/2}\int_0^\infty e^{-\alpha y}\sin\alpha x \sin\alpha x_b \frac{d\alpha}{\alpha^2}$$

(4.d)

$$-\frac{1}{4}\frac{x_b}{\pi}^{3/2} y\int_0^\infty e^{-\alpha y}\cos\alpha x_b \sin\alpha x \frac{d\alpha}{\alpha^2} + \frac{1}{4}x_b^{3/2}\int_0^\infty e^{-\alpha y}\cos\alpha x_b \cos\alpha x \frac{d\alpha}{\alpha^2}$$

Equation (1.d) now becomes

$$\underline{\underline{I}}$$

$$\frac{1}{4}\frac{x_b}{a}^{3/2}\Big|^0 - \frac{1}{4}\frac{x_b}{\pi}^{3/2}\int_0^\infty e^{-\alpha y}\sin\alpha x \sin\alpha x_b \frac{d\alpha}{\alpha^2}$$

(5.d)

$$-\frac{1}{4}\frac{x_b}{\pi}^{3/2} y\int_0^\infty e^{-\alpha y}\cos\alpha x_b \sin\alpha x \frac{d\alpha}{\alpha^2} - \frac{1}{4}x_b^{3/2}\int_0^\infty e^{-\alpha y}\cos\alpha x_b \cos\alpha x \frac{d\alpha}{\alpha^2}$$

$$\underline{\underline{II}} \qquad\qquad \underline{\underline{III}}$$

where integral III is ½ of Integral (5.47), which we shall now integrate by parts to get

$$\overset{III}{-\frac{7}{4}\sqrt{b}^{3/2}\int_0^\infty e^{-a\gamma}\cos ax\sqrt{b}\cos ax\,\frac{da}{a^2}} =$$

$$-\frac{7}{4}\frac{\sqrt{b}^{3/2}}{a}\Bigg|^0 + \overset{IV}{\frac{7}{4}\sqrt{b}^{5/2}\int_0^\infty e^{-a\gamma}\cos ax\sin ax\sqrt{b}\,\frac{da}{a}} \qquad (6.d)$$

$$+\overset{V}{\frac{7}{4}\sqrt{b}^{3/2}\gamma\int_0^\infty e^{-a\gamma}\cos ax\sqrt{b}\cos ax\,\frac{da}{a}} + \overset{VI}{\frac{7}{4}\sqrt{b}^{3/2}x\int_0^\infty e^{-a\gamma}\cos ax\sqrt{b}\sin ax\,\frac{da}{a}}$$

so that equation (5.d) becomes

$$\overset{I}{-\frac{7}{4}\frac{\sqrt{b}^{5/2}}{x}\int_0^\infty e^{-a\gamma}\sin ax\sin ax\sqrt{b}\,\frac{da}{a^2}} - \overset{II}{\frac{7}{4}\frac{\sqrt{b}^{3/2}\gamma}{x}\int_0^\infty e^{-a\gamma}\cos ax\sqrt{b}\sin ax\,\frac{da}{a^2}} \qquad (7.d)$$

$$+\overset{IV}{\frac{7}{4}\sqrt{b}^{5/2}\int_0^\infty e^{-a\gamma}\cos ax\sin ax\sqrt{b}\,\frac{da}{a}} + \overset{V}{\frac{7}{4}\sqrt{b}^{3/2}\gamma\int_0^\infty e^{-a\gamma}\cos ax\sqrt{b}\cos ax\,\frac{da}{a}}$$

$$+\overset{VI}{\frac{7}{4}\sqrt{b}^{3/2}x\int_0^\infty e^{-a\gamma}\cos ax\sqrt{b}\sin ax\,\frac{da}{a}}$$

Considering now Integral $\overline{V}$, we have

$$\frac{1}{4}\sqrt{b}^{3/2}\gamma\int_0^\infty e^{-a\gamma}\cos\alpha\sqrt{b}\cos\alpha\frac{da}{a} = -\frac{1}{4}\sqrt{b}^{3/2}\gamma$$

$$\overline{VII}$$

$$+\frac{1}{4}\sqrt{b}^{3/2}\frac{\gamma^2}{\pi}\int_0^\infty e^{-a\gamma}\sin\alpha\cos\alpha\sqrt{b}\frac{da}{a} \qquad (8.d)$$

$$(-\overline{II})$$

$$+\frac{1}{4}\sqrt{b}^{3/2}\frac{\gamma}{\pi}\int_0^\infty e^{-a\gamma}\cos\alpha\sqrt{b}\sin\alpha\frac{da}{a^2} + \frac{1}{4}\sqrt{b}^{3/2}\frac{\gamma}{\pi}\int_0^\infty e^{-a\gamma}\sin\alpha\sin\alpha\sqrt{b}\frac{da}{a}$$

$$\overline{VIII}$$

Substituting into equation (7.d) we get

$$-\frac{1}{4}\sqrt{b}^{3/2}\gamma - \frac{1}{4}\frac{\sqrt{b}^{5/2}}{\pi}\int_0^\infty e^{-a\gamma}\sin\alpha\sin\alpha\sqrt{b}\frac{da}{a^2}$$

$$\overline{I}$$

$$\overline{IV}$$

$$+\frac{1}{4}\sqrt{b}^{5/2}\int_0^\infty e^{-a\gamma}\cos\alpha\sin\alpha\sqrt{b}\frac{da}{a} + \frac{1}{4}\sqrt{b}^{3/2}\pi\int_0^\infty e^{-a\gamma}\cos\alpha\sqrt{b}\sin\alpha\frac{da}{a} \qquad (9.d)$$

$$\overline{VI}$$

$$\overline{VII}$$

$$+\frac{1}{4}\sqrt{b}^{3/2}\frac{\gamma^2}{\pi}\int_0^\infty e^{-a\gamma}\sin\alpha\cos\alpha\sqrt{b}\frac{da}{a} + \frac{1}{4}\sqrt{b}^{5/2}\frac{\gamma}{\pi}\int_0^\infty e^{-a\gamma}\sin\alpha\sin\alpha\sqrt{b}\frac{da}{a}$$

$$\overline{VIII}$$

Finally, we also have

$$\frac{1}{4}\sqrt{b}^{5/2}\int_0^\infty e^{-a\gamma}\cos\alpha\sin\alpha\sqrt{b}\frac{da}{a} = \qquad (10.d)$$

$$\overline{IV}$$

$$= \frac{1}{4} r_b^{3/2} \frac{y}{x} \int_0^\infty e^{-\alpha y} \sin\alpha x \sin\alpha r_b \frac{d\alpha}{\alpha} \qquad \text{VIII}$$

$$+ \frac{1}{4} r_b^{3/2} \frac{}{x} \int_0^\infty e^{-\alpha y} \sin\alpha x \sin\alpha r_b \frac{d\alpha}{\alpha^2} \qquad (-\text{I})$$

$$- \frac{1}{4} r_b^{1/2} \frac{}{x} \int_0^\infty e^{-\alpha y} \sin\alpha x \cos\alpha r_b \frac{d\alpha}{\alpha} \qquad \text{IX}$$

which then gives us

$$- \frac{1}{4} r_b^{3/2} y$$

$$+ \frac{1}{4} \left(r_b^{3/2} x + r_b^{3/2} \frac{y^2}{x} - r_b^{1/2} \frac{}{x} \right) \int_0^\infty e^{-\alpha y} \cos\alpha r_b \sin\alpha x \frac{d\alpha}{\alpha} \qquad \text{VI, VII, IX} \qquad (11.d)$$

$$+ \frac{1}{2} r_b^{3/2} \frac{y}{x} \int_0^\infty e^{-\alpha y} \sin\alpha x \sin\alpha r_b \frac{d\alpha}{\alpha} \qquad \text{VIII}$$

The integrals in equation (11.d) are to be found in Gradshteyn and Rhyzik ((1965), p. 492), so that equation (1.d) now becomes

$$- \frac{1}{4} r_b^{3/2} y - \frac{1}{8} r_b^{3/2} \frac{y}{x} \ln \left[\frac{y^2 + (r_b - x)^2}{y^2 + (r_b + x)^2} \right] \qquad (12.d)$$

$$+\frac{7}{4}\left(r_b^{3/2}x + r_b^{3/2}\frac{y^2}{x} - r_b^{7/2}\frac{}{x}\right)\cdot\frac{1}{2}\tan^{-1}\left(\frac{2yx}{y^2+r_b^2-x^2}\right)$$

In a similar manner integrals (5.48) and (5.49) give us

$$\frac{r_b^{7/2}}{7}\cdot\frac{1}{2}\tan^{-1}\left(\frac{2yx}{y^2+r_b^2-x^2}\right) + r_b^{5/2}\frac{y}{x}\ln\left[\frac{y^2+(r_b-x)^2}{y^2+(r_b+x)^2}\right] \qquad (13.d)$$

while integrals (5.50) and (5.51) can be shown to equal

$$\left(-\frac{21}{8}r_b^{3/2}x - \frac{21}{8}r_b^{3/2}\frac{y^2}{x} + \frac{7}{8}r_b^{7/2}\frac{}{x}\right)\cdot\frac{1}{2}\tan^{-1}\left(\frac{2yx}{y^2+r_b^2-x^2}\right)$$

$$-\frac{7}{4}r_b^{\frac{1}{2}}x^2\cdot\frac{1}{2}\tan^{-1}\left(\frac{2yr_b}{y^2-r_b^2+x^2}\right) \qquad (14.d)$$

$$-\left(-\frac{21}{8}r_b^{\frac{1}{2}}x - \frac{21}{8}r_b^{5/2}\frac{}{x} + \frac{7}{8}r_b^{\frac{1}{2}}\frac{y^2}{x}\right)$$

Taking the sum of equations (12.d), (13.d) and (14.d) gives us

$$\left(-\frac{7}{8}r_b^{3/2}x - \frac{7}{8}r_b^{3/2}\frac{y^2}{x} + \frac{1}{8}r_b^{\frac{7}{2}}\frac{}{x}\right)\cdot\frac{1}{2}\tan^{-1}\left(\frac{2yx}{y^2+r_b^2-x^2}\right) \qquad (15.d)$$

$$-\frac{1}{4}\tan^{-1}\left(\frac{2yx_b}{y^2-x_b^2+x^2}\right)$$

$$+\left(\frac{21}{8}x_b^{\frac{1}{2}}x+\frac{1}{8}x_b^{\frac{5}{2}}\frac{}{x}+\frac{1}{8}x_b^{\frac{1}{2}}\frac{y^2}{x}\right)\frac{y}{4}\ln\left[\frac{y^2+(x_b-x)^2}{y^2+(x_b+x)^2}\right]$$

as shown in equation (5.57).